NOTICE

The quality of this microform is heavily dependent upon the quality of the original thesis submitted for microfilming. Every effort has been made to ensure the highest quality of reproduction possible.

If pages are missing, contact the university which granted the degree.

Some pages may have indistinct print especially if the original pages were typed with a poor typewriter ribbon or if the university sent us an inferior photocopy.

Reproduction in full or in part of this microform is governed by the Canadian Copyright Act, R.S.C. 1970, c. C-30, and subsequent amendments.

AVIS

La qualité de cette microforme dépend grandement de la qualité de la thèse soumise au microfilmage. Nous avons tout fait pour assurer une qualité supérieure de reproduction.

S'il manque des pages, veuillez communiquer avec l'université qui a conféré le grade.

La qualité d'impression de certaines pages peut laisser à désirer, surtout si les pages originales ont été dactylographiées à l'aide d'un ruban usé ou si l'université nous a fait parvenir une photocopie de qualité inférieure.

La reproduction, même partielle, de cette microforme est soumise à la Loi canadienne sur le droit d'auteur, SRC 1970, c. C-30, et ses amendements subséquents.

Canada

Preparation and Characterization of Mesoporous Aluminosilicates from Ca-A

Zeolite.

Ngoc Truc-Chi Vo

A Thesis

in

The Department

of

Chemistry and Biochemistry

Presented in Partial Fulfilment of the Requirements

for the Degree of Master of Science at

Concordia University

Montreal, Quebec, Canada

April 1992

© Ngoc Truc-Chi Vo, 1992

Canada

CONCORDIA UNIVERSITY
Division of Graduate Studies

This is to certify that the thesis prepared

By: Ngoc Truc-Chi Vo

Entitled: Preparation and Characterization of Mesoporous

           Aluminosilicates from Ca-A Zeolite

and submitted in partial fulfillment of the requirements for the degree of

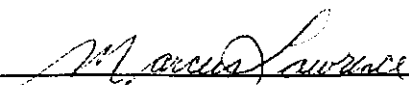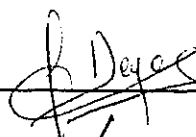   Master in Chemistry

complies with the regulations of the University and meets the accepted standards with respect to originality and quality.

Signed by the final examining committee:

_____ Chair

_____ Examiner

_____ Examiner

_____ Thesis Supervisor

_____ Thesis Supervisor

Approved by _____
           Chair of Department or Graduate Program Director

April 21, 19 92

_____
Dean of Faculty

ABSTRACT

Preparation and Characterization of Porous Aluminosilicates from CaA Zeolite.

Ngoc Truc-Chi Vo

Three methods have been developed in order to enlarge the pore size of the micropore - type zeolite into a mesopore type: a) 0.2N HCl acid treatment at 80 °C from which the time of exposure to the acid medium has a great influence on the pore size distribution of the resulting materials. b) a hydrothermal treatment followed by a mild acid treatment that can unblock the pore openings. c) finally, a treatment with 0.5M $(NH_4)_2SiF_6$. The two first methods provided mesopores of 3.5 - 4.5 nm while the last one produced larger mesopores of ca. 14 nm.

Several physico - chemical techniques were used to characterize the reaction products: BET measurements, XRD, AA Spectrophotometry, hydrophobicity measurement, bulk density, ^{29}Si- and ^{27}Al-NMR.

ACKNOWLEDGEMENT

I wish to express my sincere gratitude to my supervisor, Dr. R. Le Van Mao, for his precious guidance and direction throughout the course of this research and in the preparation of this thesis.

I would like to thank the members of my research committee, Dr. C.H. Langford and especially Dr. G. Denes who is also my co-supervisor, for his cooperation and valuable helpful discussions.

I am indebted to Mrs. J. Yao for the kind patience and interest she took in integrating me into the world of Material Sciences, on theoretical as well as practical aspects of this research. I am grateful to all the fellow members of Catalysis Research Laboratory, especially Mr. B. Sjiariel for his constant technical assistance and moral support.

Finally, I dedicate this thesis to my family who has supported and encouraged me all along this work.

TABLE OF CONTENTS

LIST OF FIGURES

LIST OF TABLES

CHAPTER I: INTRODUCTION

In order to overcome the problem of instability at high temperature in presence of air of the high-performance activated carbon and porous silicas (xero-, alcogels), other classes of molecular sieves have been synthesized. The term molecular sieve was coined by J.W. McBain to describe porous materials which can act as sieves on a molecular scale (1). The most widely known molecular sieves are aluminosilicate zeolites and microporous silica polymorphs (2).

For a long time, the largest known rings in natural zeolites and synthetic molecular sieves had been found to contain 12 tetrahedrally coordinated atoms (T-atoms) with channel diameters of 7.4 Å (3). Much work has been devoted to the search for larger rings.

Research in the field of microporous crystalline inorganic solids has followed two paths: 1) Creation of new, larger pore sized materials, 2) Enlarging the pore size of the already existing zeolites by dealumination.

Knowing that micropores have a pore size of less than 20 Å, mesopores of 20 - 500 Å and macropores are larger than 500 Å (4), the objective of this thesis is to prepare mesoporous aluminosilicates. This was attempted by enlarging the pore size of the commercial reference Ca-A zeolite via 1) hydrothermal treatments with H_2O vapor, 2) chemical treatments such as HCl acid solution or $(NH_4)_2SiF_6$ salt solution, and 3) two-step procedure combining a hydrothermal treatment with a chemical treatment or a chemical treatment with another chemical treatment.

The products are characterized by BET measurements for their specific surface

area, pore size distribution; atomic absorption spectrophotometry for elemental analysis; vapor sorption measurements for hydrophobicity degree; X-ray powder diffraction for degree of crystallinity; bulk density measurements for packing efficiency; and MAS-^{29}Si- and ^{27}Al-NMR for the chemical environment around Si and also tetrahedral vs. octahedral coordination of Al.

CHAPTER II: REVIEW OF SCIENTIFIC AND PATENT LITERATURES
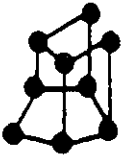
A)   Zeolite

The zeolites used as adsorbents, catalysts, ion exchangers, etc. mainly originate

from two sources: mineral zeolites (e.g. mordenite, chabazite, erionite, clinoptilolite),

and synthetic zeolites (e.g. A, X, Y, ZSM-5, etc.) (5). Structurally, zeolites consist of

a three-dimensional network of SiO_4 and AlO_4 tetrahedra with each oxygen atom being

shared between two tetrahedra to give a ratio $O/(Al+Si) = 2$. Electrical neutrality is

achieved by the inclusion of alkali or alkaline earth ions like Na^+, Ca^{++}. In addition,

interstitial voids contain water molecules which may be removed reversibly or replaced

by other species (6). The channels possess apertures between 3 and 10 Å, which are in

the dimension range of most molecules. As for the classification of zeolites, the actual

tendency is to consider the type of link of primary tetrahedra on the basis of well defined

geometric systems known as Secondary Building Units (SBU); some of these are shown

on Figure 1a, (7).

The zeolite studied is Ca-A (5A) obtained from Linde. Let us start with Na-A

(4A) zeolite, the basic compound from which all other types of A zeolite are derived,

including Ca-A zeolite.

1)   Na-A

This zeolite is represented by the formula $Na_{12}[(AlO_2)_{12}(SiO_2)_{12}]$.

27 H_2O. The SBU structure is cubic, with an edge $a_o = 12.32$ Å, D4R type,

and contains 4 AlO_4 and 4 SiO_4 tetrahedra in a rigid compact group. These

units link together to form a ring of 8 oxygen atoms in the center of each face of

1)   <u>S4R</u> (ZÉOLITHES: ANALCÍME,PHILLIPSITE,ETC)

2)   <u>S6R</u> (ZÉOLITHES: ERIONITE,OFFRETITE,T, ETC)

3)   <u>D4R</u> (ZÉOLITHES: A, ZK-4,ETC)

4)   <u>D6R</u> (ZÉOLITHES: FAUJASITE,X,Y,CHABAZITE,ETC)

5)   <u>COMPLEXE 4-1,UNITÉ T_5O_{10}</u>
                  (ZÉOLITHES: NATROLITE,THOMSONITE,ETC)

6)   <u>COMPLEXE 5-1,UNITÉ T_8O_{16}</u>
                  (ZÉOLITHES: MORDENITE,FERRIERITE,ETC)

7)   <u>COMPLEXE 4-4-1,UNITÉ $T_{10}O_{20}$</u>
                  (ZÉOLITHES: CLINOPTILOLITE,ETC)

Formule empirique : $M_{2/n}O \cdot Al_2O_3 \cdot x SiO_2 \cdot y H_2O$

Figure 1a: Models of SBU and Examples of Zeolite Structures (7).

the unit cell and an irregular ring of 6 oxygen atoms at each corner on the 3-fold axis. In the center of the unit cell is a large cavity, 11.4 Å in diameter, often called α-cage, which is connected to 6 similar cavities by the 8- membered rings which form restricted openings 4.2 Å in diameter. Furthermore, the α-cage is connected to 8 small cavities called β-cages, 6.6 Å in diameter, by the 6-membered rings which produce openings of 2.0 Å in diameter (6, Fig. 1b & 1c).

The eight Na^+ cations, called site I, are located in the β-cages. Four of them are found near the 8-membered rings. Three Na^+ ions, termed site II, are located in the α-cage which by partial blocking of the aperture, influence the adsorption of gases and vapors and regulate the pore size. The remaining Na^+ cation is located on site III, whose position is more or less displaced with respect to the sites II.

In general, removal of adsorbed water increases the intensities of the stronger Bragg peaks observed in XRD. In terms of thermal stability and decomposition products, the basic type A structure remained intact after heating in air at 350 °C and 1 atm for 475 hours and in vacuo at 350 °C for 350 hours. Zeolite type A, however, recrystallizes at 800 °C in air in less than 2 hours to a β-cristobalite-like structure. As for the adsorption properties, the critical dimension is defined as the diameter of the circumscribed circle of the cross section of minimum area. Increasing the degree of dehydration can increase the adsorptive capacity of the type A zeolite and increasing the temperature of dehydration up to 350 °C produces maximum adsorptive capacity (6). An adsorption volume for water of 833 Å^3 per unit cell is
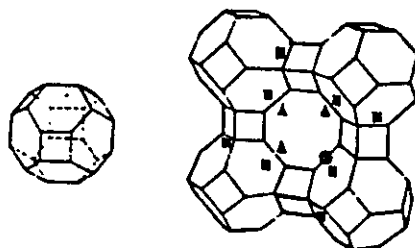
where   ▪   =   site I

          ▲   =   site II

          ●   =   site III

Figure 1b: The Archimedean Truncated Octahedron (left) and the Simple Cubic Array of Truncated Octahedra in the Zeolite Type A (right).

β-cage

α-cage

ZÉOLÍTHE A

(Structure SBU: D4R)
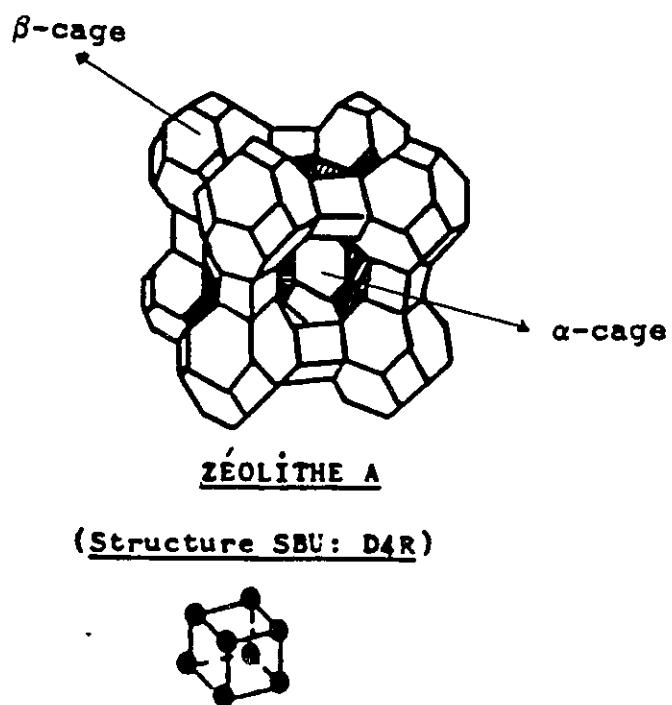
Figure 1c: A D-4-R Secondary Binding Unit of the Zeolite
Type A (7).

calculated, consisting of a 775 Å^3 cavity adsorbed by 8-membered oxygen rings and a 157 Å^3 cavity adsorbed by 6-membered oxygen rings. Finally, from the Langmuir plots, the type A zeolite surface area appears to be 750 - 800 m^2/g.

The first observed ion exchange reaction of zeolite type A was the apparent exchange reaction of Na$^+$ for H$^+$. These zeolites are unstable in acid solution but hydrogen exchange was achieved by first replacing the sodium by ammonium and subsequently heating the ammonium-exchange type A zeolite at 350 - 400 °C to liberate free ammonia. After ammonium exchange to the extent of 35 % or more of the original sodium containing material, decomposition of the ammonium zeolite destroyed the crystal structure. The selectivity of type A zeolite for Ca^{++} in 0.2N solution at 25 °C is found to be 72% (6).

2)   Ca-A

The calcium zeolite A possesses the same structure as of sodium zeolite A. Its formula is written as Ca$_6$[(AlO$_2$)$_{12}$(SiO$_2$)$_{12}$].30 H$_2$O. After exchanging Na$^+$ with Ca^{++} ions, there are 4 Ca^{++} and 4 Na$^+$ in each unit. Therefore, there is still about 33.3 % of Na$^+$, even in the parent Ca-A zeolite bought from Linde company. Hence, the eight site I positions are occupied while sites II and III are vacant, leaving the apertures completely open with a free diameter of about 5.0 - 5.6 Å. This zeolite is thermally stable at 700 °C but at 800 °C, it converts to a material amorphous to X-rays.

B)   Zeolite Modification

Instead of creating new larger and larger pore sized materials, such as the unidimensional channel system aluminophosphates [e.g. $AlPO_4$-8 with a 14-ring channel system of pore dimensions 7.9 × 8.7 Å (3), VPI-5 with 18-ring channels with free diameters of 12 - 13 Å (1)], or the three-dimensional channel system gallophosphates [e.g. cloverite with a pore opening comprising 20 T-atoms in the shape of a four-leafed clover having a body diagonal of 29 - 30 Å (8)], there are three methods of dealumination to prepare alumina-deficient, thus high-silica zeolite, and therefore to enlarge the pore size of the already existing zeolites: hydrothermal, chemical or a combination of these two treatments.

The thermal dealumination method involves calcination of the ammonium, or hydrogen, form of the zeolite at relatively high temperatures (usually over

500 °C) in the presence of steam. It consists essentially in a high-temperature hydrolysis of Si-O-Al bonds and hence, leads to the formation of neutral and cationic aluminum species. This treatment, not only causes framework dealumination, but also results in a structural rearrangement in the zeolite framework. Thus, the sites left vacant by dealumination are occupied to a large extent by silica, which leads to a very stable and highly silicious framework (USY zeolites (9a)) while the remaining, non-occupied, defect sites are occupied by hydroxyl molecules.

When chemical treatments are used, dealumination can be achieved in two ways:

1)   By reacting the zeolite with a suitable reagent in solution, aqueous or non-aqueous, such as acids [clinoptilolite, erionite, mordenite and USY

zeolites with HCl (9b)], salts [X, Y and erionite zeolites with chromium chloride solutions under reflux, leading to the formation of Si-O-Cr bonds in the framework (9c); or with solutions of ammonium fluorosilicate (9d)], or chelating agents [Y zeolites with EDTA which involves the hydrolysis of Si-O-Al bonds followed by formation of a soluble chelate between cationic, non-framework aluminum and EDTA (9e); acetylacetone (9f)].

2)   By high-temperature reactions with volatile compounds like silicon tetrachloride vapors for mordenite zeolites (9g), Y zeolites (9h). Finally, a combination of thermal and chemical dealumination has been performed for mordenite (9i) and Y zeolites (9j). High temperatures and steam will enhance the expulsion of aluminum from the framework while chemical treatment solubilizes primarily the non-framework aluminum generated during the thermal treatment, although some framework aluminum can also be removed.

According to this previous review, the Ca-A type zeolite has rarely been used for fear of getting structural collapse. However, if we treat this zeolite-type under mild conditions, very interesting products can be obtained, as we can see later on throughout this thesis.

CHAPTER III: EXPERIMENTAL

A.   Source of materials

<u>Chemicals</u>	<u>Supplier</u>
Ca-A Zeolite	Linde-Union Carbide
Na-A Zeolite	Linde-Union Carbide
Na-X Zeolite	Linde-Union Carbide
HCl [37 %]	Aldrich Chemical Company
$(NH_4)_2SiF_6$ [99.999 %]	Aldrich Chemical Company
$CaCl_2.2H_2O$	Fisher Scientific
CH_3COONH_4	Fisher Scientific
H_2SO_4	J.T. Baker Inc.
Lithium Tetraborate [99.9+ %]	Aldrich Chemical Company
Potassium Carbonate Sesquihydrate [99 %]	Aldrich Chemical Company
Bentonite	Fisher Company
n-Hexane [99+ %]	Aldrich Chemical Company
CCl_4	J.T. Baker Inc.
Hydrogen Peroxide [30 %]	A.C.P. Company

B.   Treatments

In this project, room temperature (RT) was assigned for a temperature of (24.0 ± 0.5) °C.

1)   Hydrothermal treatments

Procedure

Four boats filled with commercial Ca-A powder (Linde 5A) were centered in the computer-controlled reactor tube (Thermolyne / Omega). The samples were kept at 200 °C for one hour, under a flow of nitrogen atmosphere (10 cm / 30 sec) in order to remove all the adsorbed species from the powder. The temperature was then lowered to 120 °C in order to saturate the zeolite with H_2O for two hours at a given rate of water injection. Then, by heating very rapidly (30 °C / min) to 750 °C, the water molecules were forced to go leaving behind them the treated zeolite with a structure more or less damaged, depending on the rate of water saturation. This treatment results in the following equations quoted as eq. 1 and eq. 2.
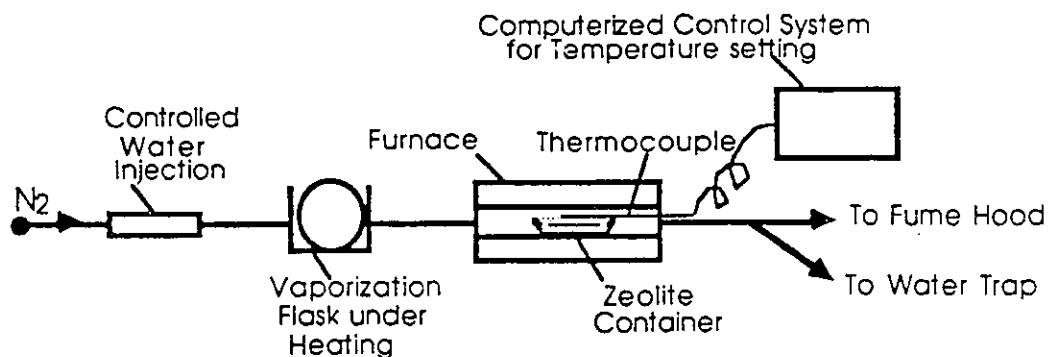
Figure 2: Hydrothermal Treatment Apparatus.

Framework Dealumination (10)

$$(1)$$

② $Al(OH)_3 + H^+(Z) \longrightarrow Al(OH)_2^+(Z) + H_2O$
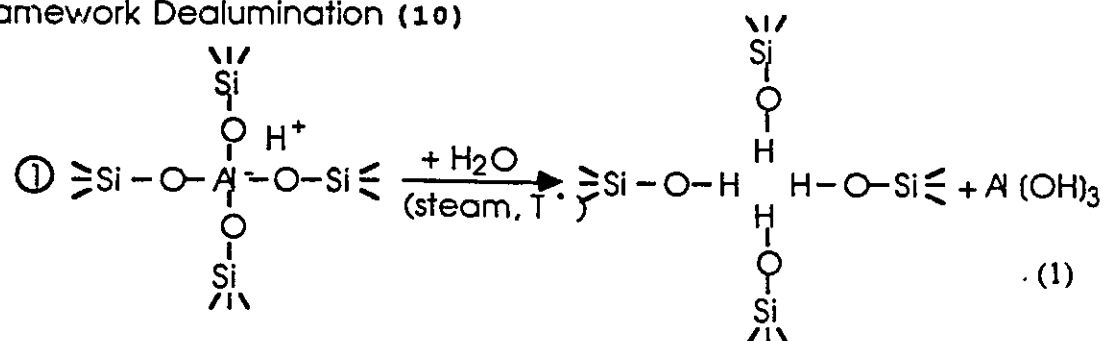
Framework Stabilization (10)

$$(2)$$
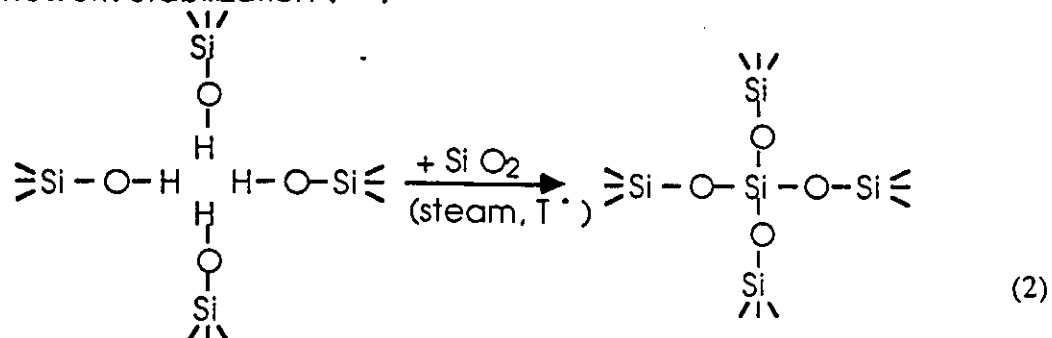
2) Chemical treatments

a) HCl treatments

Procedure

The acid solution of 0.2N HCl was heated to 80 °C first and next, the sample of 1 : 10 weight per volume ratio of Ca-A zeolite was added into it and stirred for the required time, at the same temperature. At the end, the solution was filtered on a Buchner funnel, washed with a large amount (three times with a volume of about the same volume as the reaction mixture volume) of water and then allowed to dry at 120 °C overnight. For treatments longer than three hours, the acid solution was changed to a fresh one every three hours; this included filtering, washing and drying. The reaction of this treatment is given in eq. 3 below.

$$\equiv Si-O-\underset{\underset{Si}{\overset{|}{O}}}{\overset{\overset{Si}{\overset{|}{O}}}{Al}}-O-Si\lesssim \ + \ 4\,H^{+} \longrightarrow \ \equiv Si-O-H \quad H-O-Si\lesssim \ + \ Al^{3+}_{soln.} \tag{3}$$
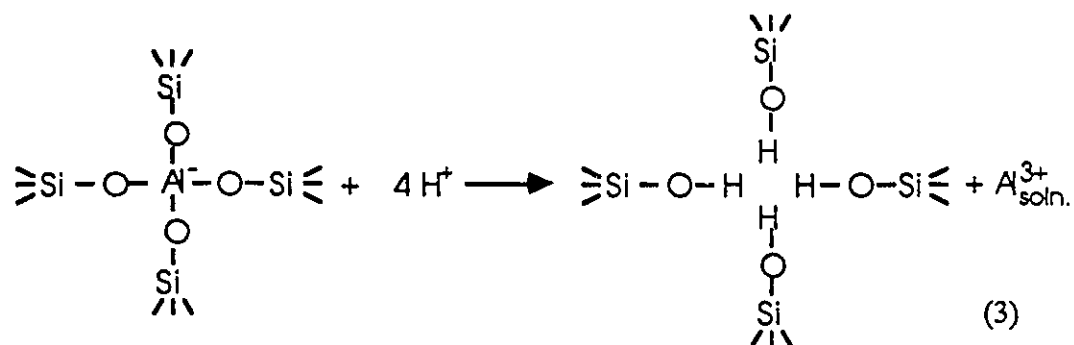
b)   (NH$_4$)$_2$SiF$_6$ treatments

Procedure

According to reference 11, a 0.5 M solution of ammonium hexafluorosilicate was added at a rate of ca. 0.30 ml / min. (or else as mentioned in detailed studies) under stirring, into a teflon beaker containing 3 g of the sample and a 225 ml solution of 0.8 M ammonium acetate at pH 7.18. Then the mixture was stirred for three hours at room temperature. After reaction, the zeolite was filtered on a Buchner funnel and washed a minimum of five times with a volume of warm (50 °C) distilled water of about the same volume as the reaction mixture each. Then the zeolite was dried in an oven at 120 °C overnight.

Controlled AFS - Pumping System

Flask containing
Zeolite to be treated

Stirring Hot Plate
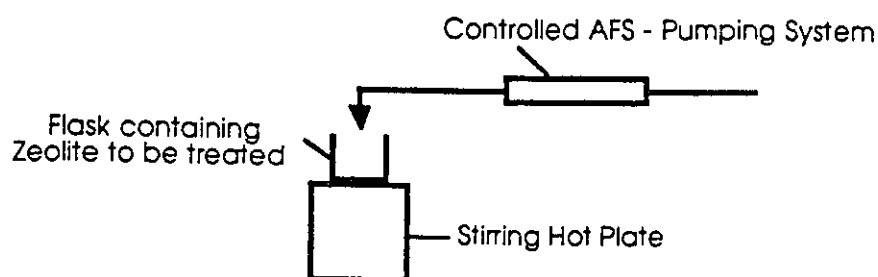
Figure 3: AFS Treatment Apparatus.

Theory

Modifying the Si / Al ratio of the framework is a good way to control the acidity of zeolite catalysts and therefore, their activity, stability and selectivity. Thus, the higher the Si / Al ratio of the zeolite framework, the lower the acid site density and the lower the coking rate will be and, consequently, the lower the catalyst deactivation. Two types of methods are used for dealuminating zeolites: 1) In the first methods, the dealuminating agent (e.g. H_2O, acids) contains no silicon, and 2) those where silicon from the dealuminating agent [e.g. $SiCl_4$, $(NH_4)_2SiF_6$] substitutes for aluminum in the framework. Since the physicochemical and catalytic properties of the resulting material depend on the method used, the first type can lead to the formation of mesopores that can cause an increase in the rate of diffusion of reactant molecules, and also the formation of aluminum deposits able to reduce diffusion and to increase the strength of the zeolite protonic sites (superacid sites). On the other hand, the second type of methods does not, and by using the method developped by Breck et al., depends greatly on the reaction time, temperature, $(NH_4)_2SiF_6$ / zeolite ratio, and washing procedure (11).

The effect of $(NH_4)_2SiF_6$ is due to the production of hydrofluoric acid (HF) by hydrolysis of Si - F bonds upon treatment at high temperature in presence of water.

$$(NH_4)_2SiF_6 \quad \rightarrow \quad 2NH_4F + SiF_4$$

$$SiF_4 + 2H_2O \rightarrow \quad SiO_2 + 4HF \tag{4}$$
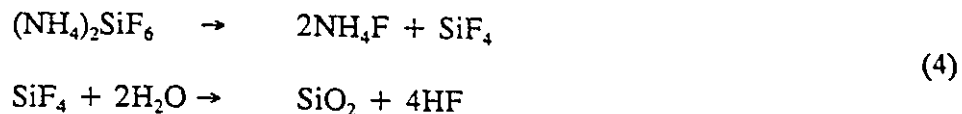
A generalized reaction scheme can be written for the reaction of zeolites with fluorosilicates (12), where M stands for cation

$$\tag{5}$$
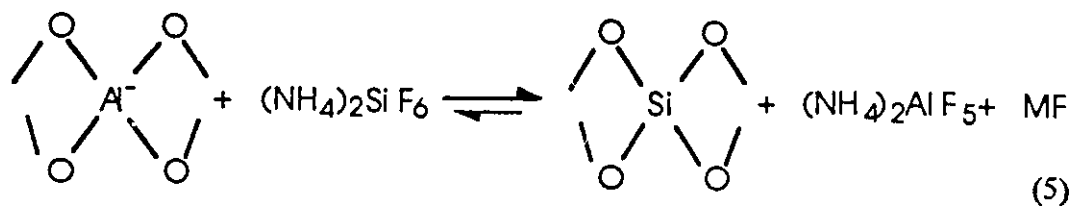
In the case of H_3O^+-mordenite (12), more aluminum was removed from the zeolite than could be accounted for by Equation 5 alone. Removal of additional aluminum from the framework may be explained in part by Equation 6. Since MF in Equation 5 is essentially HF, then

$$\tag{6}$$
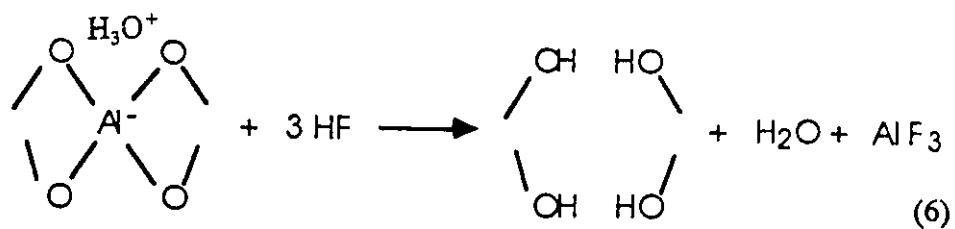
3)   "Two - step procedure" treatments

a)   Hydrothermal treatment followed by HCl treatment

The Ca-A zeolite was hydrothermally treated in order to form a range of intermediate products from 0 to 100% degree of crystallinity, such as 0, 25, 50, 75 and 100 % D.C.. These intermediate products were next treated with 0.2N HCl acid solution at 80 °C for different times of exposure. The final products were then submitted to varying characterization tests.

b)   Hydrothermal treatment followed by $(NH_4)_2SiF_6$ treatment

The Ca-A zeolite was hydrothermally treated in order to get a range of intermediate products from 0 to 100% degree of crystallinity. These intermediate products were next treated with 0.5M $(NH_4)_2SiF_6$ salt solution at room temperature for three hours. The final products were then submitted to varying characterization tests.

c)   HCl followed by $(NH_4)_2SiF_6$ treatment

The Ca-A zeolite was treated with 0.2N HCl acid solution at 80 °C for varying times of exposure. The intermediate products were next treated with 0.5M $(NH_4)_2SiF_6$ salt solution at room temperature for three hours. The final products were then submitted to different characterization tests.

4)   Cation-exchange capacity (C.E.C.)

Procedure

According to the procedure described in reference 13, the samples of AT(6), AFS(0.32) and pure Ca-A zeolite were ion-exchanged with 5% NaCl solution at room temperature for two hours in order to check if "retro-exchange" property does exist in these cases. Then the final mixture was filtered, washed with a large amount (three times with a volume of about the same volume as the reaction mixture) of H_2O and finally dried at 120 °C overnight.

C.   Physico-chemical characterization techniques

The main techniques used in the present work to characterize the samples include BET measurements (specific surface area, pore size distribution), atomic absorption spectrophotometry for elemental analysis, relative affinity index (RAI), X-ray powder diffraction, bulk density, and MAS-Solid State NMR (chemical environment of the ^{29}Si and ^{27}Al components).

1)   BET

1.1)   BET Specific surface area

The most useful method to determine the total surface area of a solid material which requires non-specific physical adsorption, is called BET method (Brunauer, Emmett and Teller). The surface area, which is a very important textural parameter of a solid, can be used to define the morphology and surface characteristics. The specific surface area (A) is the measure of the accessible surface area per unit mass of solid, where this surface is the sum of the internal surface area associated with pores and of the external surface area developed by the outer boundary of the particles (14).

The determination of A includes the following steps:

i)   Setting up the adsorption isotherm by measuring the volume of nitrogen adsorbed versus the relative pressure of the adsorbate,

ii)   Evaluating the monolayer capacity (V_m) from the isotherm, and

iii)   Converting V_m into A by means of the molecular area (a_m).

The theory of BET is based on a kinetic model of the adsorption process of Langmuir, in which the surface of the solid was regarded as an array of

adsorption sites. The BET theory is based on the following three assumptions:

(a)   There is no interaction between molecules adsorbed in the first layer of a homogeneous surface with equivalent sites for localized adsorption.

(b)   Each molecule in the first layer is a possible site for adsorption of a molecule in the second layer, and so on in order to get a multilayer adsorption.

(c)   With the exception of the first layer, the heat of adsorption is equal to the molar heat of condensation and the evaporation - condensation conditions are identical in all others.

The physical and mathematical treatment of these hypotheses leads to the following BET equation:

$$\frac{P}{V(P_o-P)} = \frac{(C-1)P}{V_m C P_o} + \frac{1}{V_m C} \qquad (7)$$

where P: equilibrium pressure of the adsorbate

P_o: saturated vapour pressure of the adsorbate in the condensed state

V: volume of gas adsorbed at STP

V_m: volume of gas at STP corresponding to the formation of a monolayer coverage

C: a constant varying with the adsorbent - adsorbate interactions which is related to the differential heat of

adsorption E_A and to the heat of liquefaction E_L by the following relation:

$$C = \exp\frac{(E_A - E_L)}{RT} \tag{8}$$

where R: ideal gas constant

T: absolute temperature

The graph of $P/V(P_o - P)$ versus P/P_o at low pressure $(0.05 < P/P_o < 0.35)$ should give a straight line and hence, one should be able to derive C & V_m. As mentioned previously, the BET method for calculation of specific surface area (A) involves two additional steps:

a)   evaluation of the monolayer capacity (V_m) from the isotherm. To obtain a reliable value of V_m from the isotherm, it is necessary that the monolayer be virtually complete before the build-up of high layers starts; which is met if the BET parameter C is neither too low nor too high $(50 < C < 150)$.

b)   conversion of V_m into A by means of the molecular area (a_m). Since nitrogen comes the closest to meeting these conditions when adsorbed on an extensive range of solids, it has become the most generally used

adsorbate for surface area determination. The specific surface area of the adsorbent is then given by

$$A = a_m \frac{(V_m N)}{V} \qquad (9)$$

where N: Avogadro constant

a_m: area occupied by one molecule of adsorbate. $a_m(N_2)$ of 16.2 $\mathring{A}^2$ is the widely accepted value.

1.2)   Pore size distribution measurement

The pore size distribution is defined as the distribution of the specific area versus the pore size.   It is an important textural parameter for the determination of morphology and pore structure of a porous solid.   Depending on the pore size range of a solid, the appropriate technique is applied:

Mercury porosimetry has been widely used to measure macropores (75 $\mathring{A}$ < pore radius < 75,000 $\mathring{A}$).   It is a technique based on the determination of mercury volume which penetrates into the solid as a function of an externally applied pressure.   Unfortunately, since our samples contained macropores, mesopores and micropores, it was not possible to apply this technique (15).

Techniques based on nitrogen adsorption / desorption isotherms make use of the desorption loop of an adsorption isotherm to relate the amount of adsorbate lost in a theoretical desorption step to the average size of pore emptied in the step.

A pore loses its condensed liquid adsorbate at a pressure related to the pore radius by the Kelvin equation (on the assumption of cylindrical pores where the adsorbate surface tension, contact angle and molar volume being known for the adsorption temperature. However, even when a pore has been emptied of condensed liquid, multi-layers of adsorbed molecules remain on the inner surface of the pores and these muti-layers continue to thin down as desorption proceeds. Therefore, the measured desorption is made up of removal of condensed liquid from some pores, plus the adsorbate lost from the surfaces exposed in earlier steps.

These techniques consist of:

(a)   The t-plot analysis method which was recently developed by Lippens and de Boer (16): in addition to measuring macropores and mesopores, it gives a detailed analysis of the micropores. This method consists of plotting the adsorption isotherm (Langmuir type) in terms of the volume of gas adsorbed versus t (the statistical film thickness of the adsorbed gas on the walls of the pores) and by extrapolating to the intercept (t = 0), the micropore volume can be obtained (Fig. 4a). However, the adsorption has to be performed at very low surface coverage using special microvolumetric apparatus to deliver microquantities of gas to be adsorbed on the surface.

(b)   The classical method consists of adsorption of N_2 at saturation under liquid nitrogen and then by applying vacuum, the adsorbed adsorbate is gradually removed. At $P/P_o \rightarrow 1$ where P_o is the saturation
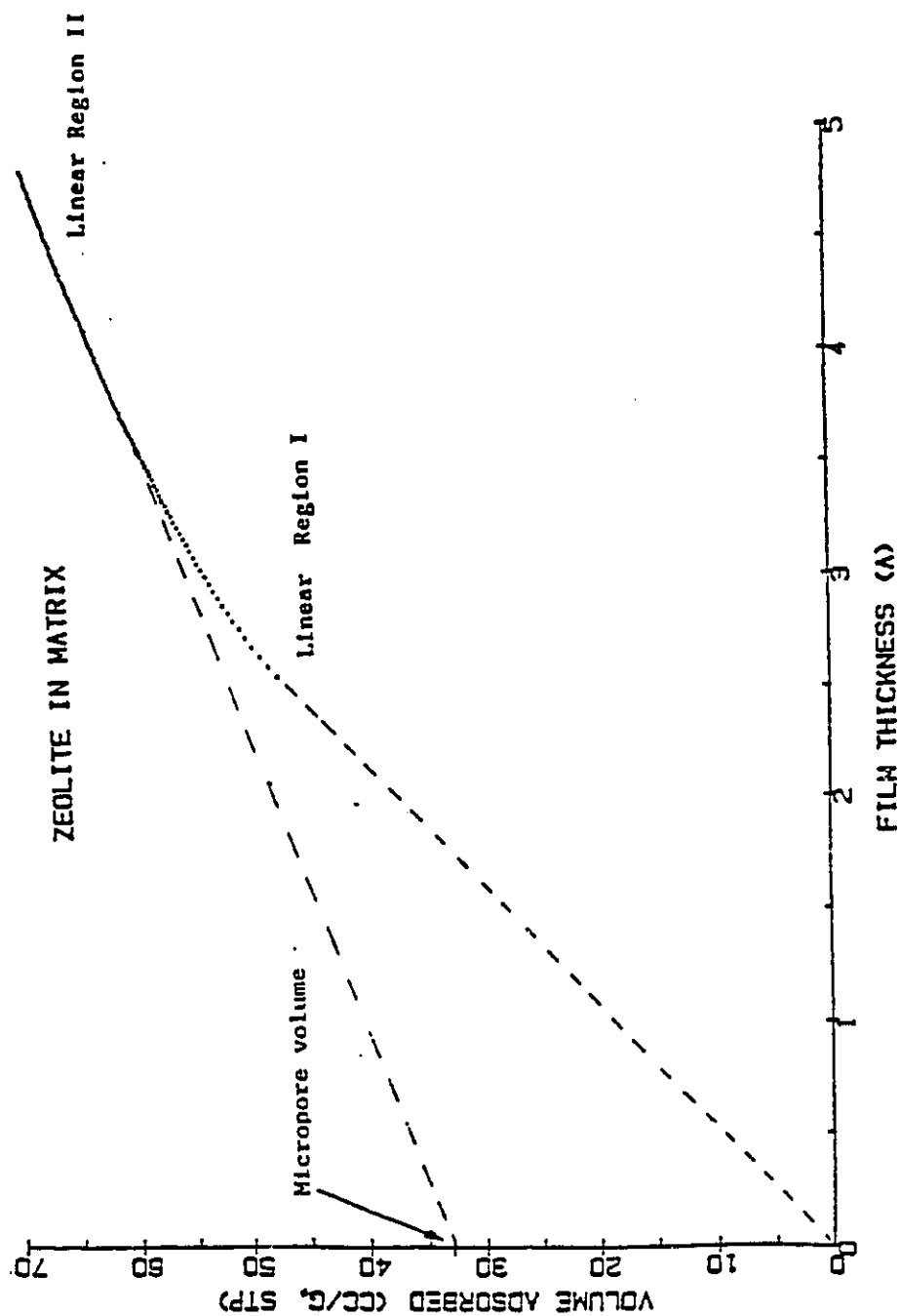
Figure 4a: A t Plot of Volume Adsorbed Versus Film Thickness.

pressure, all the pores are completely filled with adsorbed and condensed nitrogen. When the pressure is lowered by small increments, a small amount of nitrogen will first evaporate from the meniscus formed at the ends of the larger pores. Hence, a desorption isotherm of volume desorbed versus pore radius is established. The pore size distribution of a mesoporous solid may be calculated from the desorption isotherm of a vapor with the aid of the Kelvin equation:

$$\ln \frac{P}{P_o} = -\frac{2 \eta V}{RT} \cdot \frac{1}{r_K} \cos \Theta \qquad (10)$$

where P/P_o: relative pressure of vapor in equilibrium with a meniscus having a radius of curvature r_K

η: surface tension of liquid adsorbate

V: molar volume of liquid adsorbate

R: ideal gas constant

T: absolute temperature

θ: contact angle between the capillary condensate and the adsorbed film on the walls

The concept of capillary condensation and its quantitative expression in the Kelvin equation is, indeed, the basis of virtually all the various procedures for the calculation of pore size distribution (17). When capillary condensation occurs

during the course of isotherm determination, the pore walls are already covered with an adsorbed film, having a thickness t determined by the value of the relative pressure. Capillary condensation therefore, does not occur directly in the pore itself but rather in the inner core (Fig. 4b).
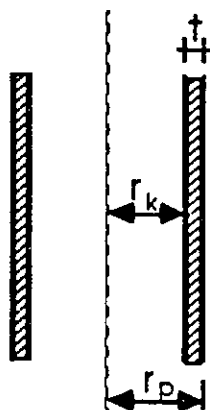
Figure 4b: Cross-section along pore axis.

The conversion of an r_K value to a pore size requires recourse to a model of pore shape and a knowledge of the angle of contact θ (it is assumed that $\theta = 0$ hence $\cos \theta = 1$). Several methods which make use of Kelvin's equation and attempt to correct the Kelvin radius have been proposed. However, all these computation methods can give an accurate assessment and measurement of the macro- and mesopores but not the micropores.

Pore size distributions can be computed using a simplified model proposed by Pierce (18), based on the application of Kelvin's equation to nitrogen desorption isotherms, from which the following is proposed:

(i)   all pores have cylindrical geometry.

(ii)   the Kelvin equation is applicable for computing the pore radii from the relative pressures at which desorption occurs.

(iii)   the film thickness remaining on pore walls after the inner capillary volume is desorbed is the same as on a non-porous surface at the same relative pressure (area of the core walls is identical to area of the pore walls, as desorption progresses). By summing the values of pore area, δA_p, for each successive group of pores over the whole pore system, a value of cumulative surface area $S_{cum} = \Sigma \ \delta A_p$ is obtained (18). And this cumulative surface area represents the total pore area of macro- and mesopores and excludes the pore area of micropores since the validity of Pierce's method only extends down to a pore radius of 15 Å.

c)   Since the method of Pierce is very approximate, Barrett, Joyner and Halenda (BJH) introduced another which seems to give better results (18a).

During the multi-layers desorption calculations, the surface area was assumed to be planar whereas it is actually curved because of the curvature of the pore walls. A correction factor is then required to counterbalance this overestimation.

Barrett et al. used a factor C, and assigned a choice of constant values to it such as 0.9, 0.85, or 0.8, etc. (according to the approximate

range of sizes of pores expected). This procedure gives reasonably accurate results for pores down to radii of 35 Å, with the lower limit for pores of 7 Å. The final equation becomes

$$\Delta V_p = R_n (\Delta V - C \Delta t \Sigma S_p) \tag{11}$$

where ΔV_p: actual volume of pore

R_n: factor $= [r_p/(r_K + \Delta t)]^2$

ΔV: amount of adsorbed material lost in a desorption step

C: factor $= (r_p\text{-}t)/r_p$

Δt: multi-layer thinning for the same step

ΣS_p: sum of pore areas for the preceding step

d)   Cranston & Inkley overcame the error of multi-layers desorption overestimation by multiplying S_p for each pore size range by its individual value of C instead of summing S_p (18b). This method is much too laborious as calculation proceeds down to small pore sizes.

e)   Dollimore & Heal proposed a method which does not require any approximation for multi-layer desorption as used in the method of Barrett et al., nor does it involve the tedious calculations of that of Cranston & Inkley (18c).

As for the most generally used adsorbate, nitrogen, adsorption at −195.8 °C, the Halsey equation is used to obtain values of t

$$t = 4.3 \left(\frac{5}{\ln \frac{P}{P_o}} \right)^{\frac{1}{3}} \tag{12}$$

By processing through several arithmetic calculations, the following is obtained:

$$\Delta V_p = R_n (\Delta V - \Delta t \Sigma S_p + 2\pi t \Delta t \Sigma L_p) \tag{13}$$

where ΣL_p: sum of the lengths of pores

The adsorption values are read off from the isotherm giving V_{ads}. Since the intervals of r are not constant, the quantity $\Delta V_p / \Delta r$ has to be found, where Δr is the pore range over the step. These quantities are plotted against r_p, permitting us to follow well the pore volume distribution.

1.3) Adsorption - Desorption Isotherms

A sorption isotherm is a plot of sorbed volume versus equilibrium pressure, the temperature being kept constant.

As we know, Brunauer et al. (15) proposed the classification which relates the shape of the isotherms to both the mean pore size of the adsorbent and the intensity of adsorbate - adsorbent interactions. Figure 5a represents
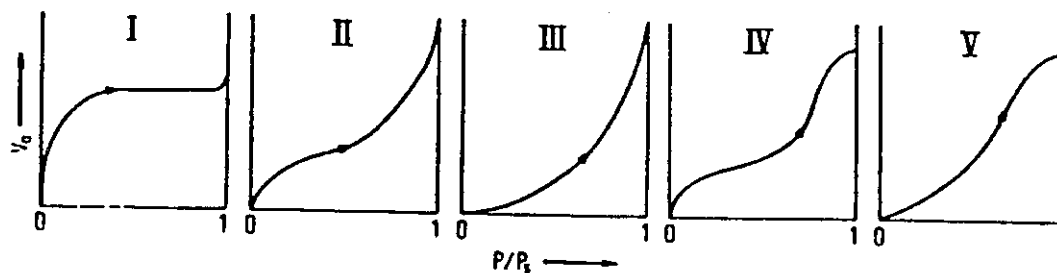
Figure 5a: The Five Types of Adsorption Isotherms according to Brunauer et al (15).
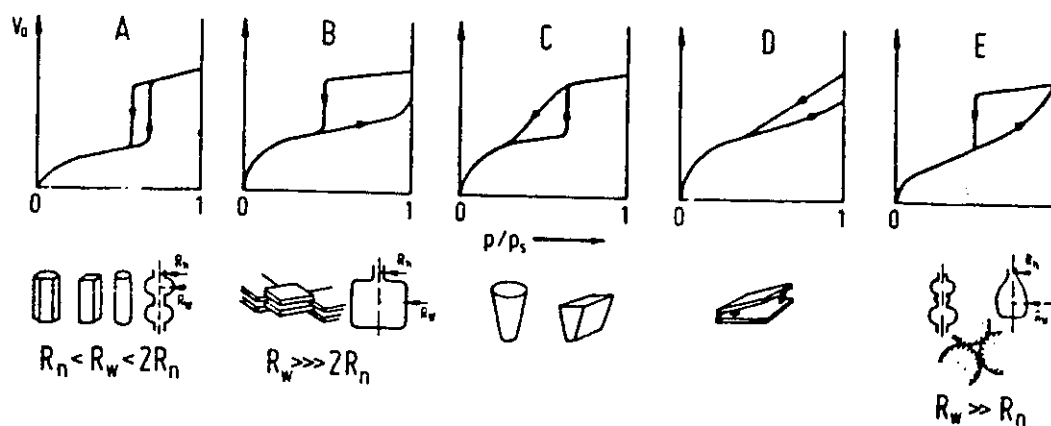
Figure 5b: The Five Types of Hysteresis Loops and the Associated Pore Shapes, as proposed by de Boer (15).

five types of adsorption isotherms: type I is characteristic of microporous adsorbents, types II and III are observed for macroporous adsorbents and types IV and V for mesoporous adsorbents. Contrary to types II and IV, type III and V isotherms are rather unusual and correspond to very weak adsorbate - adsorbent interactions.

Even though the shape of the isotherm usually gives a rather good idea of the mean size of the pores present in the solid, when a mixture of different types of pores are present in the adsorbent, it can be difficult to relate the shape of the isotherm to one definite group. As a result, an easier method was introduced (15): based on the shape of the hysteresis loop which is always observed with isotherms of types IV and V and sometimes with types II and III. De Boer (15) proposed the classification of the hysteresis loops into five main groups, each of which relates to the general shape of the pores present in the solid (Fig. 5b). Type A is associated with cylinder-shaped pores of rather constant cross section. Type B points to the presence of slit-shaped pores. Types C and D which are rather unusual, derive from types A and B respectively and indicate the presence of cone-shaped pores (type C) and pores formed by non-parallel plates (type D). Finally, type E which occurs very frequently, corresponds to "ink-bottle" pores, spheridal cavities or voids between close-packed spherical-like particles.

Another terminology was defined by the Commission on Colloid and Surface Chemistry including Catalysis (4). Figure 5c shows four main types of hysteresis loops. Type H1, formely type A, is often associated with porous material known to consist of agglomerates or compacts of approximately uniform
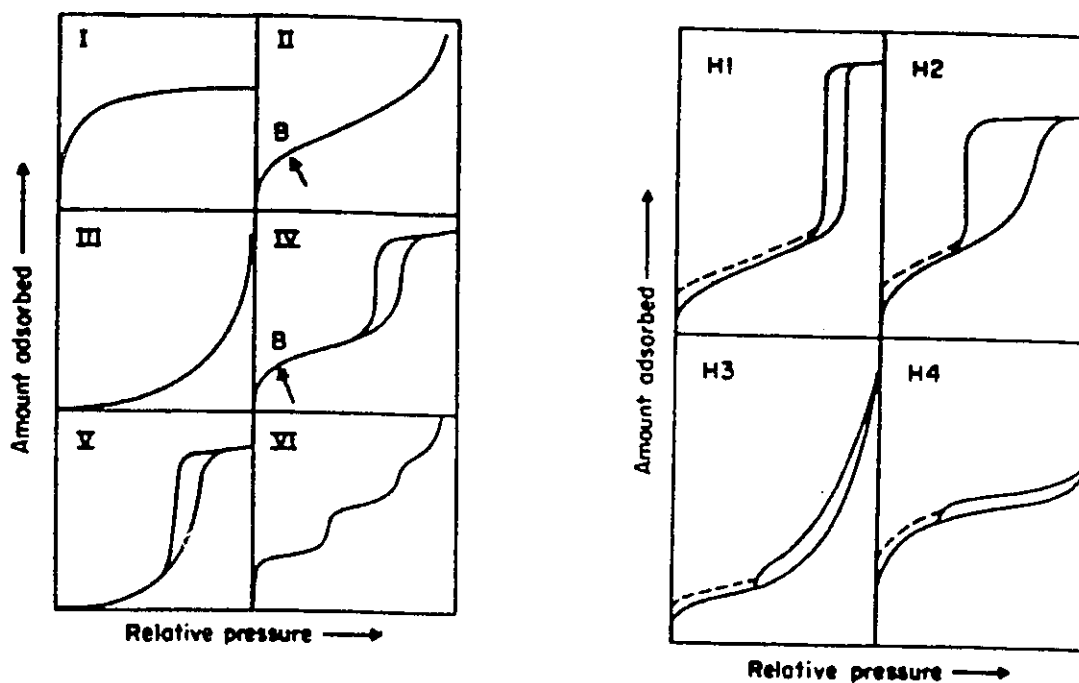
Figure 5c: Types of Physisorption Isotherms (left) and Hysteresis Loops (right), defined by the Commission on Colloid and Surface Chemistry, including Catalysis.

spheres in fairly regular array, and hence to have narrow distributions of pore size. Many porous adsorbents such as inorganic oxide gels and porous glasses tend to give type H2, formely type E, loops. The type H3 - formely type B - loop, which does not exhibit any limiting adsorption at high P/P_o, is observed with aggregates of plate-like particles giving rise to slit-shaped pores. At last, the type H4 loop is often associated with narrow slit-like pores.

1.4)   Instrument used

The ASAP 2000 system, as shown in Figures 6a and 6b, consists of either one or two analyzers and a multi-function control module. The separate internal vacuum systems are included in the analyzer: one one - port for sample analysis and one two - ports for sample preparation. Between the vacuum pump and the manifold in both the degassing and the analysis system, are located the in - line cold traps. The sample saturation pressure (P_o) tube is located next to the sample analysis port beneath which is conveniently located the automatically-operated elevator with liquid nitrogen (LN_2) Dewar mount. Connectors are put near each sample preparation port for mounting of heating mantles and thermocouples. Controls and indicators on a swing - open control panel can provide operation of the vacuum systems, degas valves and heating mantles for sample preparation. Finally, the control module consists of a computer equipped with an ASAP 2000 software (19).

The software follows the principles of the BET surface area, Halsey thickness and BJH pore volume distribution.
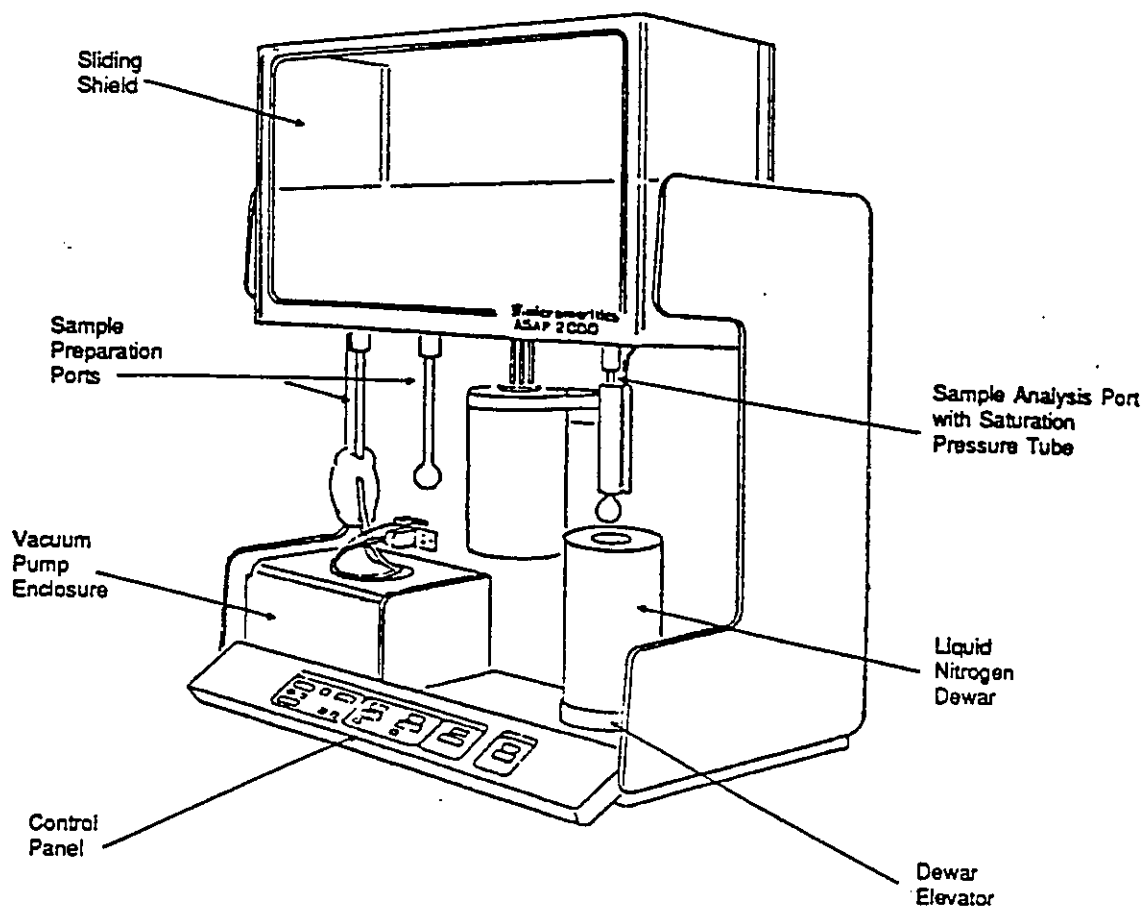
Figure 6a: ASAP 2000 System.
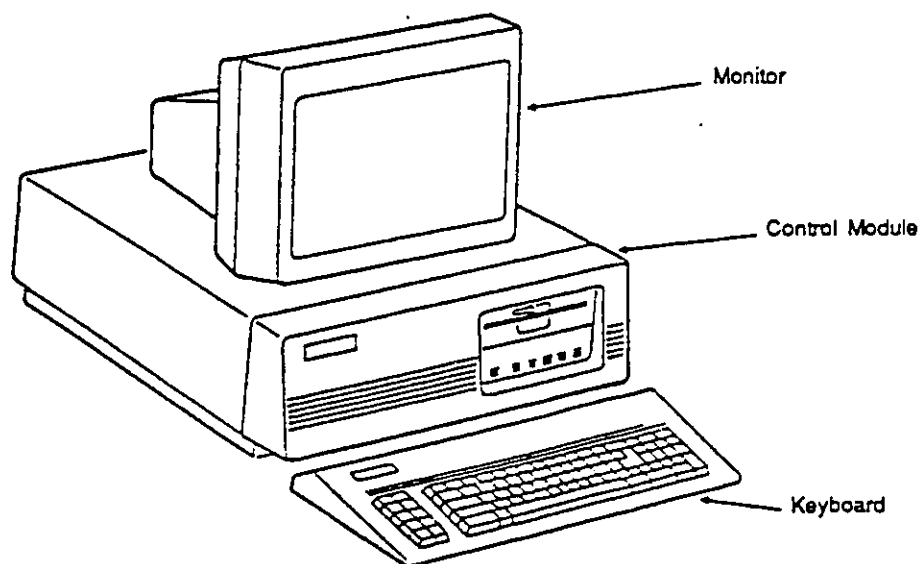
Figure 6b: The Control Module.

1.5) Procedure

Each sample was heated at 120 °C in air overnight before performing the BET analysis (especially in the case of zeolites which adsorb a lot of moisture). First, the clean and empty testing BET tube was degassed down to less than 10 μmHg pressure, and then weighed. Next about 0.5 g of sample, which was allowed to cool in the dessicator, was introduced into the empty tube. Then, the tube containing the sample was evacuated while heating with heating tape wrapped around the tube and by using a heating mantle, at 250°C for three hours, to allow pressure to decrease below 10 μmHg. Then the testing tube was once again weighed in order to obtain the weight of the degassed sample. By introducing all the required data to the ASAP 2000 program of the BET Micromeritic (TM) apparatus, the analysis was automatically performed in about six hours, with this particular Ca-A zeolite. This instrument gives the results within a range of $\pm$ 7% (19).

2) Atomic Absorption Spectroscopy

2.1) Theory

Atomic absorption spectroscopy (AAS) was used for elemental analysis of Al, Ca, Na. Si expressed as SiO_2 was obtained by substracting the sum of the oxides of Al, Ca, Na percentages from 100.

AAS is based on the principle that metal atoms absorb electromagnetic

radiations at frequencies which are characteristic of each metal, and the amount of light absorbed is a function of the metal concentration. This is one of the most used analytical tool in the modern analytical laboratory, mainly by the use of the hollow - cathode discharge lamp as a light source and the use of atomizers to provide rapid and efficient atomization of liquid samples. With current instrumentation, however, the method is not suitable for qualitative or simultaneous multi-element analysis.

Quantitative analysis by AAS is based on the measurement of the radiant energy absorbed by free atoms in their gaseous state. Because the spectra of gaseous atomic species consist of well-defined narrow lines at wavelengths characteristic of the element involved, it is a high selectivity - technique. The samples (solution or solid) are vapourized, commonly by flames, electrical heating or lasers; and on further heating the vapour dissociates into free atoms. Figure 7a shows a simple presentation of the process.

Since the element of interest does not usually exist as free atoms in any common solution but is in the ionic state or in a molecular form, it is necessary to generate a population of free neutral atoms of the element of interest in order to observe AA signals. The metal atoms are then capable of strongly absorbing radiation at discrete characteristic wavelengths, which coincide with the narrow emission lines of the particular metal generally provided by a hollow cathode lamp. Hence, the theory of AA concerns the formation of free atoms from the sample, which are in an unexcited ground - state level, and their absorption of radiation (20).
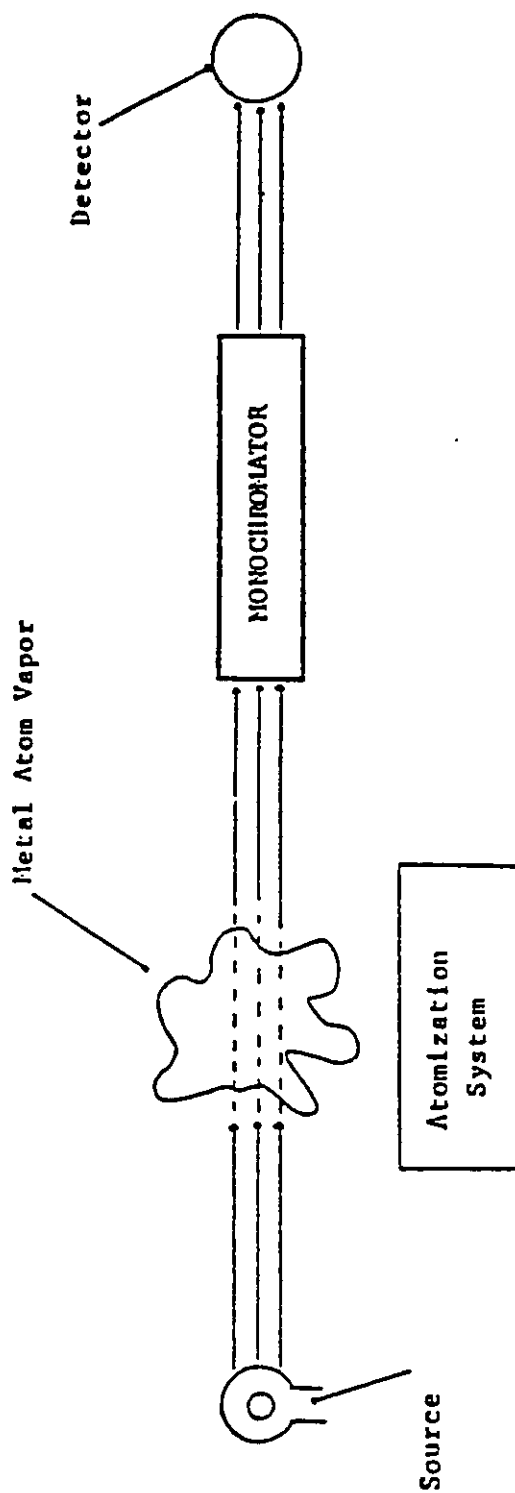
Figure 7a: A Schematic Presentation of the Concept of
Atomic Absorption Spectroscopy.

Because most of the atoms remain in the ground state, absorption is greatest for resonance lines resulting from transitions originating from the ground state and this therefore, greatly restricts the number of absorption lines that can be used in AA. The degree of absorption depends on the population of atoms in the ground state and the ability of these absorbing atoms. Such a degree of absorption is an expression of the line intensity and represents the probability that an atom will undergo a transition in unit time.

The degree of absorption is a function of the concentration of the metal in the sample while the absorption follows Beer's law - the absorbance is directly proportional to the path length in the flame. Both of these variables are difficult to determine. However, the path length can be held constant and the concentration of atomic vapour is directly proportional to the concentration of the analyte in the solution being aspirated (21). As with Lambert's law, we have

$$I = I_o \exp(-K_v B) \qquad (14)$$

where I: intensity transmitted by the sample

   I_o: incident intensity

   K_v: absorption coefficient characterizing the intensity of the absorption line

   B: horizontal path length of the flame or thermal source

Since the physical property actually measured is the absorbance A, we have then

$$A = \log(\frac{I_o}{I}) = K_\nu B \log e = 0.4343 K_\nu B \tag{15}$$

The absorbance is directly proportional to the absorption coefficient K_ν which is directly proportional to the number of absorbing atoms and therefore to the concentration of the solution. Thus, plots of absorbance at the specified wavelength against concentration should yield linear relationships.

2.2) Instrumentation

There are two parts with essentially different functions: the means whereby the population of ground state atoms is produced from the sample and the optical system. The basic components of AA spectrometers include:

(a)   A radiation source to emit the spectral line of the element of interest.

(b)   An atomization system (flame or furnace) to provide sufficient energy for analyte dissociation and vaporization as free atoms.

(c)   A monochromator for spectral dispersion and isolation of the spectral line to be measured.

(d)   A detector and data - logging device to measure, amplify and

display the results (22).

The most critical component of an AA spectrophotometer is the source. The hollow cathode lamps which have been used almost exclusively as the radiation source for most elements, emits strong sharp lines of appropriate wavelength characteristic of the desired element. This radiation then passes through a flame into which the sample solution is sprayed as a fine mist. Under the experimental conditions, the predominent ground state atoms, thermally generated by the flame, absorb the resonance radiation from the source lamp and reducing hence the intensity of the incident beam (23).

The monochromator and the slits isolate the desired resonance line from other radiations emitted by the source and allow it to fall on the photomultiplier detector which then converts the light signal into an electrical one. Since the range of wavelengths detected is determined primarily by the hollow - cathode source, the monochromator and slits serve primarily to minimize the detected background radiation from the flame and also to remove extraneous lines emitted by the hollow cathode filler gas. The emitted radiation corresponding in wavelength to the monochromator setting is inevitably present in the flame, due to excitation and emission by the analyte atoms. The thermally excited emission by the analyte atoms is therefore discriminated by modulating the source of radiation and using an A.C. amplifier: the unmodulated emission is not detected. The signals generated by the photoelectric detector are amplified by an amplifier tuned to the frequency of modulation while the radiation emitted by the flame is not modulated, and gives therefore no resulting output signal (24).

Since reducing the sample to the free atomic state is necessary to achieve absorption by atoms, the most common atomization device for atomic spectroscopy consists of a nebulizer and a burner (25). The nebulizer converts a sample solution into a fine spray or aerosol which is then fed into the flame. A diagram of a typical commercial laminar slow burner is shown in Figure 7b. The analyte solution is first aspirated from the sample container through a capillary tube by suction (venturi action) caused by rapid flow of support gas (oxidant) past the capillary tip (Fig. 7c). The resulting aerosol is next mixed with fuel and flows past a series of baffles which remove all but the finest droplets. Finally, the aerosol, oxidant and fuel are burnt in a slotted burner.

The flame evaporates the solvent, decomposes and dissociates the molecules into ground state atoms. Its use as the atom cell in analytical AA is at present, by far the most widely used method to obtain a population of free analyte atoms.

2.3) Instrument used

A Perkin - Elmer model 503 AA spectrophotometer utilizing a double - beam optical system and a Perkin - Elmer model 56 digital recorder were used. The dispersion optical system included also a high quality diffraction grating monochromator.

A laminar flow (premix) burner was used, equipped with two single - slot burner heads: a 10-cm long and a 5-cm long for air - acetylene and nitrous oxide - acetylene, respectively. The burner heads were held in place by

Figure 7b: A Schematic Diagram
              of a Perkin-Elmer
              Laminar Flow Burner.
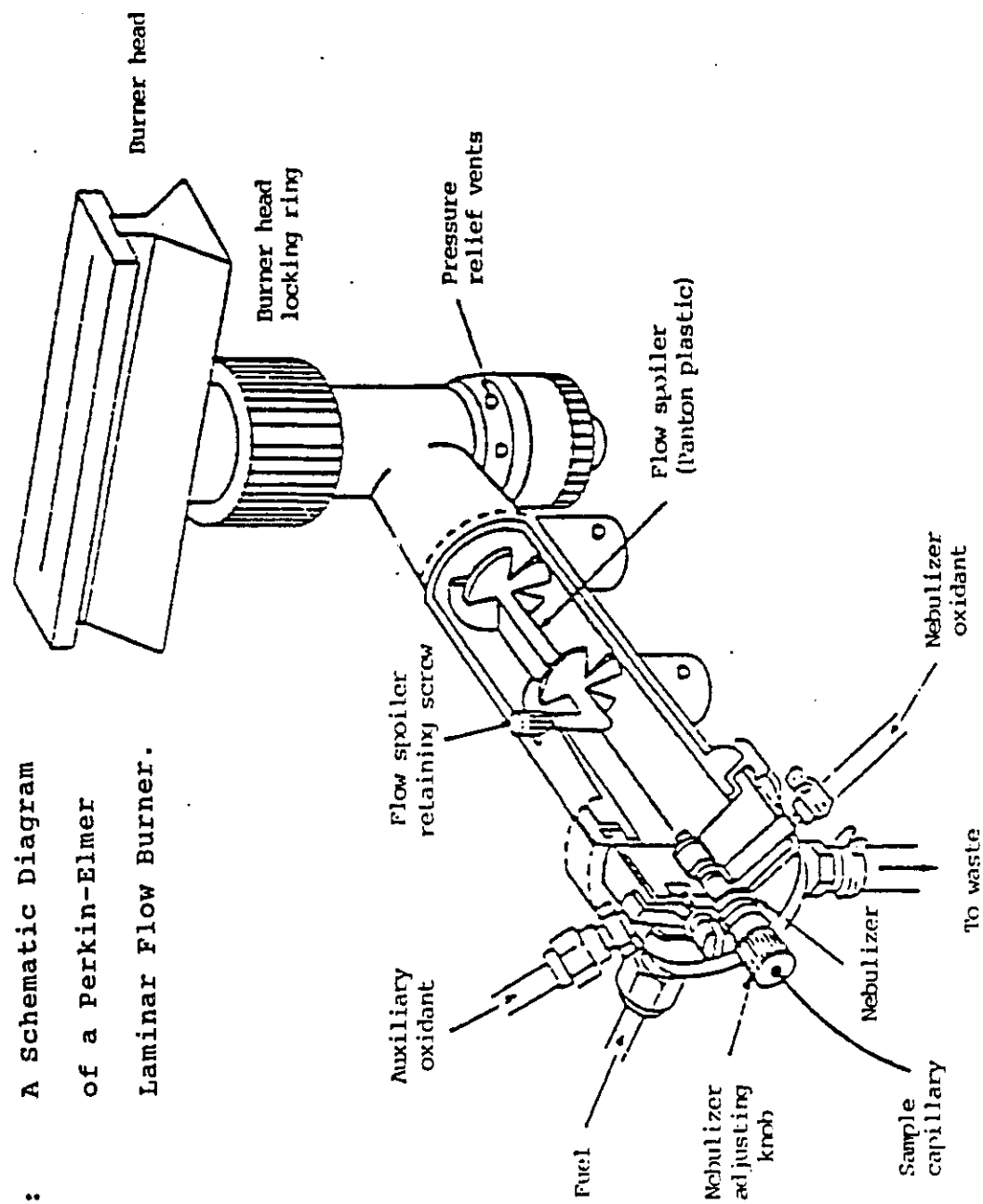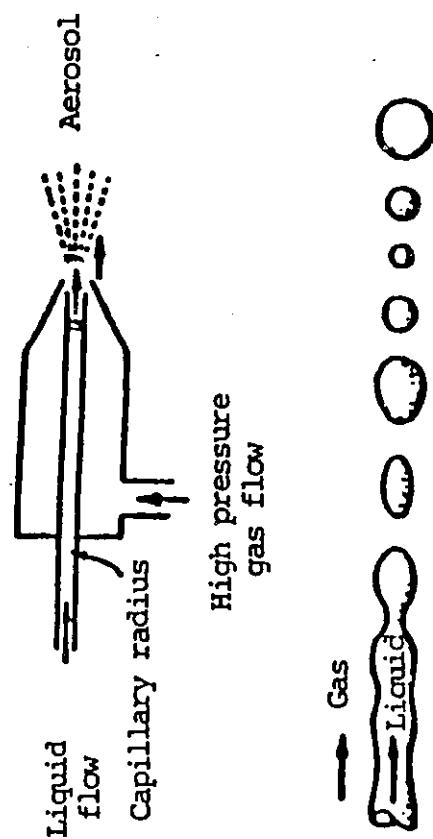
Figure 7c: Aspiration of Sample Solution into the
              Nebulizer by Venturi Action.

stainless steel cables and a safety pin interlock.

2.4) Procedure

The sample was accurately weighed (about 0.1 g) in a platinum crucible, ignited in a 750 °C - furnace for one hour, then reweighed to obtain the dry weight. A 0.9 g of fusion mixture of potassium carbonate and lithium tetraborate in ratio 2 : 1 was added to the zeolite material, mixed and ashed in the furnace for another half an hour. The resulting mixture was then transferred to a 150-ml beaker and digested with a strong mineral acid mixture of 4 mls of concentrated HCl and 10 mls of 10 % H_2SO_4 solution. The beaker was covered with a watch glass to avoid sample loss. The mixture was gently heated on a hot plate until a clear solution was obtained. Then 4 mls of 30 % hydrogen peroxide was added and the dissolution mixture was further digested for a few minutes until effervescence has stopped.

The cooled solution was then transferred to a 100-ml volumetric flask and diluted to the mark with distilled water. Appropriate dilute solutions were prepared from this stock solution. The standard solutions were prepared from 1000.0 ± 0.2 ppm metal solutions supplied by Fischer Scientific Company Limited and stored in polyethylene bottles, while the sample concentrations were determined by using the following equation:

$$\% Element = \frac{R_a}{R_{std}}(\frac{C_{std}}{W_a})(V_a)(\frac{M}{F})(100\%)(d.f.) \tag{16}$$

where % Element is in oxide form

R$_a$: reading obtained from sample solution

R$_{std}$: reading obtained from standard solution

C$_{std}$: concentration of standard solution (ppm)

W$_a$: weight of dried sample (g)

V$_a$: volume of original sample solution used (ml)

M: molecular weight of element in oxide form (g/mole)

F: formula weight of element (g/mole)

d.f.: dilution factor determined by equation

$$d.f. = \frac{V_{ds}}{V_{ad}}$$ (17)

where V$_{ds}$: volume of diluted sample solution (ml)

V$_{ad}$: volume of aliquote taken from dilution (ml)

The silicon to aluminum ratio was defined as:

$$\frac{Si}{Al} = 0.5[\frac{W(SiO_2)}{W(Al_2O_3)} \frac{MW(Al_2O_3)}{MW(SiO_2)}]$$ (18)

where W: weight percents

MW: molecular weights

Measurements on each sample were performed in duplicate, or repeated for another time (again, in duplicate) if necessary. The % error on all measured values must be within 5%.

3) Adsorption of Water and n-Hexane Vapors

3.1) Theory

Adsorption capacities of zeolites were determined by a vapor sorption apparatus (26). These measurements are important since useful information such as pore - channel dimensions, total pore volume and adsorption affinities with respect to various adsorbates may be obtained.

Traditionally, water adsorbate has been used to determine the adsorption capacity of porous solids. However, since the synthesized silica-rich ZSM zeolites show a strong hydrophobic character and a high affinity for some hydrocarbons such as n-hexane and cyclohexane (27), they thus provide water adsorption capacities substantially lower than those of classical zeolites. Therefore, water is not a good absorptive medium for these hydrophobic materials. Several people including R. Le Van Mao, have shown that the volume of n-hexane adsorbed by silica-rich zeolites is much higher than the volume of water adsorbed (26, 27). The volume ratio of adsorbed n-hexane to adsorbed water is called the relative affinity index (R.A.I.), and gives the degree of hydrophobicity of an inorganic material.

3.2) Apparatus

The vapor adsorption apparatus (Figure 8) consists mainly of two parts: a chamber for evacuation at high temperatures and a vapor adsorption system. Special tubes are also designed so that the zeolite samples can be covered by a porous disc in order to avoid sucking the zeolite in the vacuum system when evacuating. The vacuum in the Pyrex chamber is obtained with the help of a rotary pump and controlled by a Piroli vacuumstat. Finally, the adsorption system includes an adsorption chamber and a vaporization flask, which can both be maintained at the desired temperature (25, 23 or 0 °C) by a variety of thermostatic baths.

3.3) Procedure

In agreement with the procedure described in (26 and 27), the sampling tubes were evacuated ($< 4 \times 10^{-2}$ Torr), accurately weighed, and then filled with 1 g of sample specimen each. Next they were degassed down to less than 4×10^{-2} Torr at 285 °C for 4 hours. After cooling to ambient temperature, the specimen tubes were weighed again, placed rapidly into the adsorption chamber and evacuated to about 10^{-2} Torr. The same low pressure was obtained in the evaporation flask with this time, the empty adsorbate holder. Then, still isolated from each other, both the sampling tubes and adsorbate holder were placed in their respective thermostatic baths. Once the required pressure was reached, 10 mls of adsorbate was poured into the adsorbate holder. Then, the evacuated samples were brought into contact with water or n-hexane vapor

Table I: Operating Conditions for n-Hexane and Water Adsorption

Adsor-bate	Critical diameter	Vaporiza-tion tempera-ture	Vapor pressure	Adsorp-tion tempera-ture	Time required
	Å	°C	Torr	°C	hr
n-hexane	4.9	0	45	25	4
H_2O	2.8	23	22	25	overnight
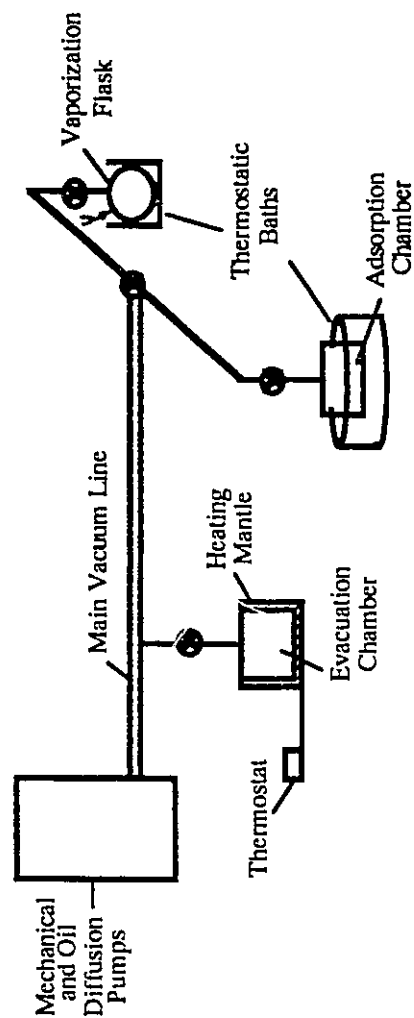
Figure 8: Vapour Adsorption - Vaporization Apparatus.

until equilibrium was established, under operating conditions mentioned in Table I. Finally, the sampling tubes were weighed and hence, the equilibrium adsorption capacity was calculated. From these sorption data, it enabled us to calculate the affinities of the zeolite toward n-hexane vapor against water vapor and also, its relative affinity index value:

$$Wt.(\%) = \frac{Wt.adsorbedvapor}{Wt.activatedzeolite}(100) \tag{19}$$

$$V(\%) = \frac{Wt.(\%)}{density} \tag{20}$$

$$R.A.I. = \frac{V(\%)ofn-hexane}{V(\%)ofwater} \tag{21}$$

Measurements on each sample were performed in duplicate, or repeated for a third time, if necessary, in order to assure that the % error on all measured values are within 5%.

4) X-Ray Powder Diffraction

4.1) Theory

X-ray diffraction (XRD) is a powerful technique for phase

identification, quantitative phase analysis, structure determination and the study of the crystallinity of solids. In this work, the XRD technique was used to investigate the effect of the hydrothermal treatment as well as the mineral acid treatments [HCl or $(NH_4)_2SiF_6$] on the crystallinity of the zeolites.

X-ray diffraction can be applied to any solid crystalline materials such as mineral, inorganic or organic compounds because all crystalline materials are made of atoms, ions or molecules arranged in a regular repetitive three-dimensional array.

A crystal type can be defined in terms of the lengths of the sides of its smallest repeating structure which is called a "unit cell". The regular repetition of the unit cell gives rise to planes throughout the crystal, and therefore, each crystal structure is characterized by a unique set of families of parallel planes at different orientations. The distance between two adjacent planes of a given family is called d-spacings (Fig. 9a). It results that each crystalline material is characterized by unique set of d-spacings. Since the wavelengths of X-rays are of the same order of magnitude as the interplanar spacings and can be constructively scattered from them to give a diffraction pattern, a unique X-ray pattern for each crystalline material can be obtained which allows, the identification of crystalline materials.

The most common source of X-rays for analytical work is the X-ray tube that is basically a highly evacuated tube in which is mounted a tungsten filament cathode and a metal target anode. X-rays are produced by bombarding the anode with high energy electrons which are obtained by
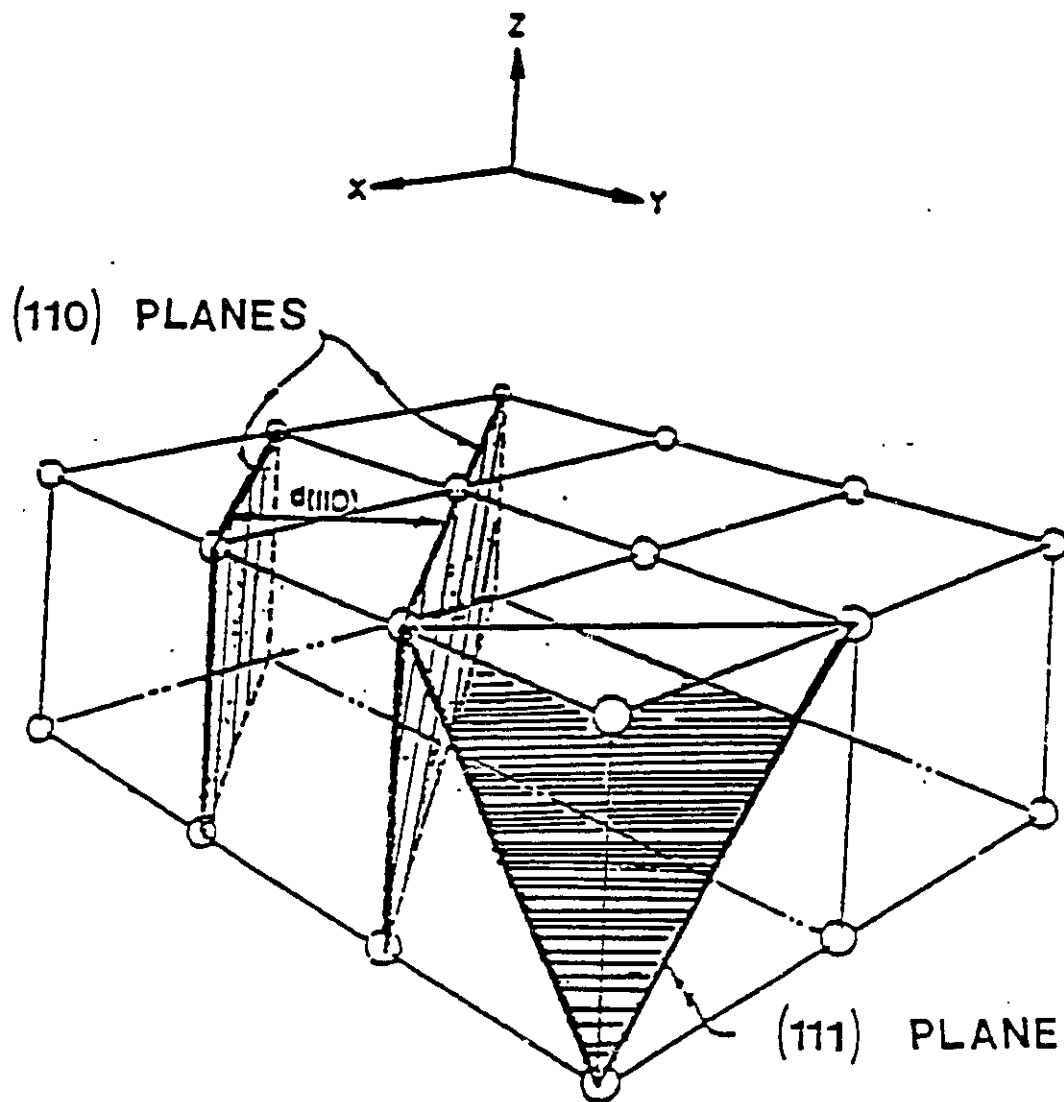
Figure 9a: Representation of a Simple Cubic Crystal
              Structure Showing Atoms, Two Adjacent (110)
              Planes and the Interplanar Spacings d (110)
              Between Them.

thermal emission from the tungsten filament or wire, and are accelerated towards the target metal (28).

Because each electron in the crystal scatters part of the radiation coherently when an X-ray beam encounters an atom, electrons act, therefore, as secondary sources of X-rays. All of these separate radiation waves can combine either constructively or destructively to give a resultant emitted wave. Knowing that the amplitude of the emitted wave depends on the number of electrons emitting radiation and on their respective phase differences which are in turn dependent on the path lengths of the incident and diffracted X-rays. In fact, only when the diffracted beams from the many atomic planes are in phase, that is when the path differences from crystal planes of the X-ray beam are equal to the integral number of wavelengths, a strong diffracted beam (constructive interference) will thus occur. The cumulative effect of this scattering from the regularly spaced centers of the crystal is a diffraction of the beam.

An X-ray beam incident on a crystal will be diffracted by the regularly repeating array of scattering centers which are the electron clouds surrounding the atomic nuclei, in the crystal. As demonstrated by the reflection analogies shown in Figures 9b, 9c and 9d, the angle through which the X-ray diffracts depends upon the spacing between the planes of the atoms in the crystal. Hence, the Bragg equation was derived as follows:

$$n\lambda = 2\,d\,\sin\theta \qquad\qquad (22)$$
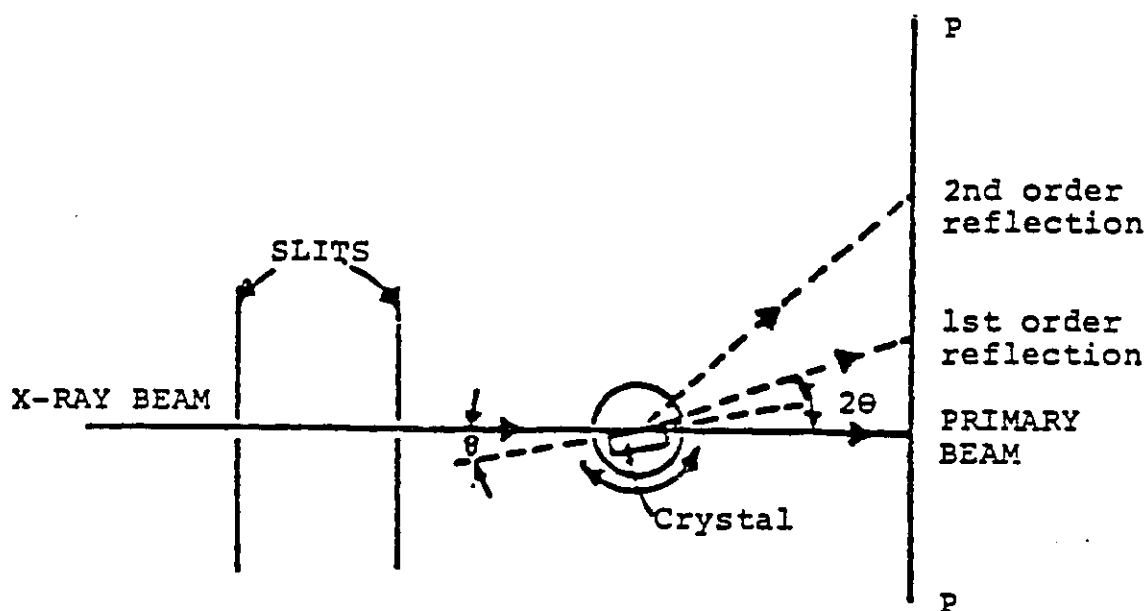
Figure 9b: Diffraction of Radiation from a Crystal.

Crystal planes (h, k, l)
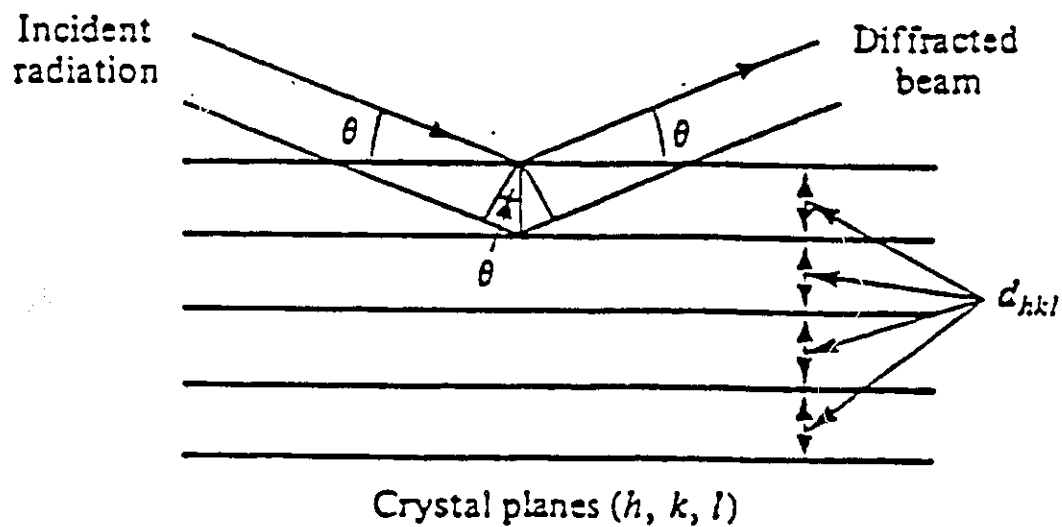
Bragg condition: $n\lambda = 2d_{hkl} \sin \theta$

Figure 9c: Reflection Analogy of X-Ray Diffraction.

Scatter slit

Receiving parallel
slit assembly

Line focus

Divergence parallel
slit assembly

Receiving slit

Divergence slit

Counter

Specimen

Receiving
slit

Goniometer
arc—0° to 165°

Center of
focusing circle

Focusing
circle

Anode

Take-off angle

2θ

θ

Line focus

90°
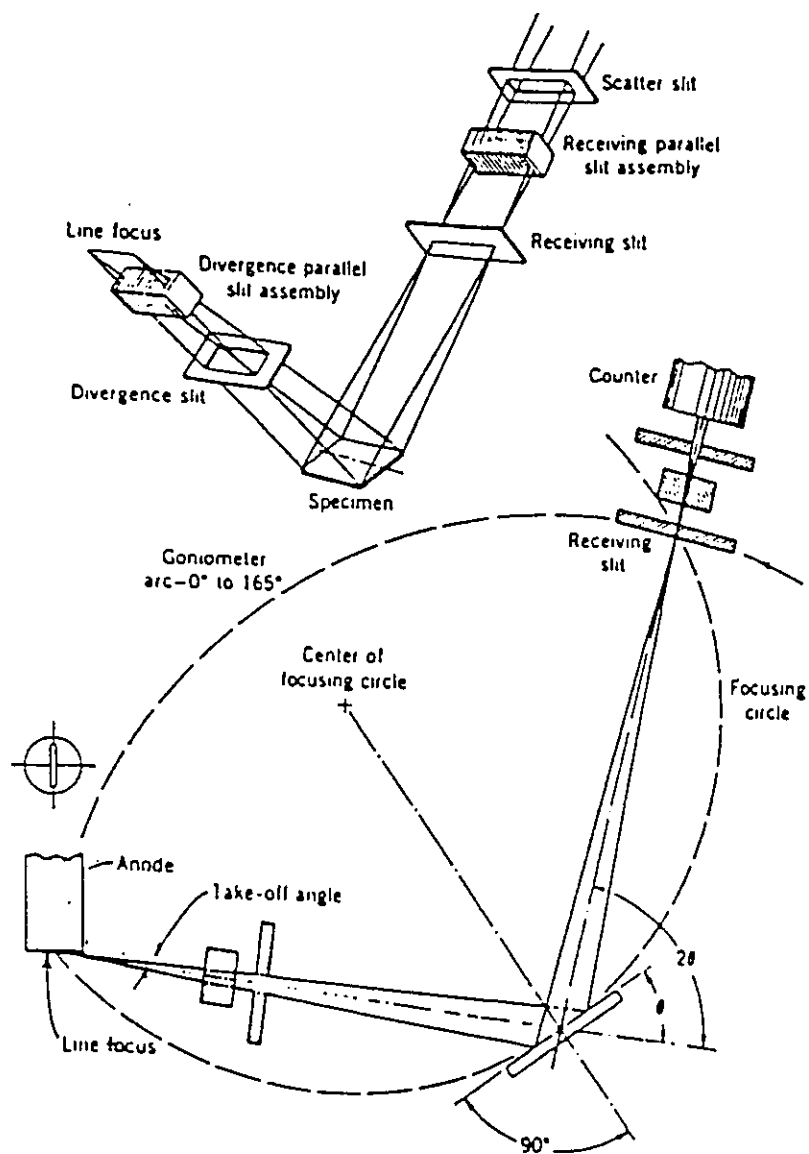
Figure 9d: A Schematic Arrangement of the Line Focusing X-
Ray Powder Diffractomer.

where n: an integer, expressing the order of diffraction

λ: X-ray wavelength

d: interplanar spacing

θ: angle of diffraction

In order for diffraction to occur from a particular family of atomic planes, they must be properly oriented with respect to the incident X-ray beam and, the diffraction intensity is related to the electron density for that specific arrangement. Diffraction only occurs for a particular angle θ that satisfies Bragg's law.

The powder method is the most frequently used for phase identification whereas the single crystal diffraction method is best suited for crystal structure determination. A diffraction pattern of all possible planes will be obtained if a monochromatic beam of X-rays strikes a fine homogeneous powder, which consists of an enormous number of small crystallites randomly oriented in every possible direction. And therefore, a significant number will be expected to be oriented in such ways as to fulfill the Bragg condition for diffraction from every possible interplanar spacing.

A powder diffraction pattern may be obtained either by surrounding the sample with a strip of photographic film in an appropriate camera (Debye-Scherrer method) or by using a more popular device, the powder diffractometer. The diffractometer includes a movable detector (most commonly a scintillation counter) whose signal is fed to an amplification and pulse height analysis system,

which outputs to a chart recorder in older systems and to a computer in more modern equipment. The sample is located at the center of a mechanical goniometer and during data accumulation the sample turns at constant speed while the detector moves at twice that speed. It results that when the sample is rotated by an angle θ, the detector is rotated by an angle 2θ in order to intercept the X-ray diffracted beam.

The objective of an X-ray powder diffractometer is to measure the intensity of diffracted X-rays as a funtion of the angle θ between the incident beam and the surface of the sample. The θ angle is called Bragg angle. Typically, instruments give the intensity of X-rays versus 2θ. The 2θ values which are the angles between the incident beam and the diffracted beam can be converted to d-spacings using Bragg relation (29).

4.2) Apparatus

A Philips PW 1050 / 25 automated X-ray powder diffractometer was used with a Philips X-ray generator (PW 1130 / 00) line focussing goniometer (Figure 9d) and a scintillation counter (PW 1965 / 30). All measurements were carried out by using a Philips long fine focus copper X-ray tube. Copper K_α monochromatic radiation with $\lambda = 1.5418$ Å was obtained by using a nickel filter, on the polychromatic radiation produced by energizing the X-ray tube at 40 kV and 20 mA. Data acquisition, carried out in the step scanning mode, was computer controlled using the SIE112 software from SIETRONICS. Data processing, i.e. removal of background and peak search were carried out using

the same software package.

4.3)   Procedure

The samples were preheated at 120 °C for a minimum of three hours and then allowed to cool in a dessicator. The well-ground samples were pressed into a plexiglass holder which was mounted in the diffractometer. Each sample was scanned in the region of the peaks of interest of zeolite 5A and the counts recorded automatically. A slow scanning speed of one degree per minute was used over the range of 15 ° $< 2\theta <$ 35 °.

Peak intensities were taken as the number of counts recorded by the digital integration system during a complete scan of the peak at constant angular velocity. Background correction was applied by substracting the baseline, using the SIETRONICS software. By reference to the external standard, untreated Ca-A zeolite, the degree of crystallinity in the sample was determined:

$$D.C.(\%)=\frac{I_o}{I}(100) \tag{23}$$

where I_o: Σ peaks intensity for the sample

I : Σ peaks intensity for the external standard

According to the ASTM (30), the four strongest peaks of zeolite 5A

were chosen and used for the analysis, and this, in the range of 2θ mentioned earlier.

Measurements on each sample were performed in duplicate and the % error on all measured values must be within 5%.

5) Bulk Density

5.1) Theory

Archimedean's method is based on Archimedes principle which states that a solid immersed in a liquid displaces a volume of liquid equals to its own volume. This can be used to measure the bulk density of any powdered samples, including zeolites. The materials tested can be polycrystalline or amorphous without any restrictions. The liquid used as a wetter must be non-reactive and should not dissolve the sample. It should be stable in air and easy to handle. It should also have reasonably low viscosity, low surface tension and low volatility, since it is hard to keep constant the level of liquid in the apparatus if it evaporates fast, and this would also lower the temperature. Carbon tetrachlroride, CCl_4, was chosen as the wetting agent, since it matches best the above criteria.

The main problem when measuring the density of a powder is removing all trapped air remaining between the particles. Wetting of the sample is carried out after the sample has been pumped at a low pressure of 30 microns of mercury and while the sample is still under vacuum. Insufficient wetting is the

largest source of error and results in an abnormally lower density, because the air volume trapped between the particles result in an overestimation of the sample value as compared to the polycrystalline volume (31), and hence, an underestimation of the density.

5.2) Apparatus

The density apparatus can be described as follows:

a) Figure 10a: The glass crucible E contains the sample and is hanging from a metal rod B during weighing. The crucible and the rod are located approximately at the center of a cylindrical glass vessel and should not touch it. The glass vessel has a lower diameter part at the bottom (F) where the crucible is located during pumping. On the top of the glass vessel, a male ground glass joint G allows an air tight fit when assembled with the female counterpart H, which is equipped with a 6mm tube (D) for connection to the vacuum line (Figure 10c). The vessel has also two side arms A and C controlled by the rotoflos V1 and V2. On the top of the upper side arm (A) is located an ampoule for CCl_4, which is slowly allowed to enter the evacuated glass vessel (controlled by V1) and the inner extension of the upper arm makes CCl_4 drops fall gently on the lower part of the vessel, near the crucible. The level of CCl_4 must be constant and always the same during measurements in order to have a fixed displacement of CCl_4 by the rod B. This is achieved by opening wide rotoflo V2 to allow any excess of CCl_4
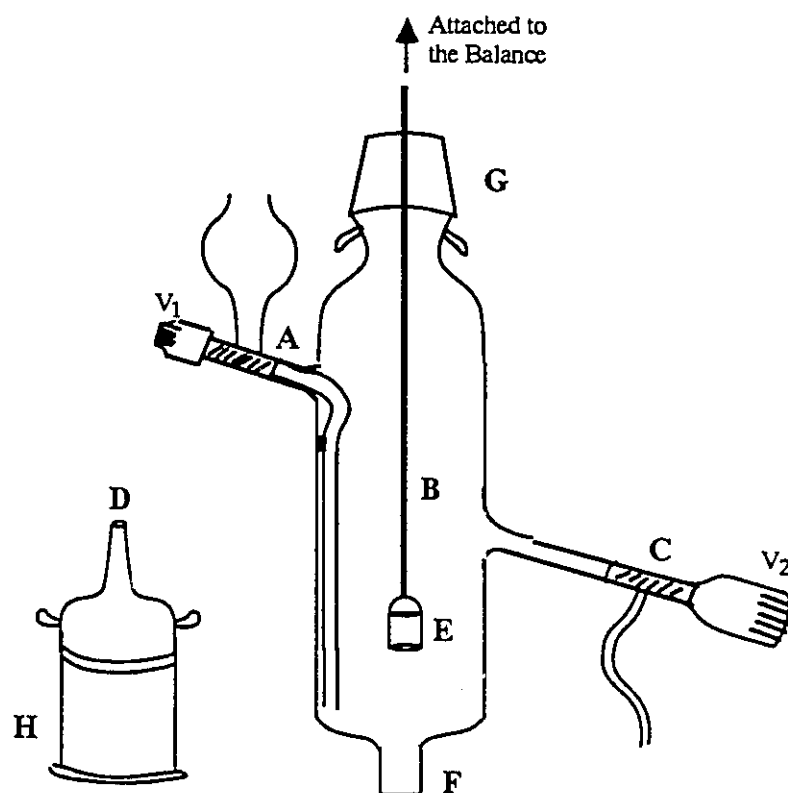
Figure 10a: Vessels used for Bulk Density Measurement.

to be evacuated through the lower side arm (C) and recuperated. A slight excess of CCl_4 must be allowed through A in order to compensate for evaporation.

b) <u>Figure 10b</u>: This figure shows the set up for weighings. The rod B holding the crucible E (see Figure 10a) enters the balance (I) through an opening in the floor of the balance, and is suspended to the hook where the tray of the balance, which has been removed, was hanging. In order to ensure an accurately defined and reproducible positioning of the glass vessel relative to the balance, an adjustable system of arms and clamps (J) are used to hold the glass vessel in position.

c) <u>Figure 10c</u>: This shows the set up during the pumping stage. The sample crucible is located in F at the bottom of the glass vessel (see Figure 10a) and is held in place with a metal rod, which prevents the crucible from floating over CCl_4 during the wetting stage, and tipping over, which would spill the sample in the CCl_4. The glass vessel is tightly connected to the vacuum line as describe earlier. Valves V1 and V2 (Figure 10a) are closed during pumping. Valves V3 and V4 are alternatively opened and closed in order to evacuate the vessel in stages; i.e. with V3 open and V4 closed, the vacuum line is evacuated using the machanical pump only, then V3 is closed and B4 is opened very slowly to equilibriate the pressure in the vessel with that in the line, while monitoring the pressure change on the vacuum gauge. Then
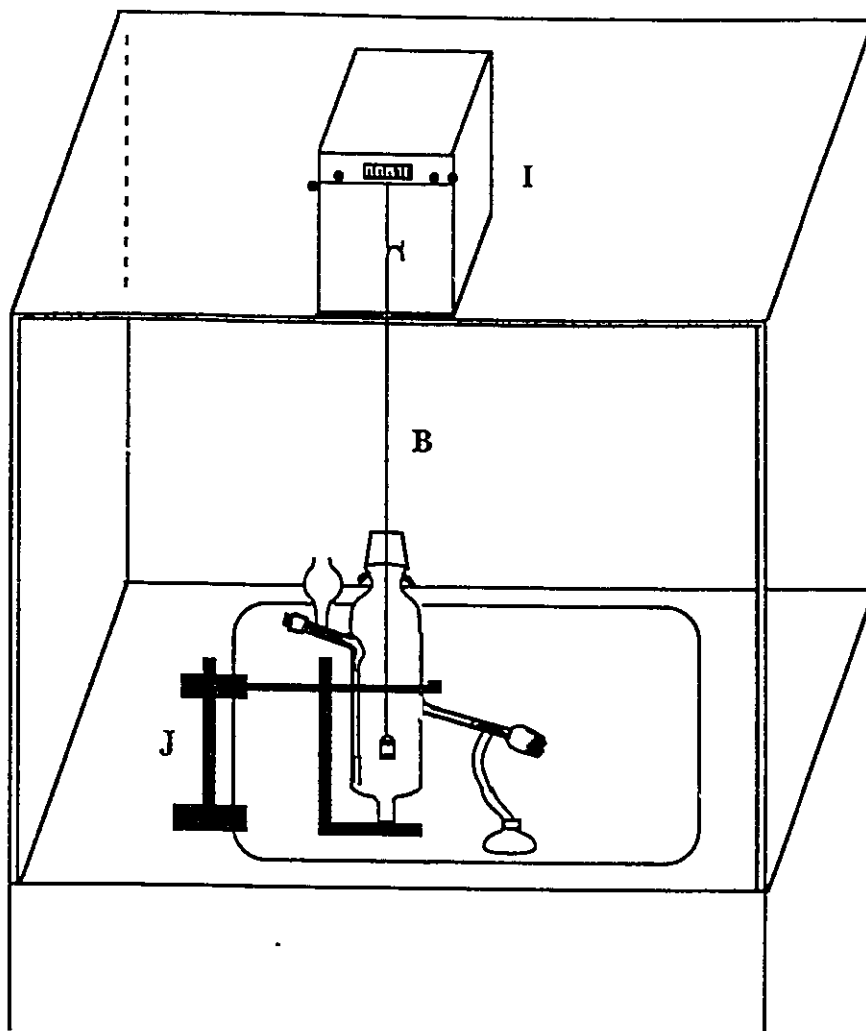
Figure 10b: Weighing Setting for Bulk Density Measurement.
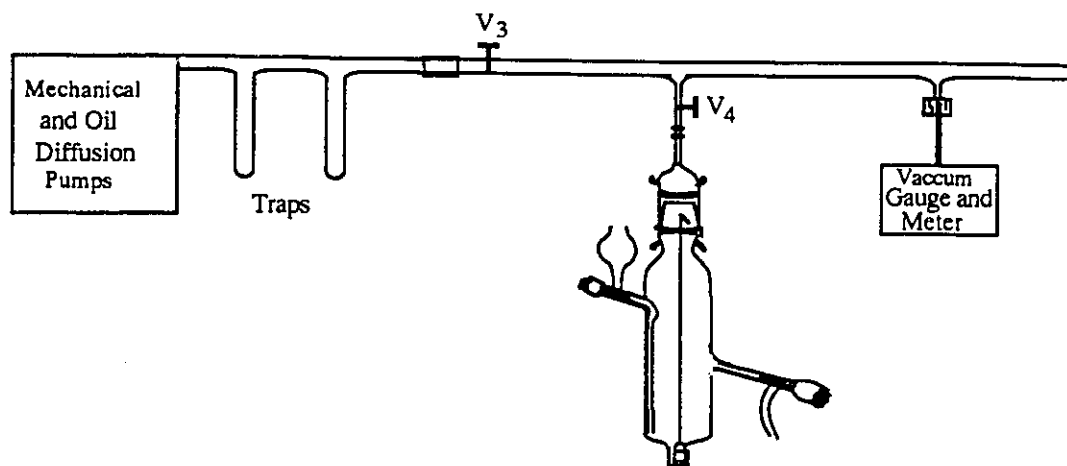
Figure 10c: Vacuum Setting for Bulk Density Measurement.

V4 is closed and V3 is opened, and the process is repeated until the pressure is down to ca. 60 μm Hg. This procedure is necessary to avoid sucking the powdered sample out of the crucible. Then both V3 and V4 are opened together, very slowly and secondary pumping is applied for one hour, with the help of an oil diffusion pump.

5.3) Procedure

Since the crucible (E) and a portion of rod B are also immersed in CCl_4, in addition to the sample, they will also displace some volume of CCl_4; the volume of CCl_4 displaced, which is measured, is the sum of that displaced by the sample, by the crucible and by the rod. The measurement of the displacement of CCl_4 by the empty crucible and rod (m_2) makes possible the calculation of the volume of CCl_4 displaced by the sample only.

After recording m_1 and m_2, approximately 1 g of sample is introduced into the crucible. Then m_3 is measured. The glassware containing the crucible with the sample is connected to the vacuum line and evacuated according to the procedure described above, then CCl_4 is allowed slowly into the vessel, which is still under vacuum until the sample is completely immersed. Then the vessel is disconnected from the vacuum line and is connected to the balance for the measurement of m_4. The density of the sample is obtained from the following formula:

$$\rho = \frac{(m_3 - m_1) \; \rho\,CCl_4}{(m_3 + m_2 - m_4 - m_1)} \qquad (24)$$

where $\rho(CCl_4)$: density of the wetting agent (CCl_4)

m_1: mass of the empty crucible

m_2: mass of the empty crucible immersed in CCl_4

m_3: mass of crucible and sample

m_4: mass of crucible and sample, after air removal, immersed in CCl_4

ρ: density $= m / v$

since v: volume of sample $= \dfrac{(m_3 + m_2 - m_4 - m_1)}{\rho\,CCl_4}$ $\qquad (25)$

and m: mass of sample $= (m_3 - m_1)$ $\qquad (26)$

Not only the liquid level but also the liquid temperature must be the same for the measurements of m_2 and m_4, in order to assure accurate subtraction of the volume of the empty crucible and the part of the rod that is immersed in CCl_4. The experimental error on density measurements, using CCl_4 as wetting agent, was found to be not larger than 2% (31). The main source of

error is usually imperfect degassing, although the technique described above was designed to minimize this effect. Slow stepwise degassing as described above usually avoids suction of powder out of the crucible. However, the high porosity of zeolites give these materials extraordinary adsorptive capacities, and this gave rise to continuous degassing which always resulted in some of the sample being blown away from the crucible.

In order to eliminate this problem, the powders were transformed into the extrudate form using bentonite as the binder agent. Several ratios of binder to zeolite were used, such as 10, 20 and 30 %. The extrudate form could be easily evacuated with no loss of sample. The values of the density for given samples were plotted versus the ratio of bentonite and extrapolation to 0 % of bentonite yielded the density of the pure samples. Each sample was performed in triplicate and its percentage of errors is given in chapter IV.

6) Magic Angle Spinning ^{29}Si- and ^{27}Al-NMR

6.1) Theory

Several new techniques have been developed that overcome the band broadening obtained when applying conventional NMR to crystalline or amorphous solids, and that make possible the acquisition of high - resolution spectra much like the ones for liquids. Modern NMR techniques which especially involve magic - angle spinning are potentially powerful for studying the local structure of silicates and other inorganic solids that have non-zero nuclear

spin nuclides (32) [^{29}Si and ^{27}Al for silicas, aluminas, zeolites and various other aluminosilicates; ^{11}B and ^{29}Si for borosilicates; etc. (33)]. The degree of structural insight achievable with MAS-NMR is exceptionally high since it probes the immediate environment of a particular nucleus more or less irrespective of whether the sample is amorphous or crystalline. The elucidation of the coordination of silicon in zeolites proves the high importance of ^{29}Si MAS-NMR. To date, ^{27}Al MAS-NMR is used to supplement the information provided by ^{29}Si MAS-NMR on alumino-silicates (34).

Most of the line broadening of NMR spectra of solids is attributable to two interactions: chemical shift anisotropy and static dipolar interactions, which in liquids average to zero because of the rapid and random motion of molecules. The line broadening represented by chemical shift (shielding) anisotropy is an inhomogeneous broadening, a superposition of spectra of randomly oriented individual nuclei with respect to relative to the direction of the applied magnetic field. Each of these nuclei has an inherently sharp line for a particular orientation of nuclear environment with respect to the static field. For highly immobile species such as those in an amorphous or powdered crystalline solid, the net result of the chemical shift anisotropy is that the entire range of chemical shift spanned by all possible orientations is present in the spectrum. The technique of MAS is to remove the chemical shift anisotropy by high-speed mechanical spinning of the rigid sample about an axis making an angle of 54.7 °, called "magic angle", to the direction of the static magnetic field (33, 35). In effect, the solid acts like a liquid when spun at that magic angle. In practice, anisotropic and static effects

in a solid average out to simulate the situation present in a liquid when rotated rapidly at that magic angle. In principle, and sometimes in practice, MAS can also be used to eliminate the other important cause of line - broadening, i.e. magic dipole - dipole interactions between pairs of nuclear magnetic moments.

6.2)   Instrumentation

The NMR spectra of zeolite materials were obtained on a Varian VXR 300 FT-NMR spectrometer operating at 59.592 MHz (78.159 MHz for ^{27}Al) using superconducting solenoid magnets and amplifiers for final radio frequency pulse generation. A VXR 4000 model computer system was used for data acquisition and processing. ^{29}Si MAS-NMR spectra were obtained using probes with a spinning rate of 26 Hz (10 Hz for ^{27}Al). All ^{29}Si and ^{27}Al line positions (chemical shifts) were referred to tetramethylsilane (TMS) and $[Al(H_2O)_6]^{3+}$ as zero chemical shift respectively. The MAS-NMR spectra were recorded at the University of Montreal.

CHAPTER IV: RESULTS & DISCUSSION

i).   Hydrothermal treatments (HT)

After a large number of experiments aimed at finding the best and reproducible conditions for hydrothermal treatment, we succeeded to produce accurately five samples of 100.0, 76.3, 50.2, 21.0 and 0.0 % degree of crystallinity (D.C.) using commercial Linde Ca-A zeolite under the conditions listed in Table II. Figure 11 shows the results of the exploratory hydrothermal treatments. It shows clearly that the degree of crystallinity decreases when the maximum temperature of treatment increases. The results of Figure 11 were used to choose the appropriate temperature of treatment in order to obtain the desired values of degree of crystallinity, i.e. ca. 75, 50, 25 and 0 %. The material looses all its crystallinity at 850 °C. Contrary to temperature, which has a large effect on the result of the treatment, the rate of H_2O injection seems to have a much milder influence on the D.C. (Figure 12). It is noteworthy that the samples labelled R (Right) always have a lower D.C. than the ones labelled L (Left), because the R samples are placed closer than the L samples to the H_2O injection source. They must have absorbed more H_2O vapor and therefore, are more suitable for the structural collapse following the abrupt evaporation of the H_2O molecules previously trapped in the silica-alumina structure of the zeolite.

The textural and nitrogen sorptive properties of the hydrothermally treated materials (labelled HT) as a function of the degree of crystallinity are given in Table III. The low values of nitrogen adsorption obtained after treatment indicates that serious pore closure occured under our conditions, in contrast to the results reported by Breck for the

Table II: Operating Conditions for HT Samples, Set-up using Results from the Exploratory Phase (Figures 11 and 12).

Sample	Run #	Maximum Temperature	H_2O injection	N_2 Flow
% D.C.	—	°C	ml / hr	ml / min
100.0	—	—	—	—
76.3	31, 32, 33L	750	30.6	20.0
50.2	38, 40, 41R	750	13.3	20.0
21.0	44, 45L	800	13.3	20.0
0.0	44, 45, 46R	800	13.3	20.0
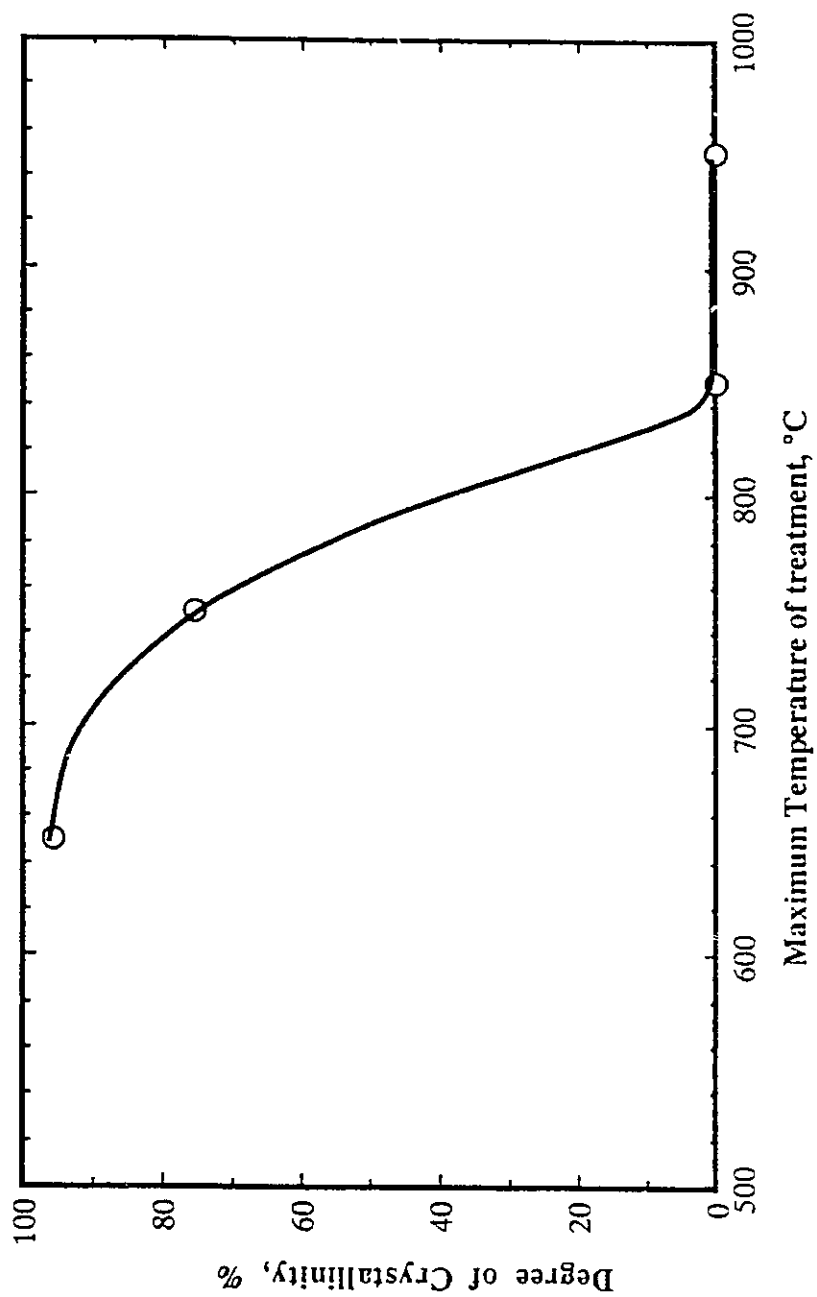
Figure 11: Variation of the Degree of Crystallinity of HT Samples
with Temperature.

(Curve obtained during the Exploratory Phase).
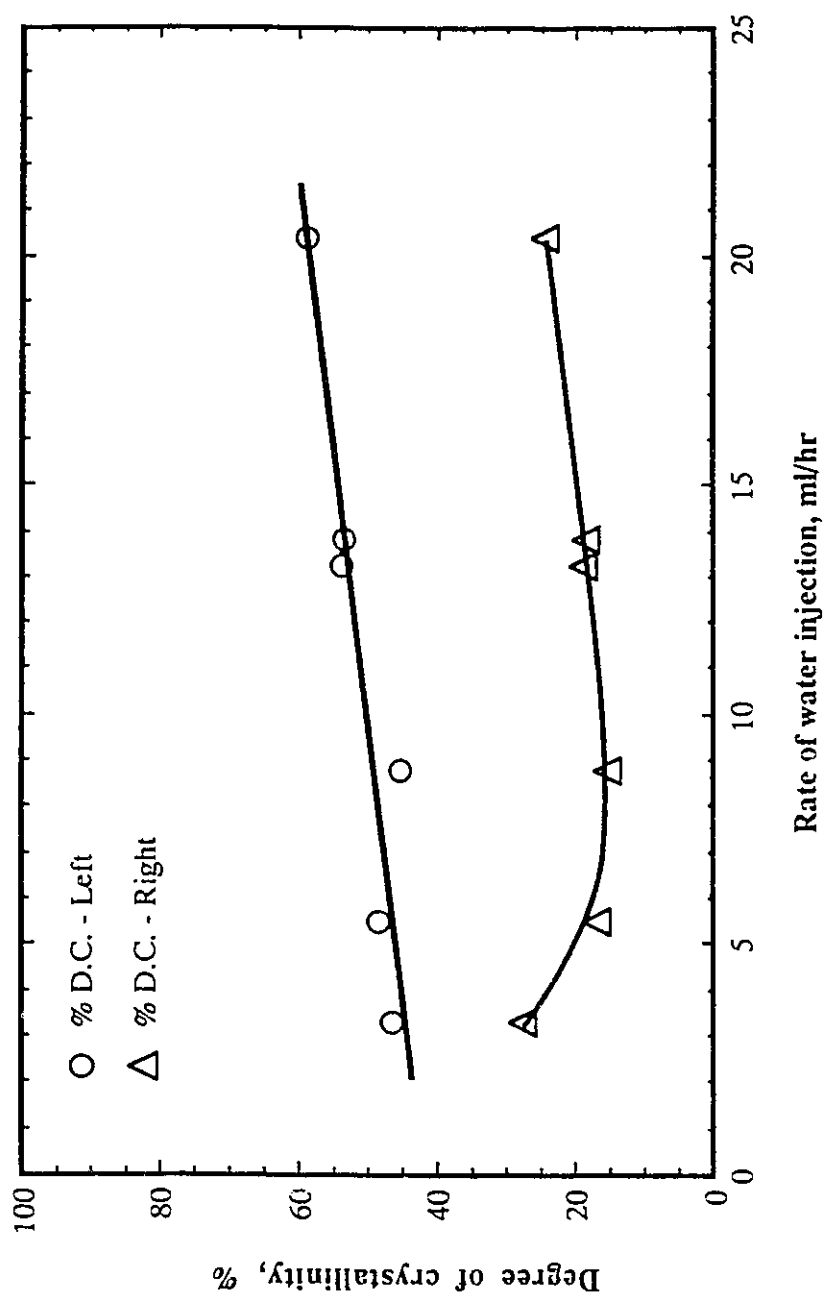
Figure 12: Variation of the Degree of Crystallinity of HT Samples
with Water Injection Rate.

(Curve obtained during the Exploratory Phase).

Table III: BET Results of HT Samples

Sample	Surface area	Volume of N$_2$ sorbed		Average pore diameter
		Total	Micropore	
% D.C.	m^2 / g	cm^3 / g	cm^3 / g	nm
0.0	7	0.019	0.012	7.3
21.0	3	0.004	0.001	4.4
50.2	26	0.007	0.005	2.3
76.3	160	0.065	0.065	1.5
100.0	531	0.258	0.234	< 1.7

hydrothermal treatment of Ca-A type zeolites (36). Furthermore, the more severe the conditions of the hydrothermal treatment, the more extensive the structural collapse, the lower the BET surface area and the more serious the pore closure phenomena which occurs during hydrothermal treatment (Tables II & III). Hence, the volumes of nitrogen, water and n-hexane adsorbed decreases sharply with the extent of the structural collapse (Table III & Figure 14). The chemical composition however, remained practically unchanged upon the hydrothermal treatment (Table IV).
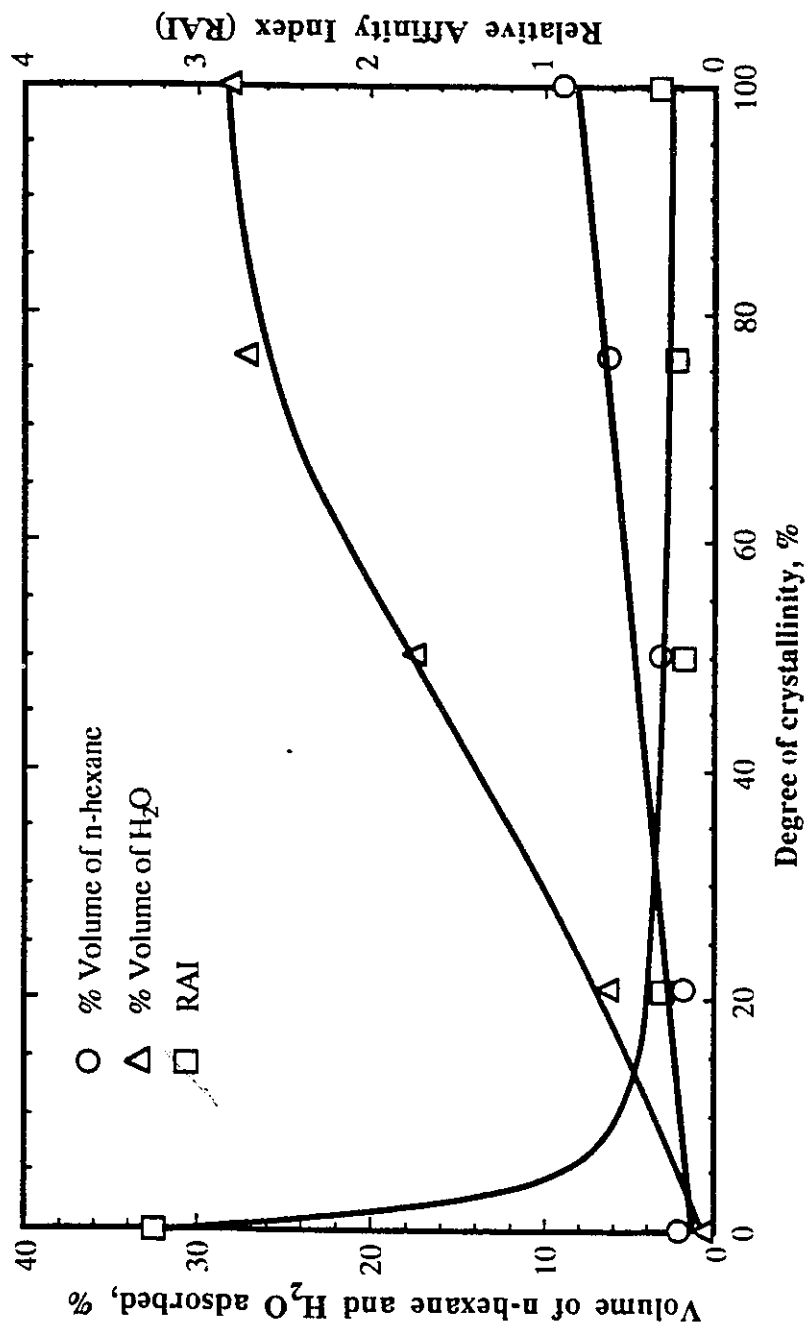
Figure 14: Vapour of n-Hexane and Water adsorbed by HT Samples.

Table IV: Chemical Composition of HT Samples

| Sample | Chemical composition | | | | Si/Al ratio |
| | CaO | Na$_2$O | Al$_2$O$_3$ | SiO$_2$ | |
% D.C.	Wt. %	Wt. %	Wt. %	Wt. %	-
100.0	15.6	7.2	38.8	38.4	0.84
76.3	14.0	6.7	38.2	41.1	0.91
50.2	15.4	7.5	37.1	40.0	0.91
21.0	13.4	6.0	34.5	46.1	1.13
0.0	14.4	6.5	36.4	42.7	1.00

ii). HCl Treatment (AT)

The second method used is the treatment of the parent Ca-A zeolite with HCl acid solution. The reaction conditions were fixed as follows: 0.2N HCl solution concentration and 80 °C reaction temperature. Hydrothermal treatment on pure Ca-A zeolite leaves amorphous species formed by removing Al from the zeolite structure, then further treatment with HCl, on a sample of 25 % D.C. for example, that resulted from the hydrothermal treatment, removes these amorphous species. Therefore, we have applied such a mild treatment with acid concentration of 0.2N on pure Ca-A zeolite. This is understandable because we do not want too severe a pore enlargement, that could lead to a serious structural collapse. As one can expect, the degree of crystallinity (Figure 15), the BET surface area as well as the volume of adsorbed nitrogen (Table V), or the weight contents in Na_2O and in CaO (Table VI) decrease with increasing time of exposure to the acid solution whereas the average pore diameter (Table V) and the Si / Al ratio increase. The water and n-hexane adsorption capacities and the relative affinity index (RAI) first increase and go through a maximum for an acid leaching time of one to two hours (Figure 16). In the first hour of treatment, the n-hexane sorption capacity exhibits a very sharp increase (multiplied by three relative to the untreated commercial Ca-A zeolite) which results in a significant enhancement of the RAI value since the increase of adsorbed water is very small. The existence of such a sharp maximum in the adsorption capacity for n-hexane, and to a minor extent for water, seems to stem not only from a surface poorer in alumina (Figure 16) but also probably mainly from a better accessibility to the sorption sites for n-hexane and water molecules, as already observed by Gnep et al. (37).
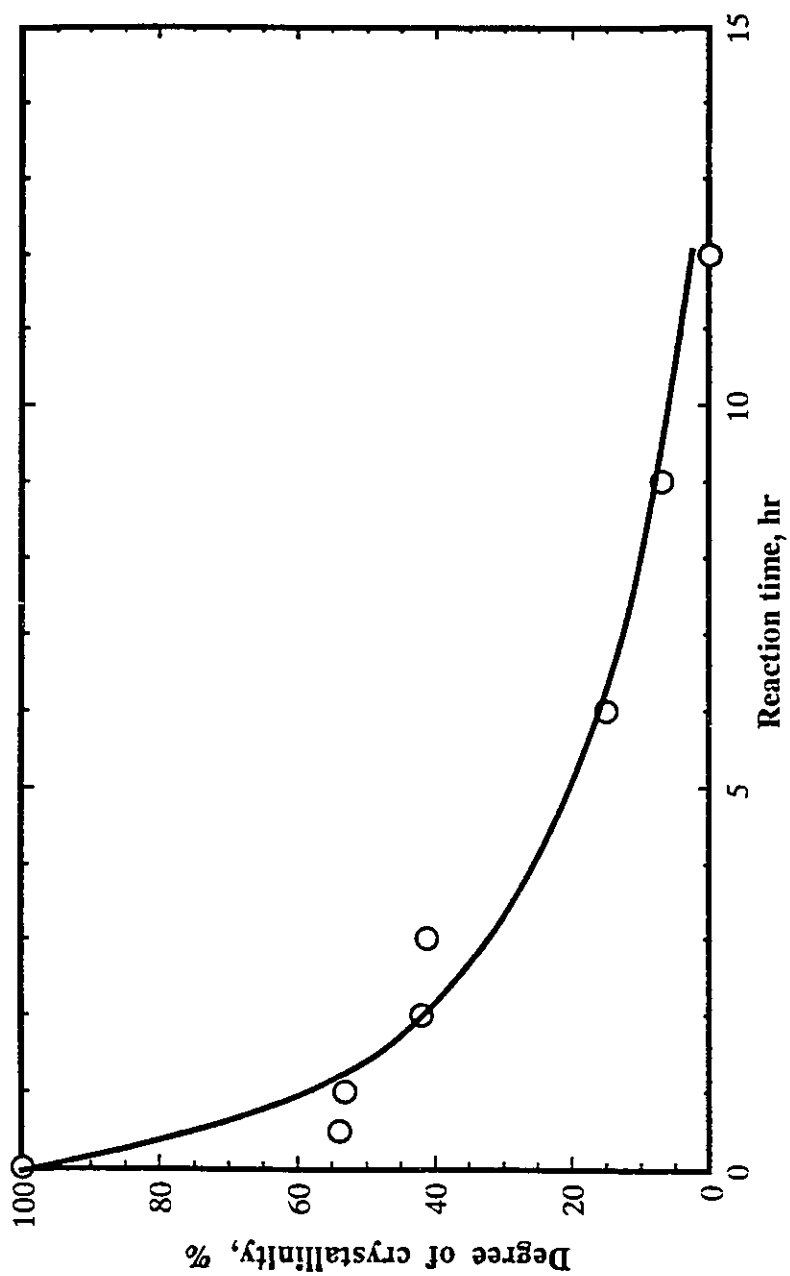
Figure 15: Variation of the Degree of Crystallinity of AT Samples with Reaction Time.

Table V: BET Results of AT Samples

| Reaction time | Surface area | Volume of N$_2$ sorbed | | Average pore diameter |
| | | Total | Micropore | |
hr	m^2 / g	cm^3 / g	cm^3 / g	nm
0.0	531	0.258	0.234	< 1.7
0.5	446	0.279	0.181	1.6
1.0	450	0.231	0.182	1.5
2.0	436	0.252	0.173	1.6
3.0	318	0.171	0.108	1.7
6.0	182	0.133	0.032	2.1
9.0	144	0.128	0.006	3.3
12.0	145	0.131	0.005	3.5

Table VI: Cnemical Composition of AT Samples

Reaction time	Chemical composition				Si / Al ratio
	CaO	Na$_2$O	Al$_2$O$_3$	SiO$_2$	
hr	Wt. %	Wt. %	Wt. %	Wt. %	-
0.0	15.6	7.2	38.8	38.4	0.84
0.5	13.9	1.8	33.9	50.4	1.26
1.0	12.9	1.6	34.3	51.2	1.27
2.0	13.2	2.7	35.3	48.8	1.17
3.0	12.2	2.8	35.2	49.8	1.20
6.0	7.6	1.2	39.4	51.8	1.11
9.0	3.0	0.3	42.5	54.2	1.09
12.0	2.2	0.1	36.6	61.1	1.41
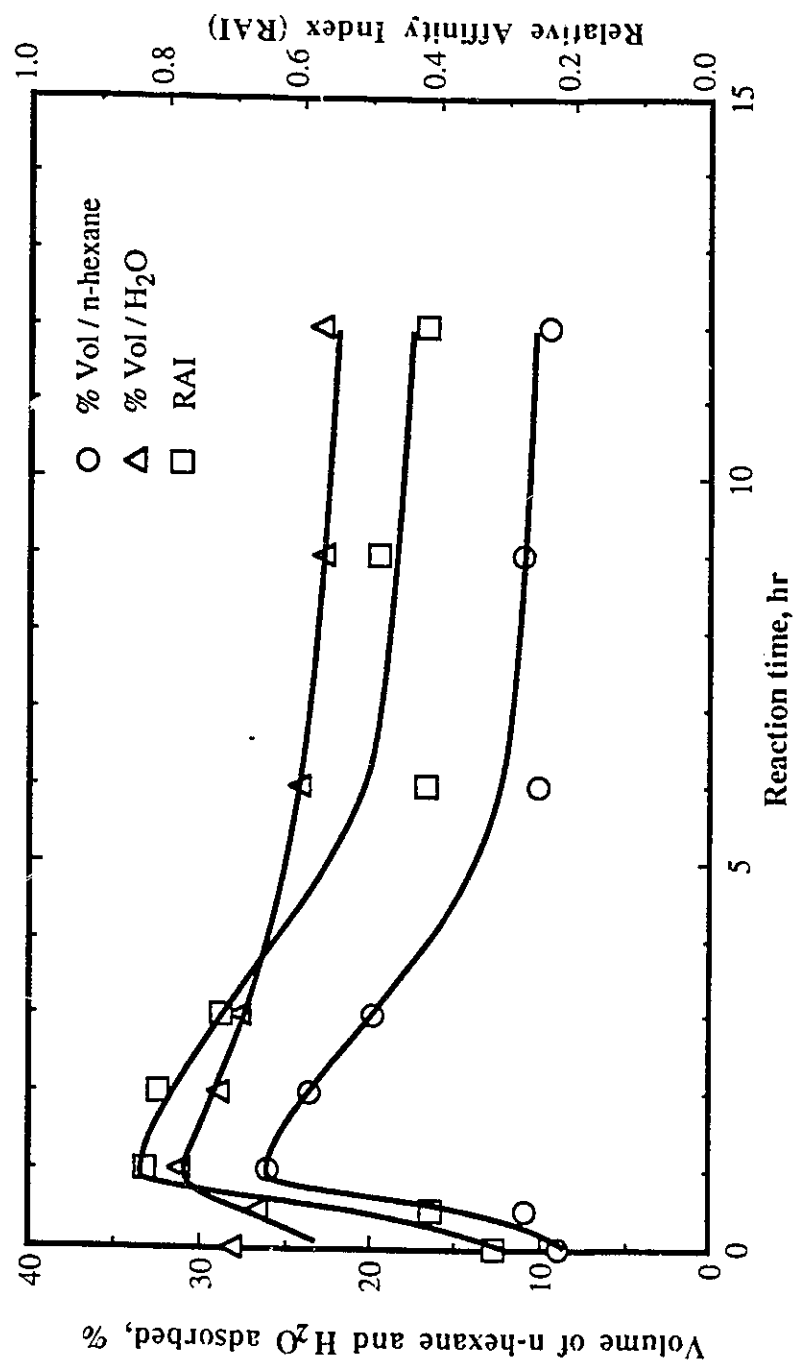
Figure 16: Vapour of n-Hexane and Water adsorbed by AT Samples.

Micropore enlargement upon acid leaching was evidenced by the following experimental results. Let us consider the plots of the differential pore volume dV/dlogD (cm_3 / g) versus the pore diameter D (nm) obtained with the parent zeolite and the various AT materials obtained upon acid treatment (Figure 17). The ratio of the volume of nitrogen adsorbed by the micropores to the total volume adsorbed in untreated Ca-A zeolite is 0.234 / 0.258 (Table V), therefore 91 % of the pores are zeolite-type micropores (pore diameter ≤ 0.43 nm) and the remaining 9 % are mesopores. The difference is due to the mesopores (ca. 3.5 - 4.5 nm diameter) the existence of which is shown on Figure 17. These mesopores may be the only portion of the zeolite pores which constitute the pore openings of the parent Ca-A particles. The mild acid treatment apparently did not create new larger size pores but gradually enlarged the already existing "zeolite - type" micropores until all these micropores had grown to the size of the "external" mesopores. As a matter of fact, the maximum for the size distribution of all AT materials is located at 3.5 - 4.5 nm. In addition, the corresponding share of pore volume increases with increasing time of exposure to the acid solution (Figure 17) while the share of pore volume corresponding to the zeolite - type micropores decreases accordingly (Table V).

The change of chemical composition of the samples as a function of the acid treatment can be related to the change in porosity. The weight percent of silicon dioxide increases significantly whereas that of sodium oxide decreases steadily in the first half hour of exposure to the acid solution (Table VI). The decrease in Ca and Al contents were fairly limited in the same time period. The loss of sodium in the first half hour of acid treatment results in an increase of the weight percent of SiO_2 because the total
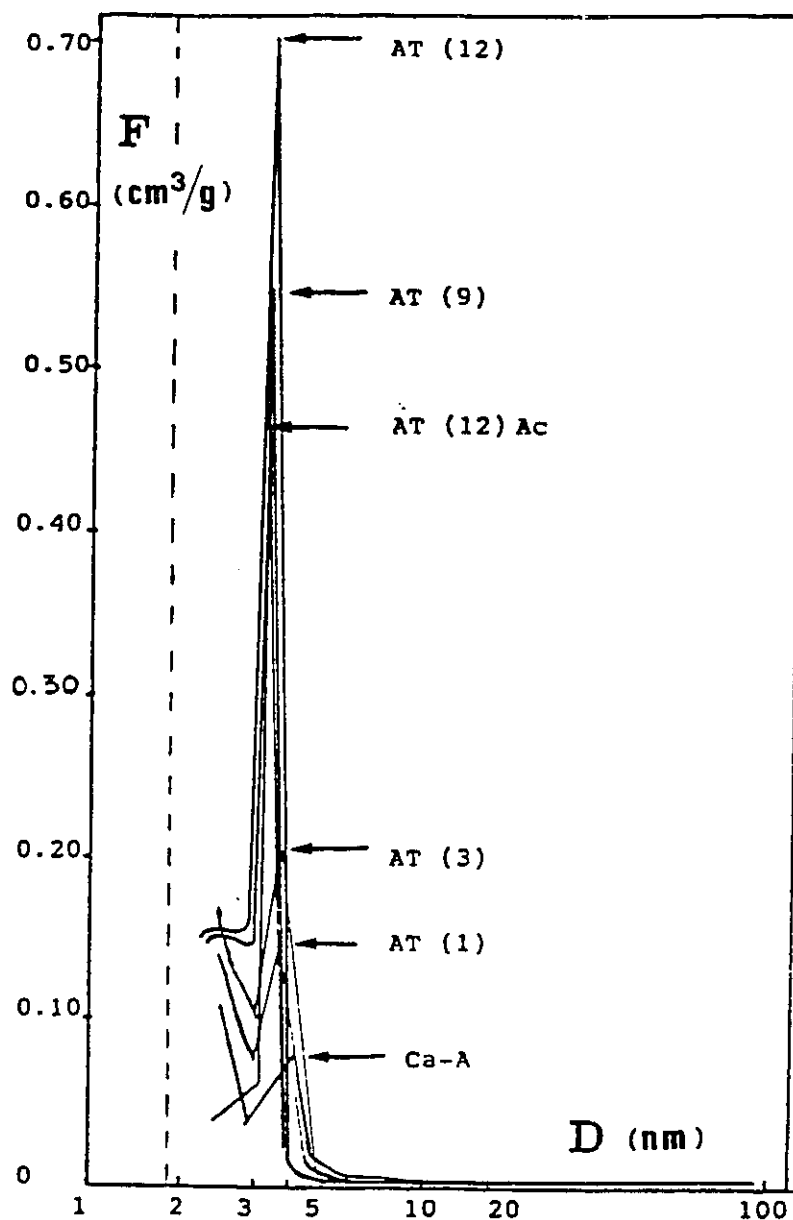
Figure 17:   Differential Pore Size Distribution of the AT
Samples (F = dV/dlog(D) as a function of the
pore diameter D - mesopore region only).
V is the pore volume as determined by nitrogen
adsorption / desorption technique. The arrows
show the function maxima. Ac = activated at
500 °C.

weight of the sample decreased and the acid treatment does not remove Si. For the same reason, if there were no loss of Al, the weight percent of Al_2O_3 should also increase. However, it is observed (Table VI) that the weight percent of Al changes little with acid treatment, therefore, some loss of Al probably occured together with the loss of Na. This is also shown by a significant but not total, loss of the zeolite degree of crystallinity (Figure 15). It has been established (36) that in the Ca-A zeolite unit cell, the eight cation sites S_1 within the β-cages are occupied by four Na^+ and four Ca^{++} ions. The main role of these cations is to compensate for the negative charges created near the tetrahedral Al atoms where tetravalent Si is replaced by trivalent Al. Thus, the almost complete disappearance of the sodium after the first half-hour of acid leaching seems to indicate that the first Al atoms removed are those which are located in the vinicity of the Na S_1 sites. Most of the other Al sites, the charge of which is compensated by Ca^{++} ions, are still intact at this stage and contributed to the preservation of a significant amount of micropores. In fact, the volume of nitrogen adsorbed by such micropores still represents 65 % of the total volume of nitrogen adsorbed (Table V).

Consequently, the mild acid treatment might follow the following scenario: first, the acid attack occurs at the outermost portion of the zeolite pores (36) and then, gradually makes its move through the zeolite particle body, selectively leaching at Na locations. Finally, a material poorer in alumina, with a higher Si/Al ratio, is obtained. Such a gradual dealumination which results in a significant loss of crystallinity and enlargement of the zeolite micropores is accompanied by a selective removal of the cations, i.e. Na at the beginning, and Ca at the end (Figure 15, Tables V & VI).

It is noteworthy pointing out that a longer exposure to the acid solution (9 and 12

hours) yielded materials with a monomodal pore distribution. There was practically no adsorption of nitrogen corresponding to the micropore region (negligible micropore adsorption values, Table V), and a fairly narrow mesopore size distribution 3.5 - 4.5 nm is observed (Figure 17). Nevertheless, these materials still have a relatively high surface area and interesting sorption properties (Table V). The aluminosilicate skeleton of such materials obtained was practically free of Na^+ and Ca^{++} cations which were replaced by H_3O^+.

Figure 18 shows the adsoption / desorption isotherms of the parent Ca-A zeolite and some AT samples. There is no hysteresis loop for the untreated Ca-A zeolite which is understandable because the hysteresis loop is always observed with the mesopore isotherms (15) whereas there is very few (9 %) mesopores present in the untreated Ca-A zeolite. The shape of the hysteresis loops of all the AT samples shown in Figure 18, which corresponds to that of H4 (4) or B (15), strongly suggests the presence of slit-shaped mesopores. For long exposure to the acid medium (AT (12)), the mesopores have a more open slit configuration than for shorter exposures. These more open slits are formed by non-parallel plates.
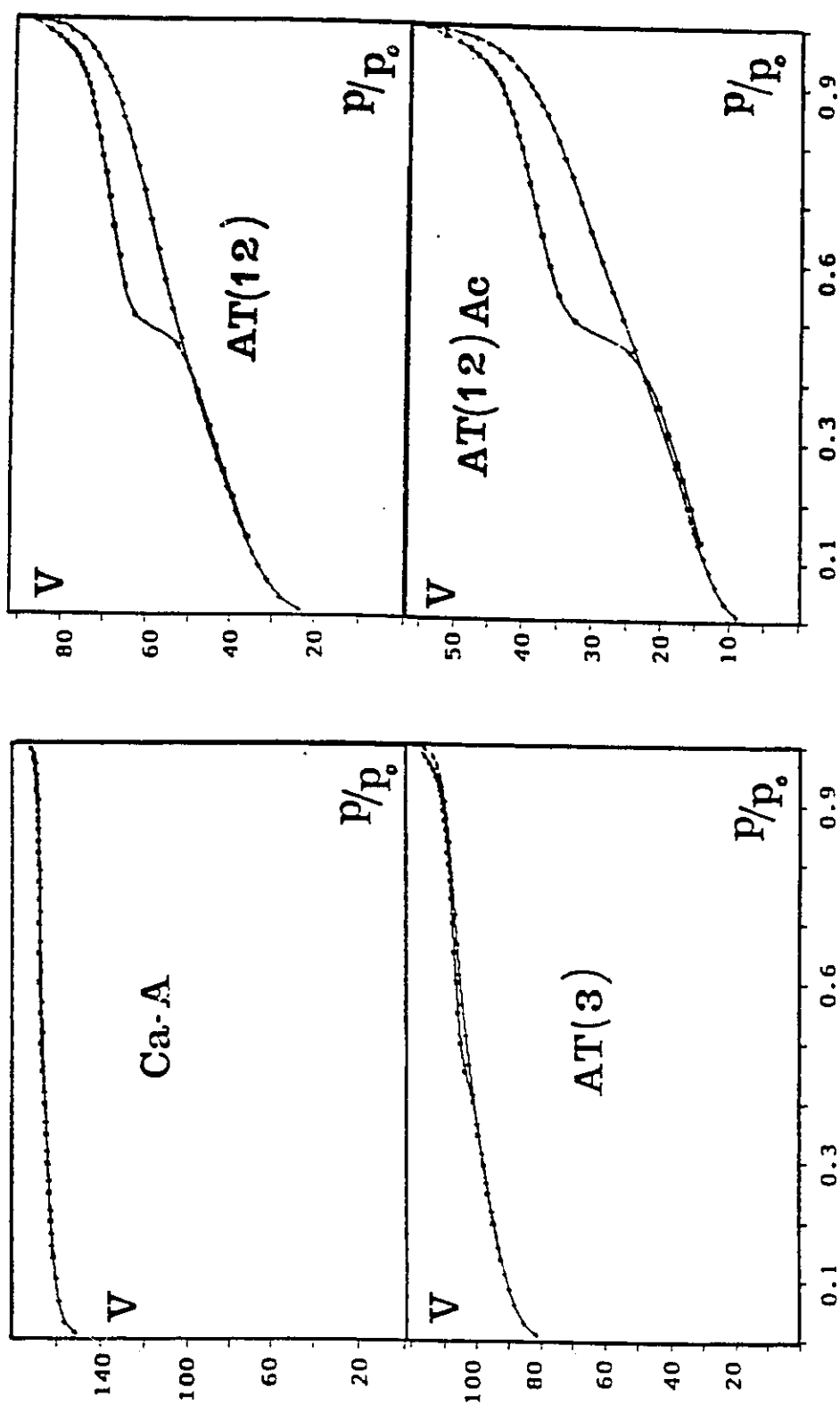
Figure 18: Nitrogen Adsorption (+) / Desorption (*) Isotherms (volume V per unit mass, in cm³/g STP, versus relative pressure P/P₀) obtained with Ca-A Zeolite and AT Samples. Ac = activated at 500 °C.

iii). (NH$_4$)$_2$SiF$_6$ Treatment (AFS)

Another chemical treatment of the zeolite consists of reacting commercial Ca-A zeolite with a salt solution such as (NH$_4$)$_2$SiF$_6$ (11). The textural and sorptive properties of ammonium hexafluorosilicate treated zeolites are shown in Table VII and Figure 19. The two samples treated at room temperature (AFS1 and AFS3) showed a pore size distribution of monomodal type, maximum of which was located at ca. 14 nm; whereas the sample treated at 80 °C (AFS1.HT) surprisingly exhibited a bimodal and much more expanded mesopore size distribution curve with a flat maximum also located at 14 nm (Figure 19). In fact, Table VII reports that the volume of nitrogen adsorbed by the micropores still represented 16 % of the total volume (0,283 cm^3 / g) while other AFS treated samples did not show any adsorption in the micropore region (< 1 %).

AFS treatment is currently used to extract some Al from zeolite structures and substitute it by Si, which thereby, provides zeolites having higher Si / Al ratios (38). According to earlier authors, this treatment essentially preserved the original zeolite pore system. In our AFS treatment, there was simultaneously a significant decrease of the Al and Na contents, relative to untreated Ca-A zeolite, whereas the Ca content remained practically unchanged (Table VII). A significant loss of crystallinity was observed (Table VII) which seems to indicate that AFS reacted with some of the Al, contained in the zeolite lattice, and with Na$^+$ according to the following equation, (12):

$$Na^+[(AlO_4)^-]_t + (NH_4)_2SiF_6 \quad \rightarrow \quad [SiO_4]_t + (NH_4)_2AlF_5 + NaF \qquad (27)$$
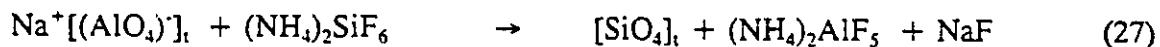
where [ ]$_t$ indicates the tetrahedral site.

Table VII:Physico-Chemical Properties of the AFS Samples
with Addition Rate of 0.30ml/min

		Unit	Sample				
			5A	AFS1	AFS3	AFS3 (rep)	AFS1. HT
A	Time	hrs	–	1	3	3	1
	Temperature	°C	–	24	24	24	80
B	D.C.	%	100	15	17	19	26
	Surface area	m^2 / g	531	128	112	97	191
	Volume of N_2 sorbed — Tt	cm^3 / g	0.258	0.323	0.314	0.394	0.283
	Volume of N_2 sorbed — MP		0.234	0.005	0.001	0.003	0.046
	Average pore diameter	nm	<1.7	10.1	11.2	14.3	4.0
	Volume adsorbed — H_2O	vol %	28.1	29.8	36.2	30.4	25.5
	Volume adsorbed — n-C_6H_{14}		9.0	16.5	14.6	14.6	7.0
	R.A.I.	–	0.32	0.55	0.40	0.48	0.35
	Chemical composition (oxide form) — Al	wt %	38.8	30.2	31.4	30.7	28.5
	Chemical composition (oxide form) — Na		7.2	1.1	1.3	1.1	0.3
	Chemical composition (oxide form) — Ca		15.6	12.3	14.7	13.3	13.2
	Chemical composition (oxide form) — Si		38.4	56.4	52.6	54.9	58.0
	Si / Al ratio	–	0.84	1.54	1.44	1.54	1.73

N.B.:
- A: Method preparation
- B: Characterization
- Tt: Total
- MP: Micropore
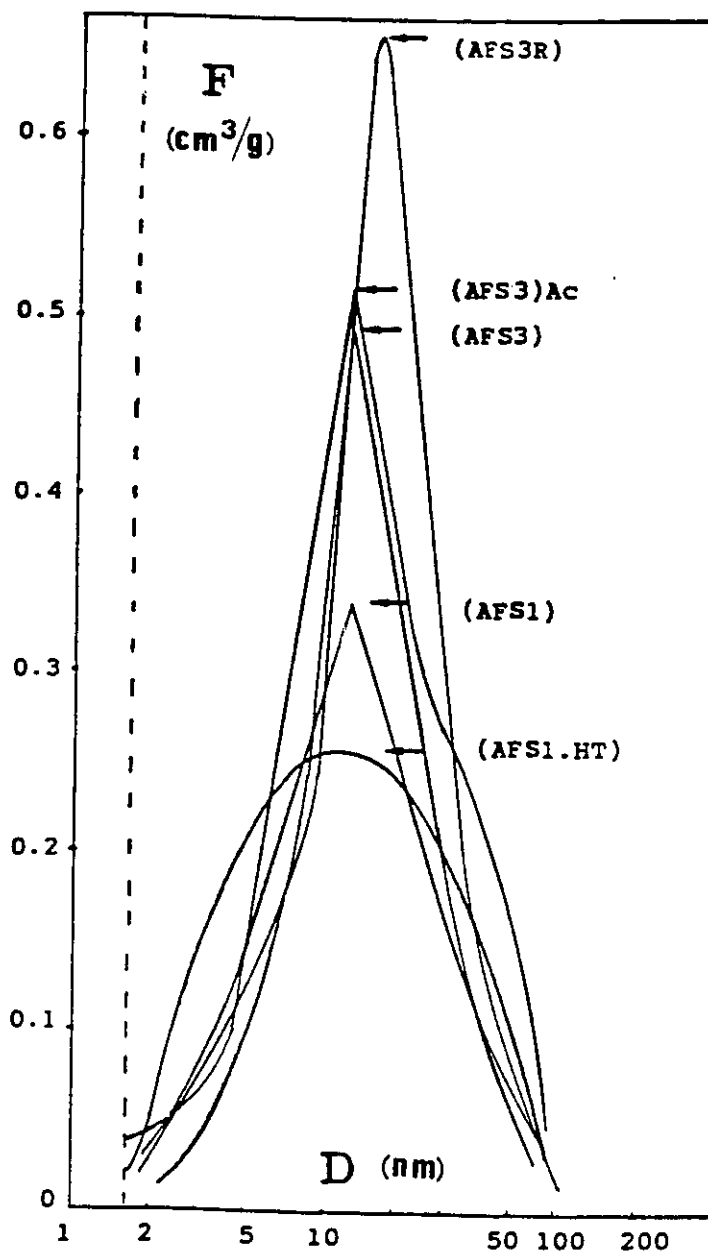
Figure 19: Differential Pore Size Distribution of AFS Treated Samples ($F = dV/dlog(D)$ as a function of the pore diameter D - mesopore region only). V is the pore volume as determined by nitrogen adsorption / desorption technique. The arrows show the function maxima. Ac = activated at 500 °C.

It should be pointed out that Ca^{++} is not affected by this reaction. At 80 °C, this reaction was probably accompanied by some HF evolution due to hydrolysis in water (11); as mentioned in chapter III:

$$(NH_4)_2SiF_6 \rightarrow 2NH_4F + SiF_4$$

$$SiF_4 + 2H_2O \rightarrow SiO_2 + 4HF \tag{4}$$
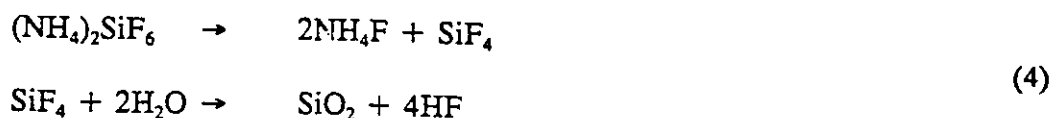
The excess HF can be expected to corrode the walls of the pore and make them collapse, thereby enlarging the pore. Because of the high corrosivity of HF, the reaction was faster (it appears finished in one hour) and more efficient, resulting in the formation of larger pores. In addition, it is restricted to the immediate vicinity of the external of the zeolite particles because the AFS concentration decreases rapidly as one moves inside the bulk of the particles. This phenomenon resulted in solid particles which had a large amount of mesopores and some remaining zeolite - type micropores (Table VII).

The rate of addition of AFS during the preparation had a noticeable effect on the final ceramic powders. As can be seen on Figure 20 and Table VIII, the degree of crystallinity and the Na_2O and Al_2O_3 content decrease with the increasing rate of addition of AFS. The volume of nitrogen adsorbed by the mesopores (Table IX) as well as the volume of n-hexane adsorbed (Table X), and the Si content (Table VIII) increased with the rate of addition AFS.

Figure 21 shows the adsorption / desorption isotherms obtained with two AFS samples reacted at ambient temperature for three hours, one of which was activated at 500 °C. The mesopores formed by the action of AFS on the Ca-A zeolite lattice
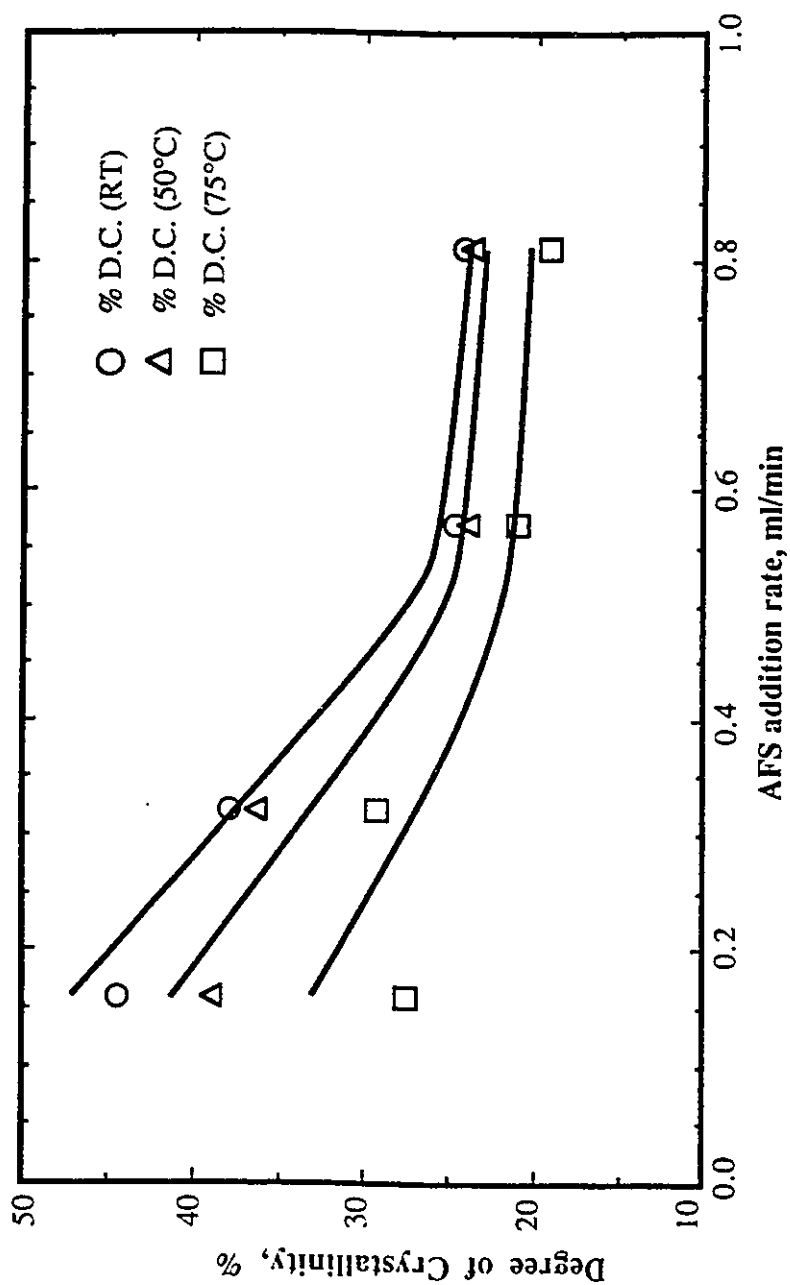
Figure 20: Variation of the Degree of Crystallinity of AFS Samples with Reaction Temperature and Rate of Addition of AFS.

Table VIII: Chemical Composition of AFS Samples

Sample		Chemical composition				Si/Al ratio
Temp.	Rate	CaO	Na$_2$O	Al$_2$O$_3$	SiO$_2$	
°C	ml/min	Wt %	Wt %	Wt %	Wt %	-
-	0.00	15.6	7.2	38.8	38.4	0.84
RT	0.16	14.1	1.0	34.4	50.5	1.25
	0.32	16.3	0.9	31.3	51.5	1.39
	0.57	16.5	0.8	30.9	51.8	1.42
	0.81	13.3	1.1	30.7	54.9	1.52
50	0.16	14.7	0.9	34.0	50.4	1.26
	0.32	14.1	0.7	33.3	51.9	1.32
	0.57	13.7	0.7	32.7	52.9	1.37
	0.81	12.3	0.6	32.7	54.4	1.41
75	0.16	15.8	0.7	36.1	47.4	1.11
	0.32	-	-	-	-	-
	0.57	14.6	1.1	35.6	48.7	1.16
	0.81	13.7	0.7	33.1	52.5	1.34

Table IX: BET Results of AFS Samples

| Sample | | Surface area | Volume of N$_2$ sorbed | | Average pore diameter |
| Temp. | Rate | | Total | Micropore | |
°C	ml / min	m^2 / g	cm^3 / g	cm^3 / g	nm
–	0.00	531	0.258	0.234	< 1.7
RT	0.16	212	0.190	0.051	3.1
	0.32	136	0.265	0.019	7.7
	0.57	138	0.306	0.016	8.0
	0.81	126	0.286	0.013	8.4
50	0.16	74	0.181	0.002	8.9
	0.32	179	0.266	0.040	4.5
	0.32 rep	115	0.187	0.020	4.3
	0.57	165	0.343	0.032	5.9
	0.81	112	0.362	0.010	10.6
75	0.16	85	0.245	0.002	10.0
	0.32	–	–	–	–
	0.57	129	0.386	0.080	7.9
	0.81	141	0.463	0.016	12.2

Table X: Volume of n-Hexane and Water Adsorbed by AFS Samples

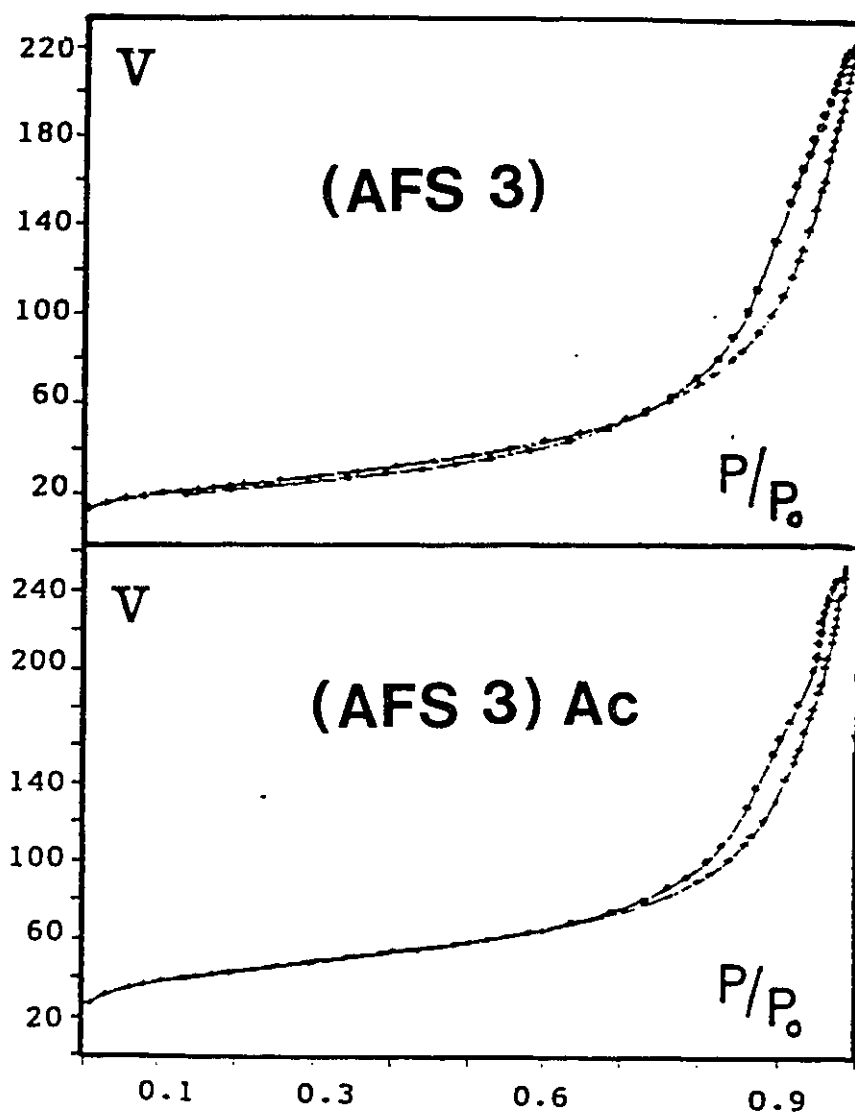| Sample		Volume sorbed		R.A.I.
Temp.	Rate	n-hexane	H₂O	
°C	ml / min	Vol. %	Vol. %	–
–	0.00	9.0	28.1	0.32
RT	0.16	16.4	29.5	0.56
	0.32	13.3	28.8	0.46
	0.57	13.7	30.2	0.45
	0.81	14.3	29.1	0.49
50	0.16	11.8	24.7	0.48
	0.32	12.2	30.4	0.40
	0.57	13.5	30.4	0.44
	0.81	14.0	31.1	0.45
75	0.16	8.3	23.7	0.35
	–	–	–	..
	0.57	–	–	–
	0.81	15.4	30.9	0.50

Figure 21:   Nitrogen Adsorption (+) / Desorption (*)

Isotherms (volume V per unit mass, in cm^3/g

STP, versus relative pressure P/P_o) obtained

with AFS Samples.

Ac = activated at 500 °C.

probably had the shape of open slits.

A bulk density study was also performed on these AFS samples. The bulk density of unreacted Ca-A zeolite could not be measured under its normal pure powder form because it could not be pumped without sample loss, due to its high adsorption properties. This problem was overcome by adding various amounts of bentonite binder and mixing them well together in order to extrudate the powder zeolite, which is not sucked out of the crucible upon evacuation. The results presented in Table XI and on Figure 22a show that the density of the extrudate varies little with the weight percent of bentonite. The small variation is linear up to 30 % weight percent bentonite and allows meaningful extrapolation to 0 % bentonite, i.e. pure zeolite sample. A linear regression of the three points give $\rho = 1.92$ g/cm^3 as the bulk density for pure Ca-A zeolite. This compares well to the theoretical value calculated from the crystal structure ($\rho = 1.96$ g/cm^3). The difference of 2% can be attributed to experimental errors such as imperfect wetting of the sample because of gases trapped inside or between the zeolite particles, which gives a larger volume and therefore, a smaller bulk density result.

It results from the test with unreacted zeolite extrudates that:

* The density increases only very slightly with the amount of bentonite;

* For 10 % weight percent bentonite, the measured density is equal to the theoretical density, this is due to the fact that the slight increase due to the presence of 10 % bentonite cancels out the slight decrease due to imperfect wetting;

* Formation of extrudates eliminates completely the risk of loosing

Table XI: Bulk Density of AFS Samples

Sample		Bulk density				
Rate $\frac{ml}{min}$	Bentonite %	ρ 1 $\frac{g}{cm^3}$	ρ 2 $\frac{g}{cm^3}$	ρ 3 $\frac{g}{cm^3}$	ρ aver. $\frac{g}{cm^3}$	$\frac{\Delta\rho}{\rho}$ %
0.00	10.0	1.99	1.94	1.95	1.96	2.6
	20.5	1.96	1.97	2.00	1.98	2.0
	30.4	2.05	2.01	2.03	2.03	2.0
0.23	10.1	1.93	1.97	1.97	1.96	2.0
0.32	10.4	1.94	1.90	1.92	1.92	2.1
0.57	10.1	1.94	1.95	1.96	1.95	1.0
0.81 (RT)	9.7	1.93	1.95	1.97	1.95	2.1
	21.1	1.95	1.93	1.96	1.95	1.5
	30.4	2.04	2.01	2.02	2.02	1.5
0.81 (50 °C)	11.9	1.95	1.99	2.00	1.98	2.5
	20.8	2.01	2.01	1.97	2.00	2.0
	30.7	2.01	1.99	1.98	2.00	1.5
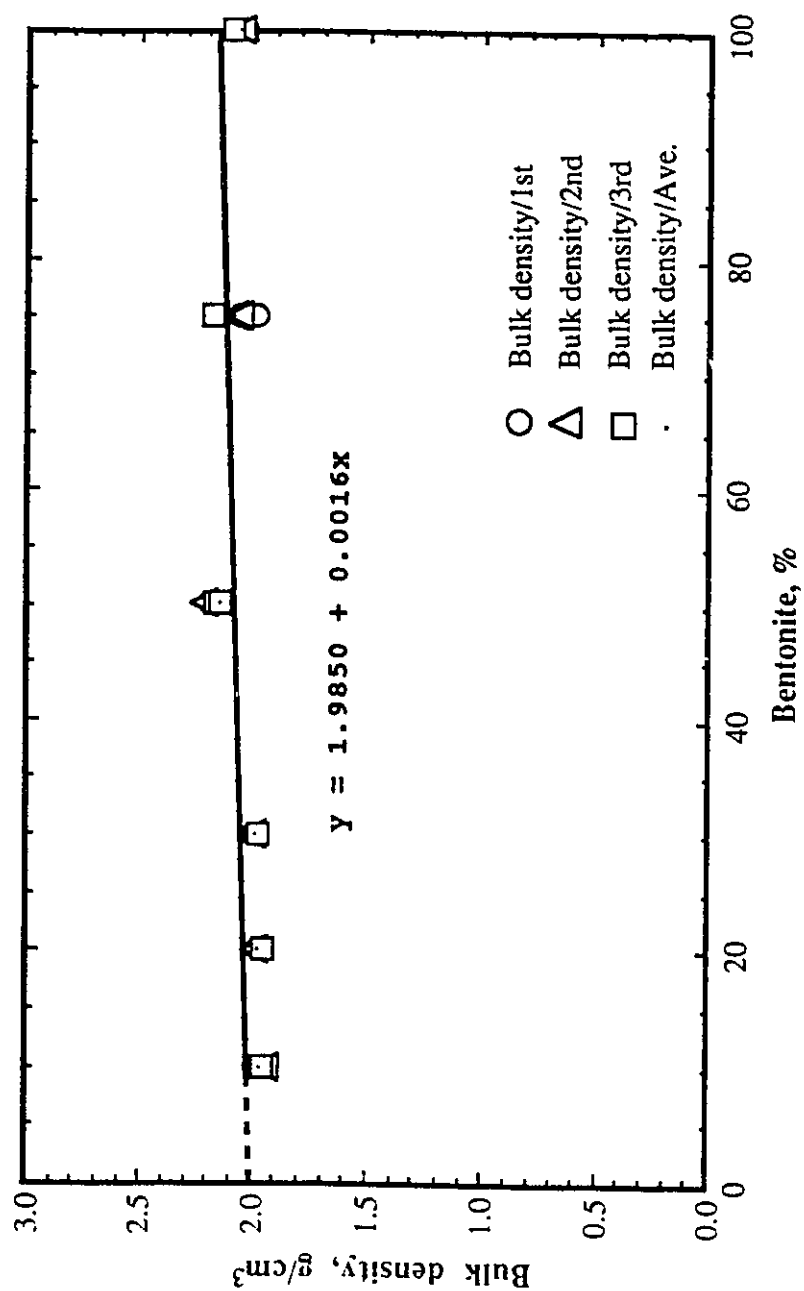
Figure 22a: Bulk Density of Extrudates of Ca - A Zeolite versus the Amount of Bentonite.
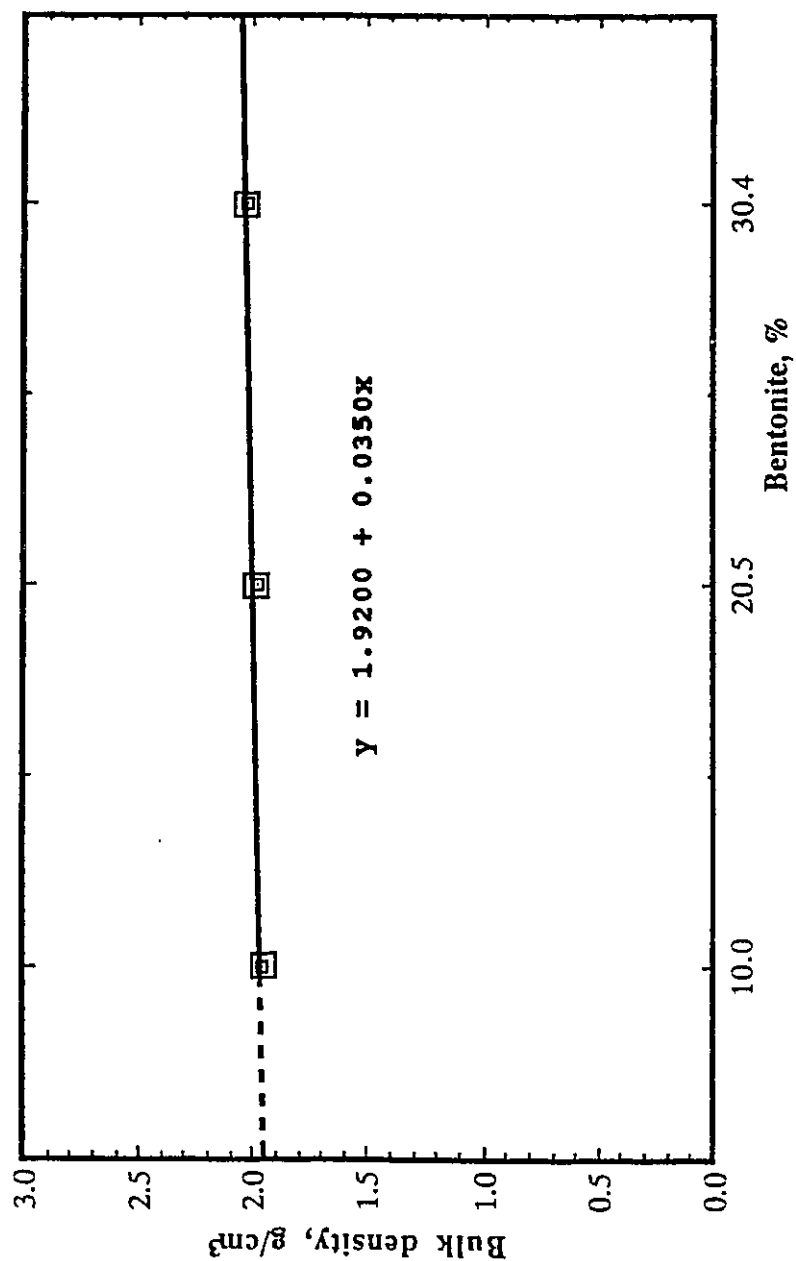
Figure 22b: Bulk Density of extrudates of Ca - A Zeolite versus the Amount of bentonite.
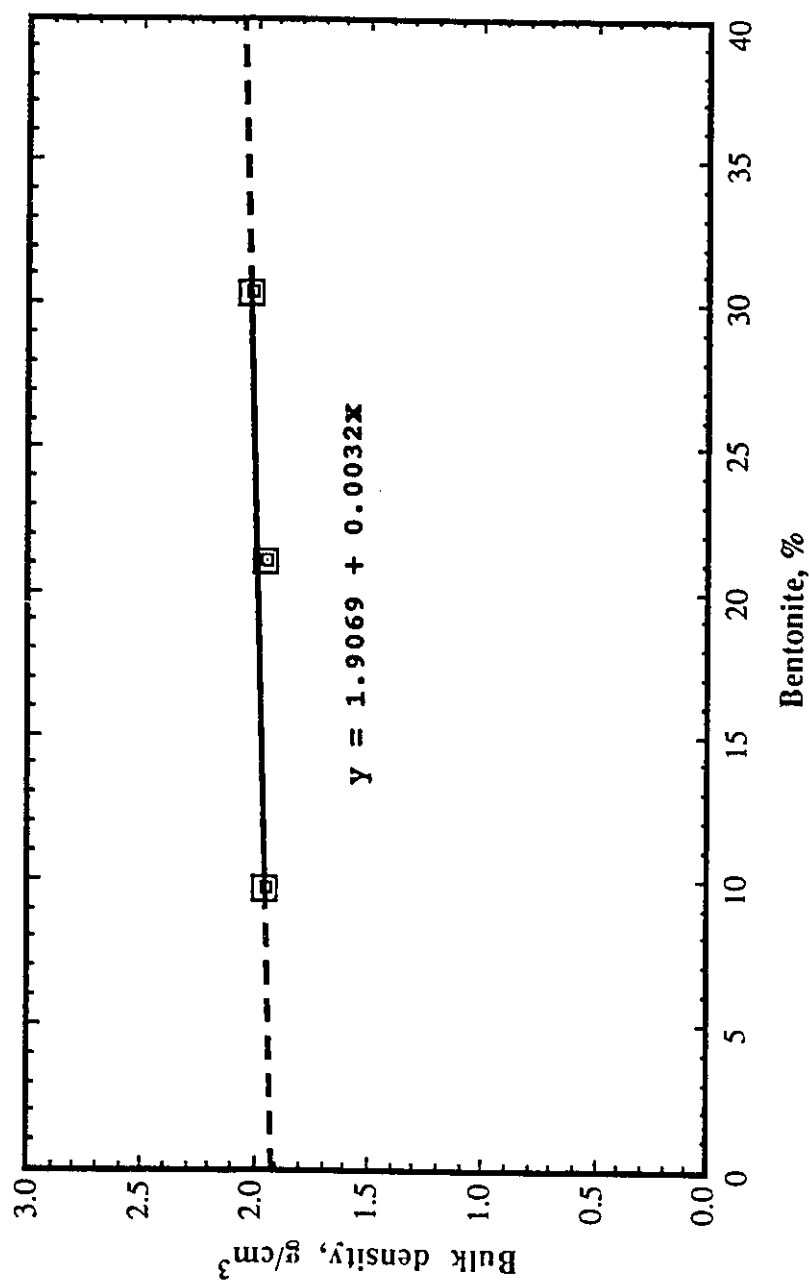
y = 1.9069 + 0.0032x

Figure 22c: Bulk Density of Extrudates of Ca - A Zeolite Treated with AFS (0.81 ml/min) at RT versus the Amount of Bentonite.
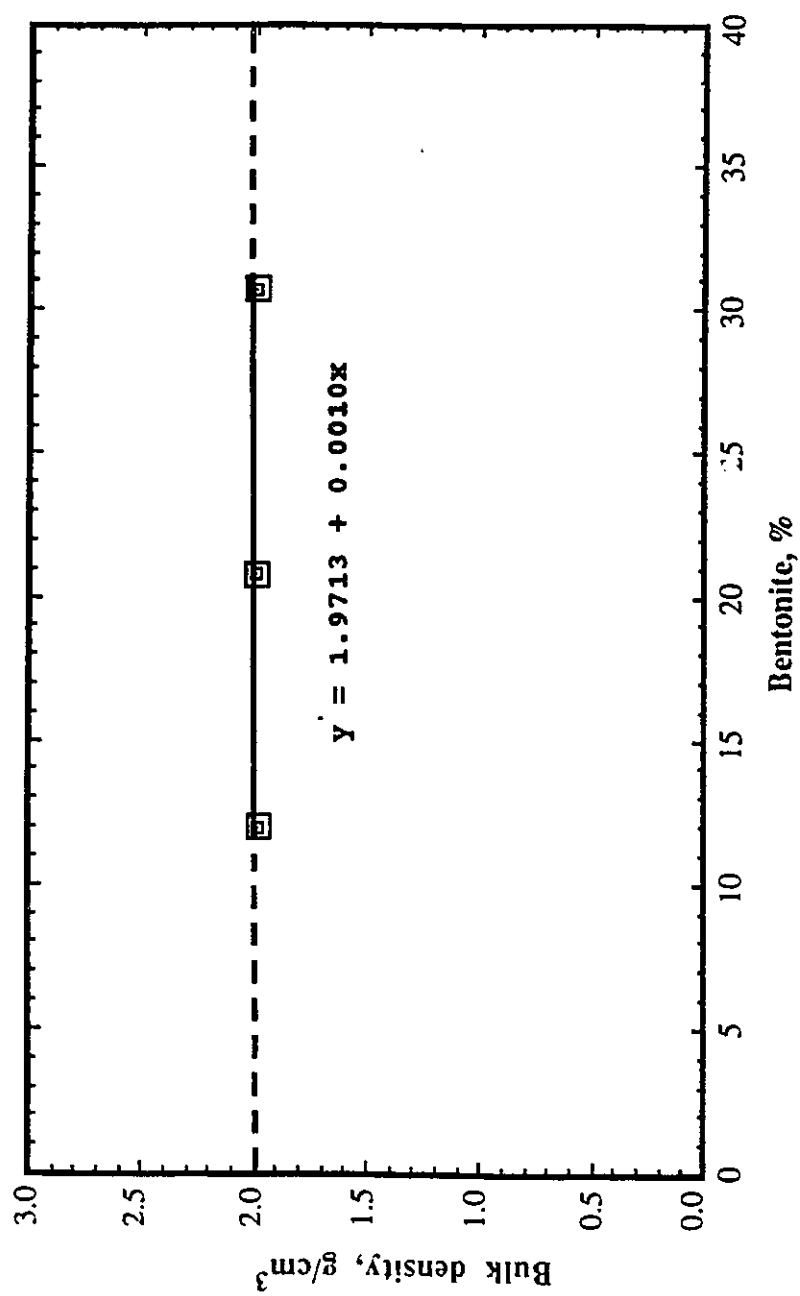
Figure 22d: Bulk Density of Extrudates of Ca - A Zeolite Treated with AFS (0.81 ml/min) at 50°C versus the Amount of Bentonite.

sample when evacuating the samples during measurements;

* Measurements are highly reproducible since the maximum relative difference between three measurements per sample is usually not higher than 2 %, which is the accepted precision for the method (31), (Table XI).

The above validates the technical approach. Therefore, all the measurements presented on Table XI were carried out on extrudates and the value obtained for 10 % weight percent bentonite (average density values of three measurements) was taken as equal to the bulk density of the pure sample.

It can be seen from Table XI that, all the samples have a density in the range of 1.92 to 1.98 g/cm³. This gives an average density of 1.95 ± 0.03 g/cm³, with 3 % difference between the two extreme values. This difference can be considered close enough to the experimental error (usually ca. 2 %), such that we can say that there is no measurable difference in the bulk density of the samples versus the reaction conditions.

Reaction of the zeolite with AFS can be expected to results in the following changes of bulk density:

* Removal of Na^+ ions and their replacement with H_3O^+, with no change of porosity: decrease of density;

* Increase of porosity due to the formation of mesopores: decrease of density if CCl_4 does not penetrate the pores. Otherwise, the formation of large pores should have little effect on the bulk density.

* Rearrangement of the aluminosilicate framework upon Al/Si substitution and collapse of walls between micropores to give mesopores: this would most likely result in a decrease of the total pore volume and

therefore the density would increase.

* Production of non-crystalline material: the density of the mixture remaining transformed zeolite / amorphous material will be equal to the weighed average of the densities of the solid components.

Since no significant change of density occur, it is most likely that the decrease of density due to loss of Na^+ is compensated for by the density of the amorphous product(s) formed. X-ray diffraction shows no shift of the Bragg peaks of zeolite, which rules out a partial collapse of the framework.

For the study of the Si environment by NMR, the spectra of samples of pure Ca-A zeolite, AFS (0.32 RT) and AFS (0.57 RT) were recorded. Let us consider first the ^{29}Si-NMR results. As shown in Figure 23, one sharp peak signal is observed at -90 ppm for unreacted Ca-A zeolite (39). Since the Si/Al ratio of pure Ca-A zeolite is one, the signal must be uniform in any direction (isotropic) which results, in a very clear and sharp peak.
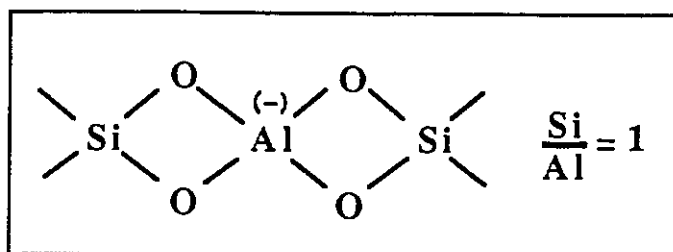
On the contrary, for the Na-Y zeolite, with a Si/Al ratio of 2.61, different chemical environments give several peaks, each corresponding to a particular environment around Si (Figure 24, (39)). A stronger magnetic field increases the separation between the peaks and therefore should yield a better resolution, this is at least in part cancelled by
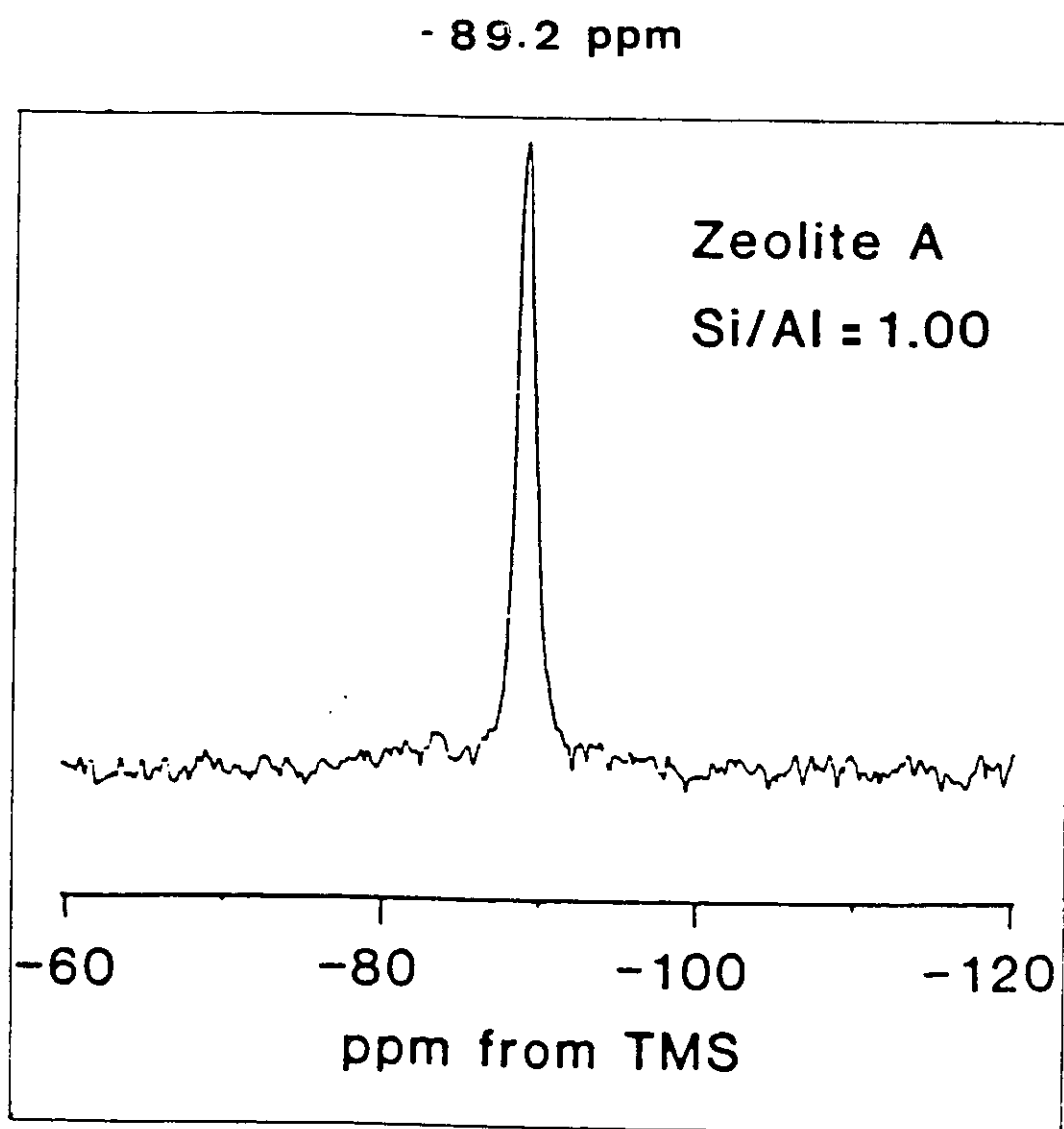
-89.2 ppm

Figure 23: ^{29}Si-MAS-NMR Spectrum of Zeolite Na-A at 79.80 MHz (39).
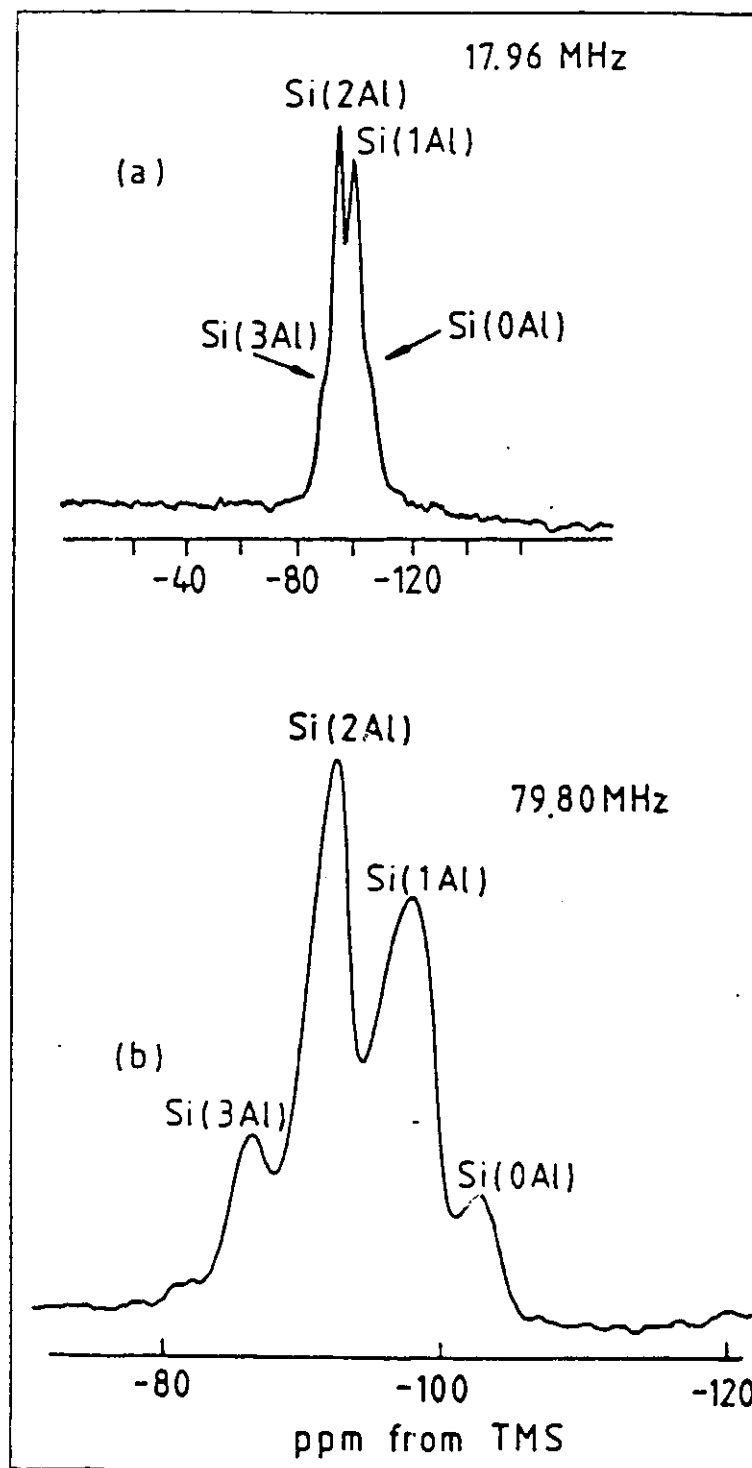
Figure 24: ^{29}-Si-Mas-NMR Spectra of Zeolite Na-Y (Si/Al = 2.61) at Two Magnetic Fields: (a) 17.96 MHz Spectrum, (b) 79.80 MHz Spectrum (39).

the fact that a stronger field also increases the line width. When treated with AFS, the Si environment is no longer the same as the one of unreacted Ca-A zeolite, i.e. some Si are not anymore surrounded by four Al, but (4-x)Al where $1 < x < 4$. Altering of the Si/Al ratio results in many overlapping peaks, and the sum of these gives one broader signal. By deconvolution, we can observe the presence of different peaks (Figures 25).

^{27}Al-NMR was also used in order to study the environment of aluminum. According to the large typical signal at 50 ppm of the ^{27}Al-NMR spectra, we can conclude that the Al which constitutes the framework is in tetrahedral form, as compared to the smaller peak of octahedral form at -25 ppm (40, 41, 42). We can also observe the presence of an impurity line at 80 ppm, which would cause the decrease of the Si/Al ratio of pure Ca-A zeolite from 1 to 0.84 (Table VIII). Even though the octahedral/tetrahedral peak area ratio of the samples treated with AFS is larger than that of unreacted Ca-A zeolite (3.19% versus 2.61% respectively), the major peak signal is still the one for tetrahedrally coordinated Al, and therefore, the tetrahedral coordination remains predominent after the treatment; however there is slight increase of octahedrally coordinated Al.

This shows that our work was successful since we managed to enlarge the pore size of the zeolite and this, without damaging the zeolite framework, since most of the remaining Al is still in tetrahedral coordination. Any further treatment just removed the octahedral Al species formed upon AFS treatment.

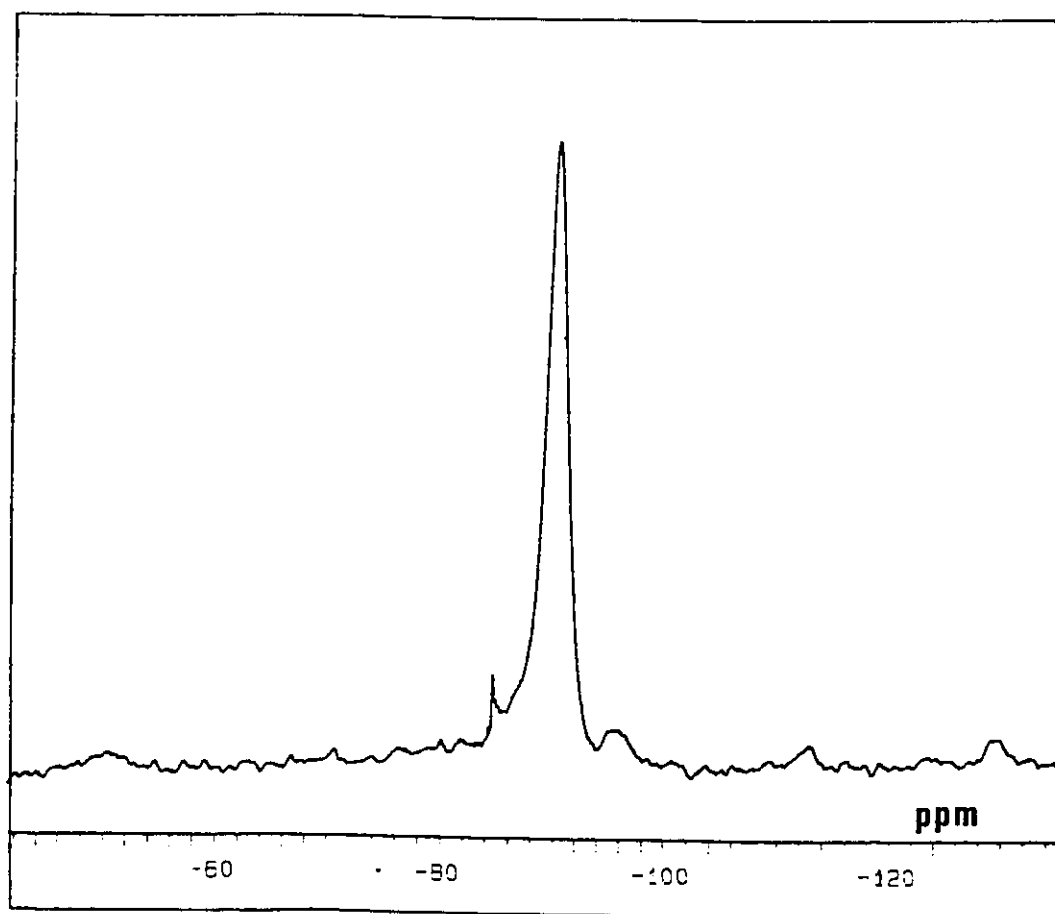**Figure 25a.1:** ^{29}Si-MAS-NMR Spectra of Untreated Ca-A Zeolite Samples.
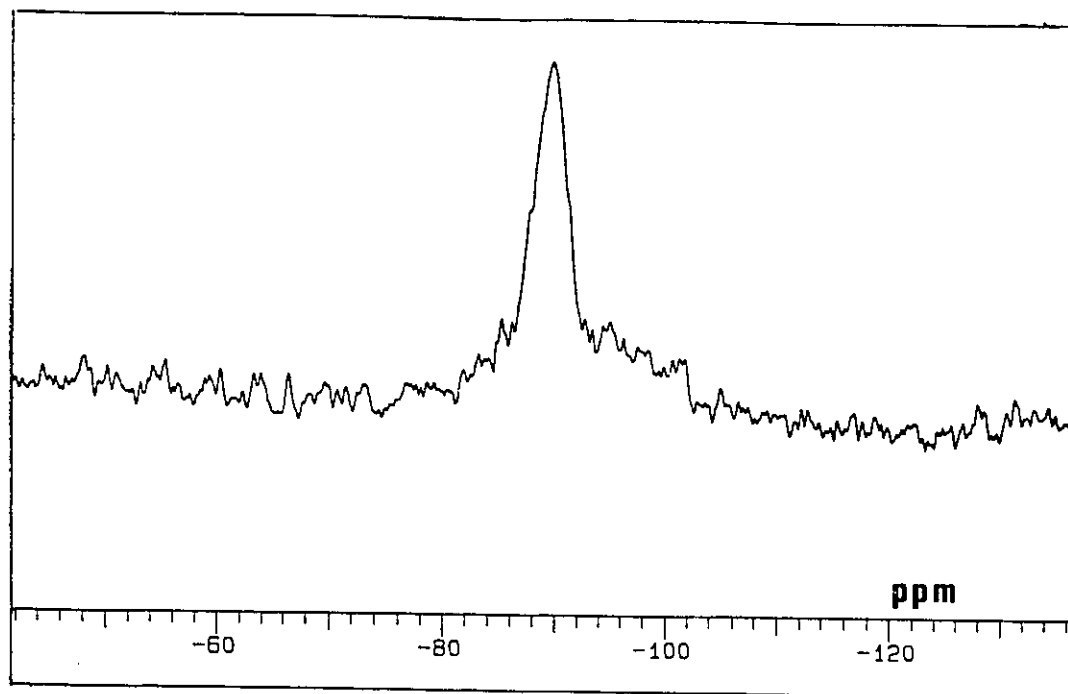
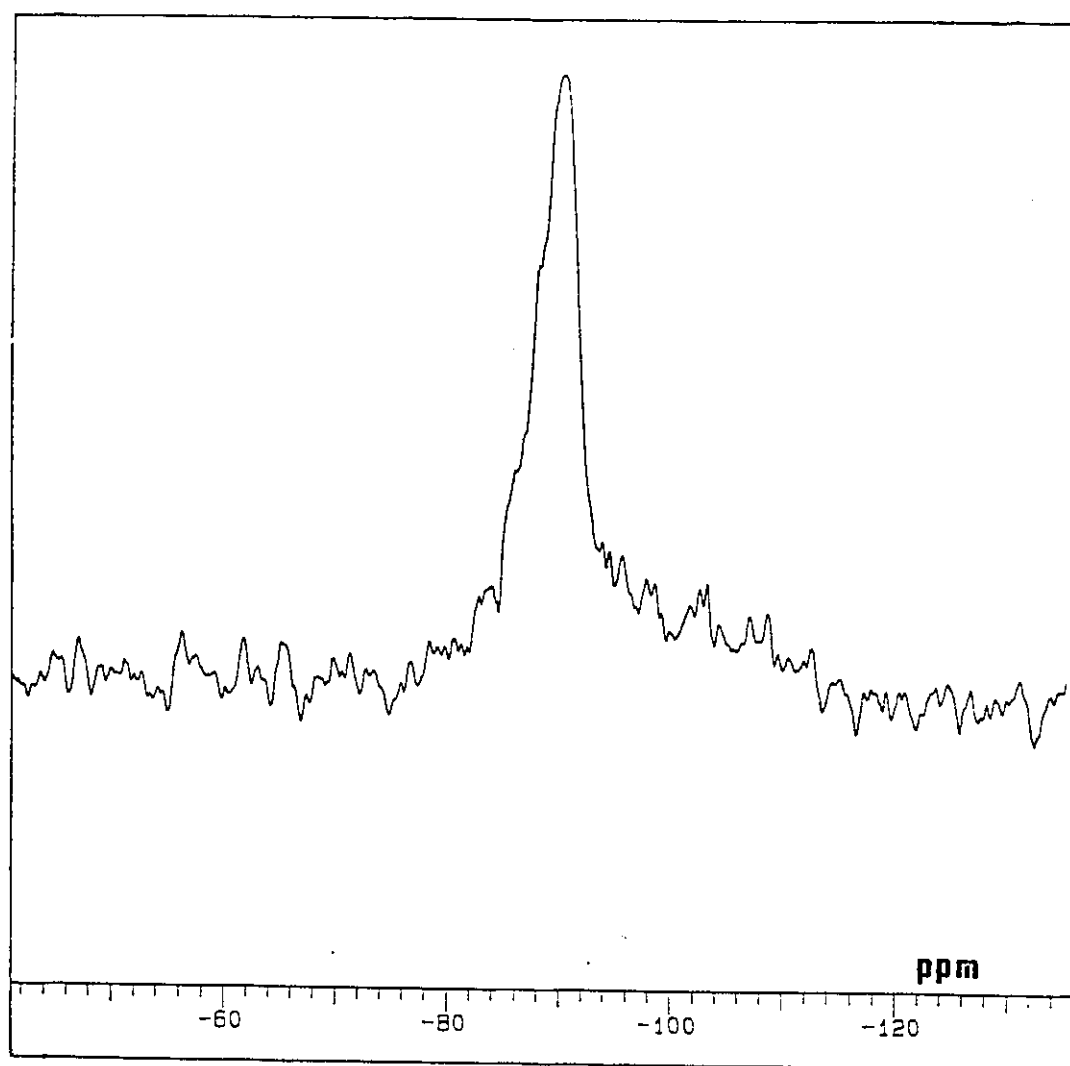Figure 25a.2: ^{29}Si-MAS-NMR Spectra of AFS(0.32)RT Samples.

Figure 25a.3: ^{29}Si-MAS-NMR Spectra of AFS(0.57)RT Samples.
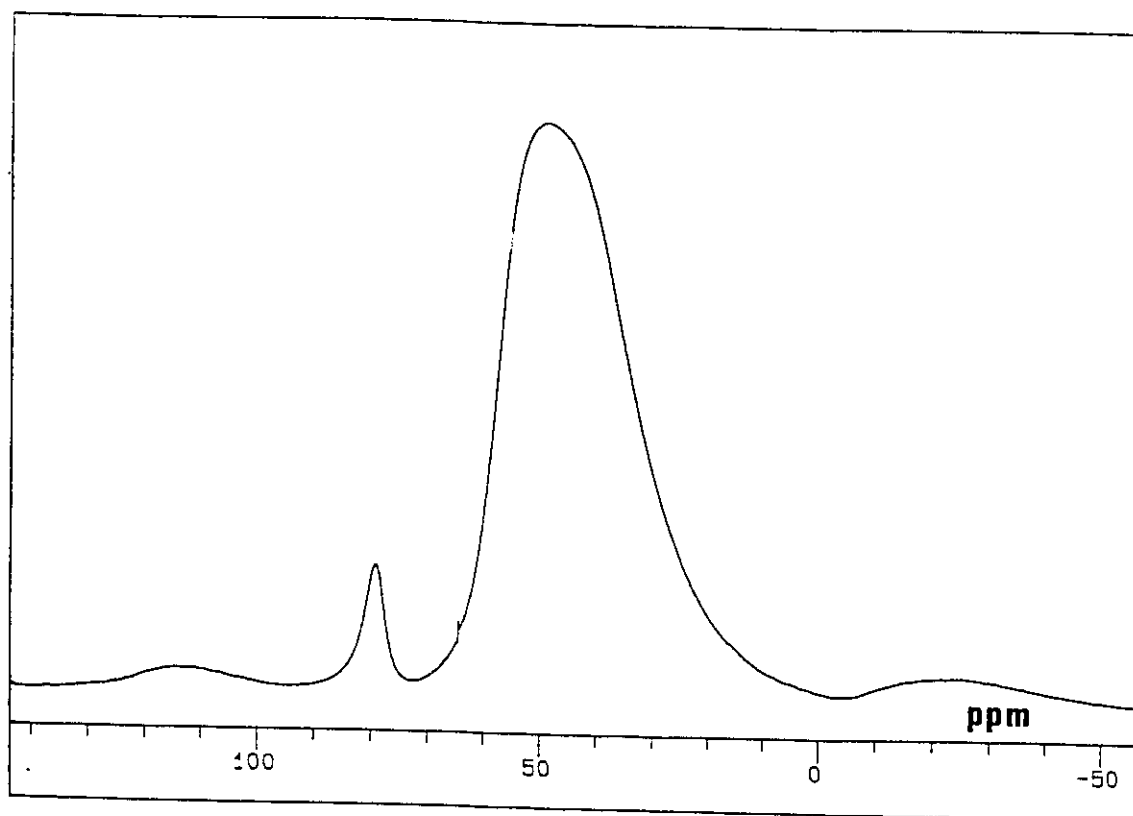
Figure 25b.1: ^{27}Al-MAS-NMR Spectra of Untreated Ca-A Samples.
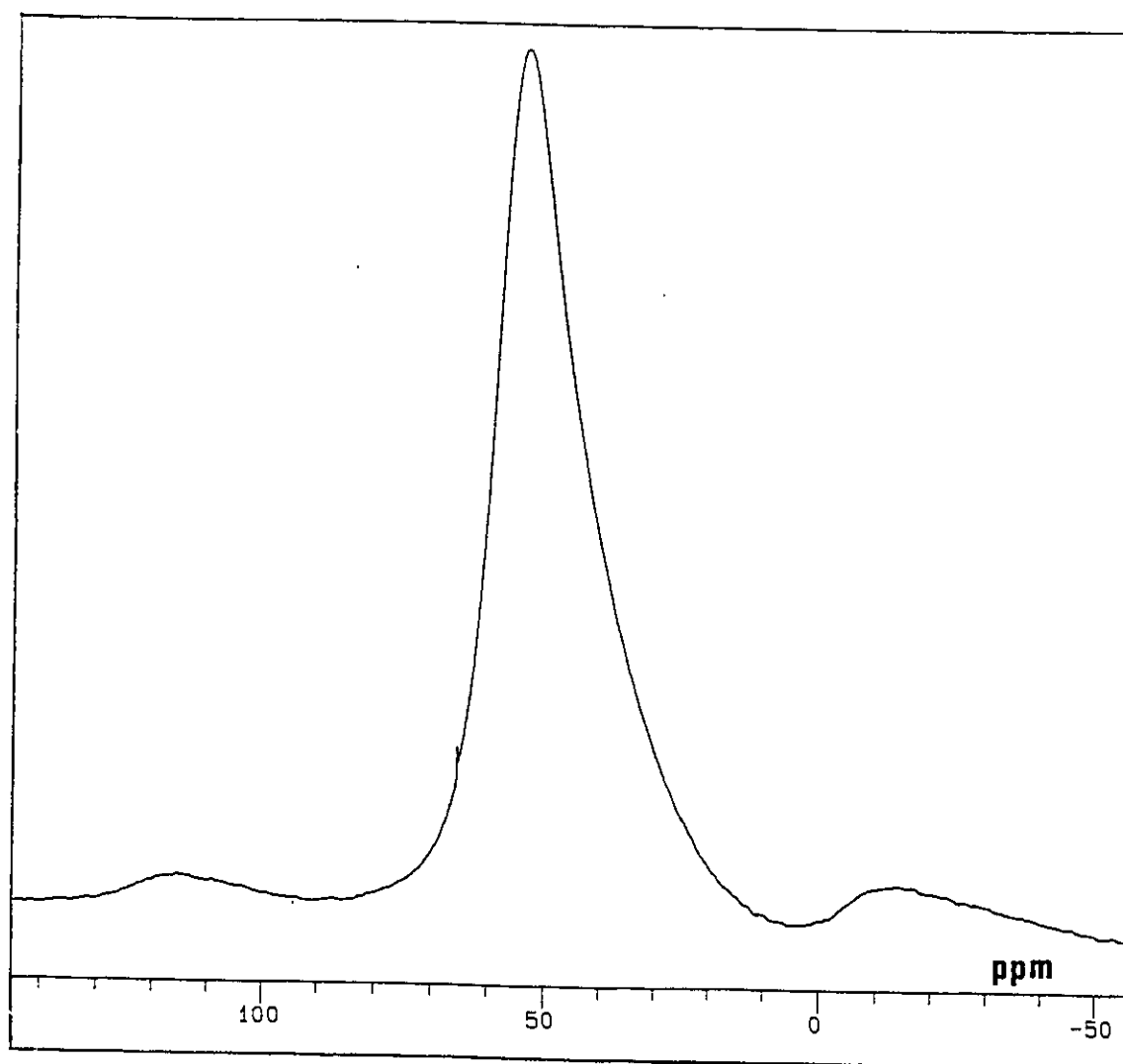
Figure 25b.2: ^{27}Al-MAS-NMR Spectra of AFS(0.32)RT Samples.
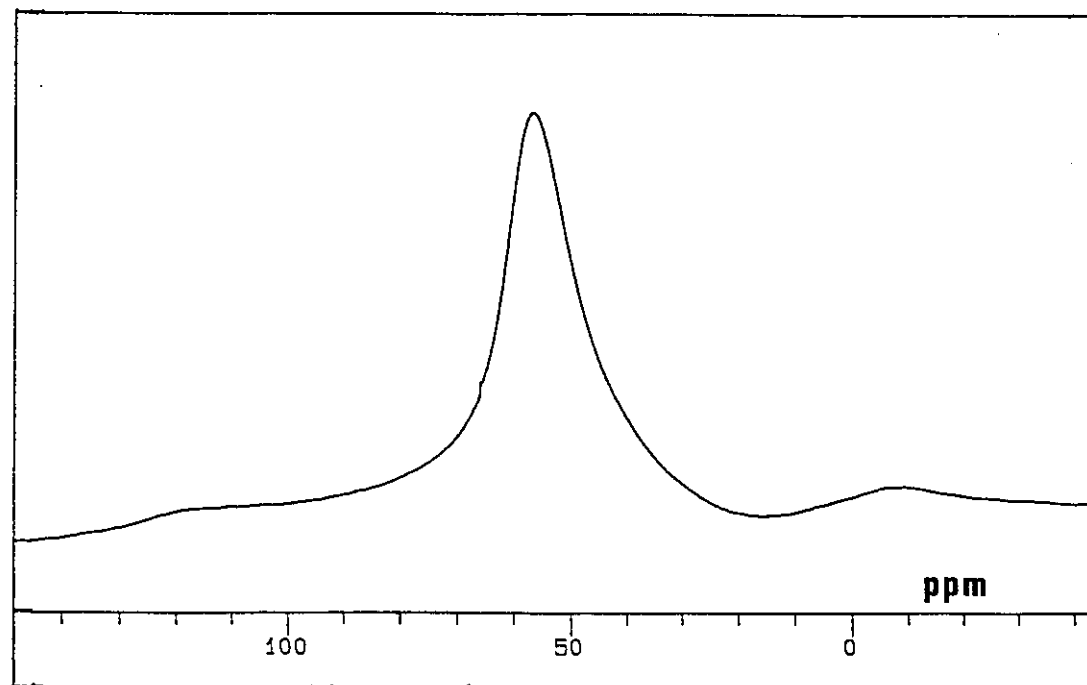
Figure 25b.3: ^{27}Al-MAS-NMR Spectra of AFS(0.57)RT Samples.

iv).   "Two - Step Procedure" Treatments

When the hydrothermally treated solids were submitted to an additional mild acid leaching, the sorptive properties of the solids were restored. This means that the acid treatment had succeeded in removing the silicon and aluminum species previously displaced from the zeolite framework by the combined action of steam and high temperature (43). Indeed, all HTA materials obtained by subsequent acid leaching of the HT solids with an aqueous solution of 0.2N HCl, exhibited much higher sorption capacities for nitrogen, water and n-hexane, than the HT materials (Figure 26, Tables XII).

The plots of the pore size distribution of three HTA materials are shown in Figure 27. The mesopores of these samples have practically the same size as the corresponding ones found in the acid treated material (Figures 17 & 27), which suggest that the pore enlargement by hydrothermal treatment might follow the same pathway as the acid treatment. The practically constant values of the Si / Al ratio, however, indicate that the hydrothermal treatment involved an undiscriminating extraction of Si and Al species from the framework rather than a selective dealumination as in the case of the mild acid treatment. Figure 28 shows the adsorption / desorption isotherms obtained with some HTA samples. The shape of the hysteresis loops suggests once again, the presence of slit-shaped mesopores.

Some studies on the hydrothermally treated solids with AFS, HTA materials with AFS or even AT samples with AFS were performed (Tables XII). It seems that the more we treat our samples, the more pore size enlargement we will get, especially with any AFS treatment. One should note the remarkable decrease of Na_2O content and increase
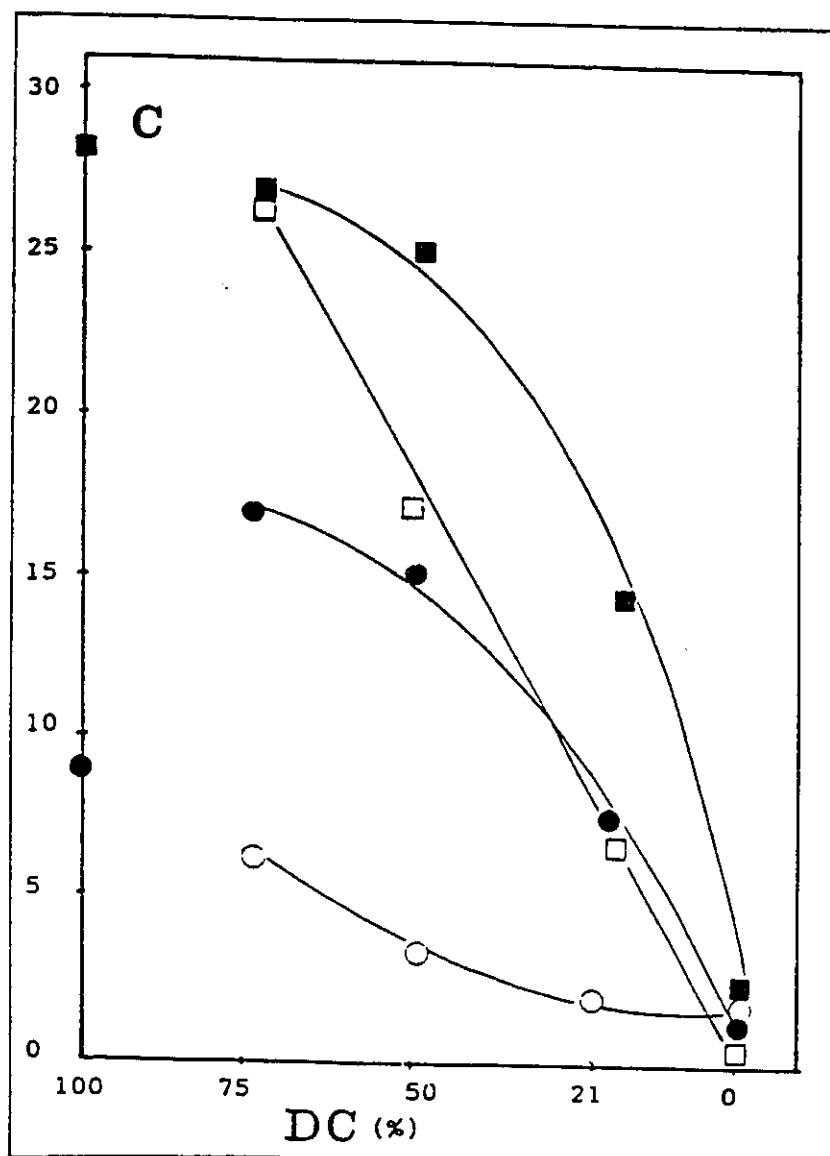
Figure 26: Adsorption Capacities C, Expressed in $cm^3/100g$, for Water ($\square$ = HT samples; ■ = HTA samples) and n-Hexane (O = HT samples; ● = HTA samples) Versus the Degree of Crystallinity (D.C.). Data reported for D.C. = 100 % are related to the parent Ca-A zeolite.

Table XIIa: Degree of Crystallinity of Samples Prepared Using the "Two – Step Procedure"

Conditions	Starting D.C.		Final D.C.
hr	%		%
AFS3	76.3		39.0
	50.2		25.0
AT(2, AFS3)	76.3		23
AT(0.5, AFS3)	100		15
AT(1, AFS3)			22
AT(2, AFS3), 700°C			6

Table **XIIb**: BET Results of Samples Prepared Using the "Two - Step Procedure"

Conditions	Starting sample	Surface area	Volume of N_2 sorbed		Aver. pore diameter
			Total	MP	
hr	% D.C.	m^2 / g	cm^3 / g	cm^3 / g	nm
AT3	100	318	0.171	0.108	1.7
	76.3	275	0.155	0.099	1.7
	50.2	261	0.193	0.097	1.8
	21.0	85	0.109	–	5.2
	0.0	13	0.016	–	4.6
AFS3	100	112	0.314	0.001	11.2
	76.3	245	0.442	0.055	4.9
	50.2	151	0.470	0.007	12.8
(500°)	100	154	0.397	0.012	9.2
AT(2, AFS3)	100	120	0.414	0.006	12.2
	76.3	188	0.270	0.032	4.0
AT(0.5, AFS3)	100	184	0.397	0.028	7.7
AT(1, AFS3)		133	0.411	0.005	11.3
AT(2, AFS3)		120	0.414	0.006	12.2
AT(2, AFS3), 400°C		152	0.440	0.016	10.1
AT(2, AFS3), 500°C		140	0.484	–	12.0
AT(2, AFS3), 700°C		77	0.332	–	16.1
AT(3, AFS3)		124	0.331	0.010	10.0
AT(12, AFS3)		108	0.131	0.004	3.6

Table XIIc: Volume of n-Hexane and Water Adsorbed of Samples Prepared Using the "Two - Step Procedure"

Conditions	Starting samples	Volume adsorbed		R.A.I.
hr	% D.C.	n-hexane Vol. %	H_2O Vol. %	-
AFS3	100	14.6	36.2	0.40
	76.3	10.4	26.1	0.40
	50.2	7.7	22.7	0.34
AT(2, AFS3)	100	5.0	21.6	0.24
	76.3	8.3	29.0	0.29
AT(0.5, AFS3)	100	11.7	29.2	0.40
AT(1, AFS3)		9.4	29.2	0.33
AT(2, AFS3)		5.0	21.6	0.24
AT(2, AFS3), 400°C		4.7	16.5	0.29
AT(2, AFS3), 500°C		5.6	18.0	0.31
AT(2, AFS3), 700°C		4.7	13.5	0.35
AT(3, AFS3)		3.8	21.2	0.18

Table **XIId**: Chemical Composition of Samples Prepared Using the "Two - Step Procedure"

Conditions	Sam-ple	Chemical composition				Si/Al ratio
		CaO	Na$_2$O	Al$_2$O$_3$	SiO$_2$	
hr	%D.C.	Wt.%	Wt.%	Wt.%	Wt.%	-
AT0	0.0	14.4	6.5	36.4	42.7	1.00
	21.0	13.4	6.0	34.5	46.1	1.13
	50.2	15.4	7.5	37.1	40.0	0.91
	76.3	14.0	6.7	38.2	41.1	0.91
	100.0	15.6	7.2	38.8	38.4	0.84
AT3	0.0	14.7	6.3	36.7	42.3	0.98
	21.0	12.7	4.7	39.3	43.3	0.93
	50.2	13.7	4.2	37.2	44.9	1.03
	76.3	13.5	4.0	38.4	44.1	0.97
	100.0	12.2	2.8	35.2	49.8	1.20
AT6	100.0	7.6	1.2	39.4	51.8	1.11
AT9		3.0	0.3	42.5	54.2	1.09
AT12		2.2	0.1	36.6	61.1	1.41
AFS3	50.2	8.3	1.2	16.3	74.2	3.86
	76.3	12.0	2.3	28.4	57.3	1.71
	100.0	14.7	1.3	31.4	52.6	1.42
AT(2, AFS3)	76.3	11.6	2.6	27.6	58.2	1.79
	100.0	12.3	0.6	30.4	56.7	1.58
AT(0.5, AFS3)	100.0	9.5	0.4	29.9	60.2	1.71
AT(1, AFS3)		13.1	0.7	30.5	55.7	1.55
AT(2, AFS3)		12.3	0.6	30.4	56.7	1.58
AT(2, AFS3), 400°C		-	-	-	-	-
AT(2, AFS3), 500°C		-	-	-	-	-
AT(2, AFS3), 700°C		12.1	0.4	30.6	56.9	1.58
AT(3, AFS3)		11.3	0.6	32.3	55.8	1.47
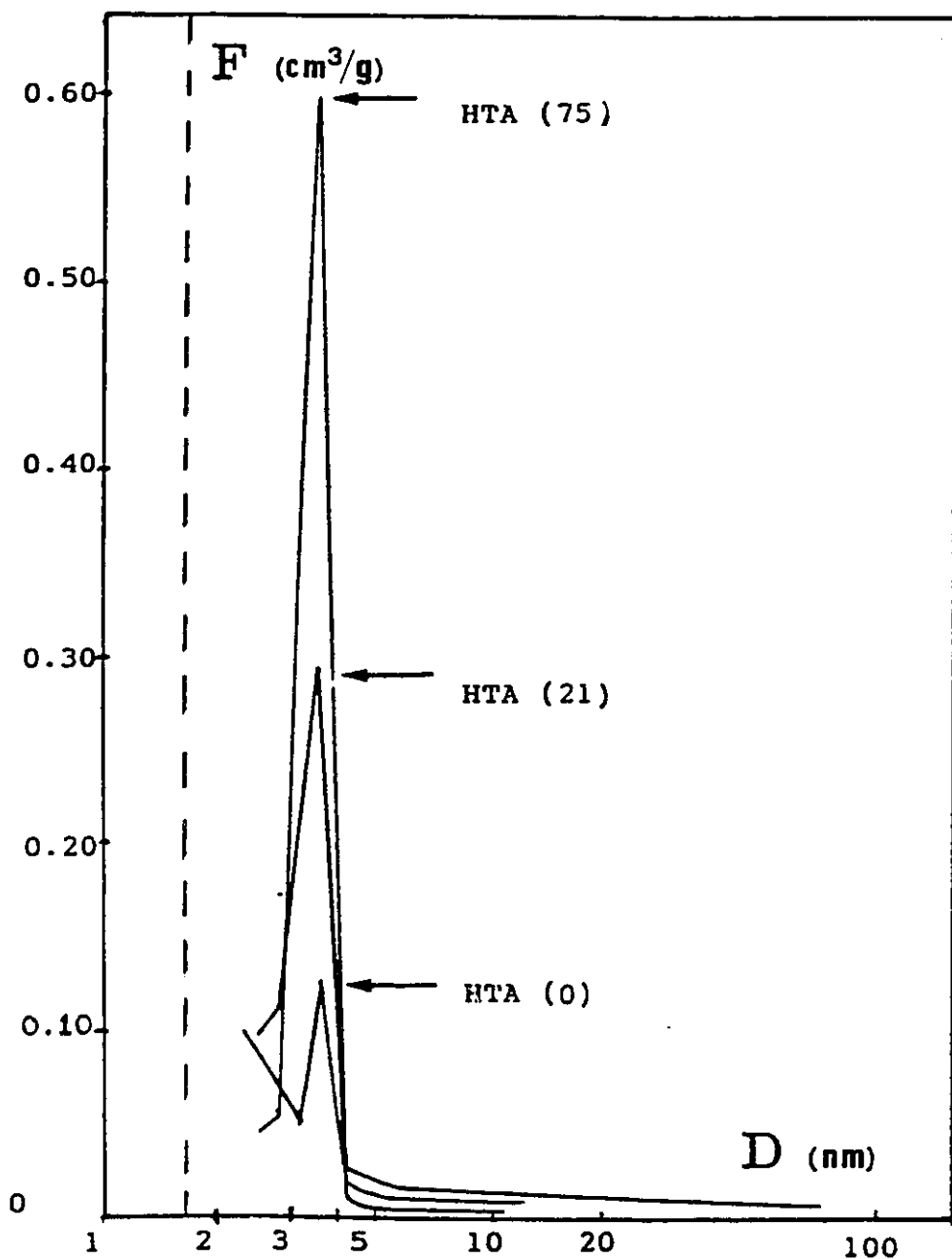
Figure 27:   Differential Pore Size Distribution of HTA
               Samples (F = dV/dlog(D) as a function of the
               pore diameter D - mesopore region only).
               V is the pore volume as determined by nitrogen
               adsorption / desorption technique. The arrows
               show the function maxima.
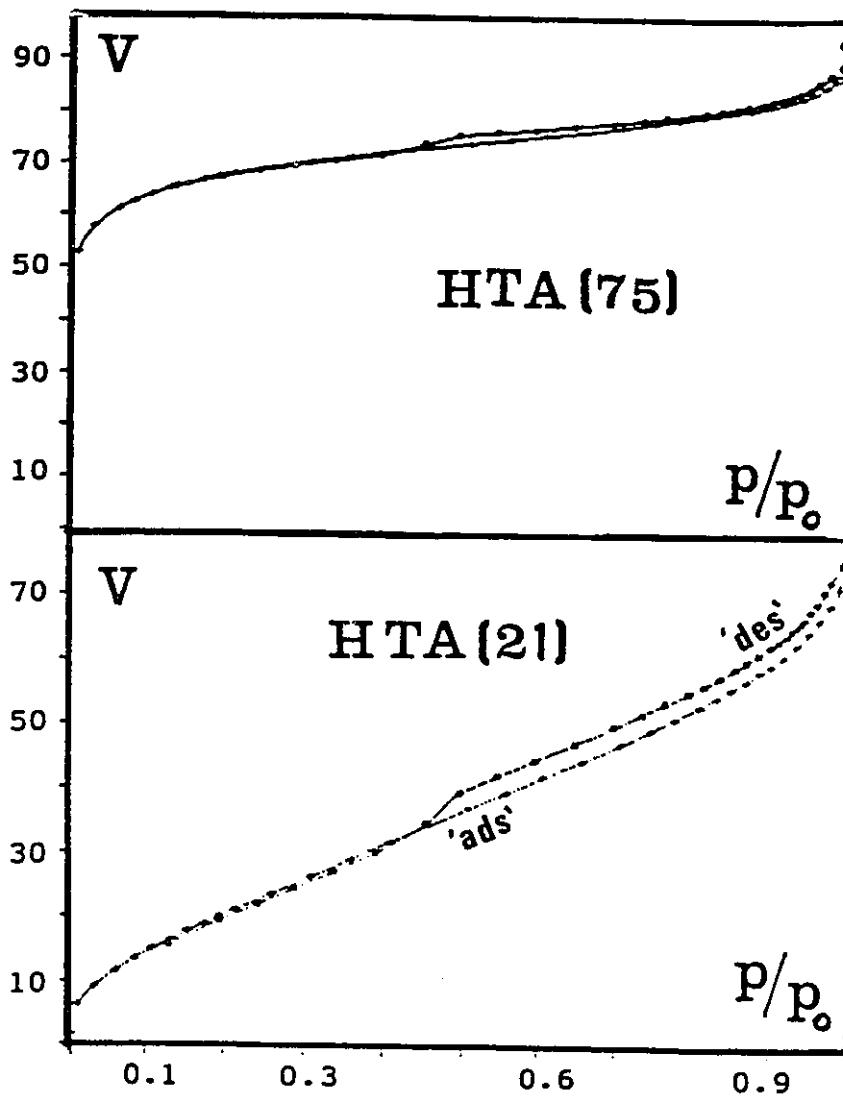
Figure 28: Nitrogen Adsorption (+) / Desorption (*) Isotherms (volume V, in cm^3/g STP, versus relative pressure (P/P_o) obtained with HTA Samples.

of SiO_2 accordingly with the high volume of sorbed N_2 by mesopores, in the case of the zeolite treated first with HCl and then by AFS (Tables XIIb and XIId).

Figure 29 summarizes the pore enlargement by various treatments, whereas Figures 30 represent the X-ray diffraction patterns of some treated samples as compared to the untreated Ca-A zeolite.
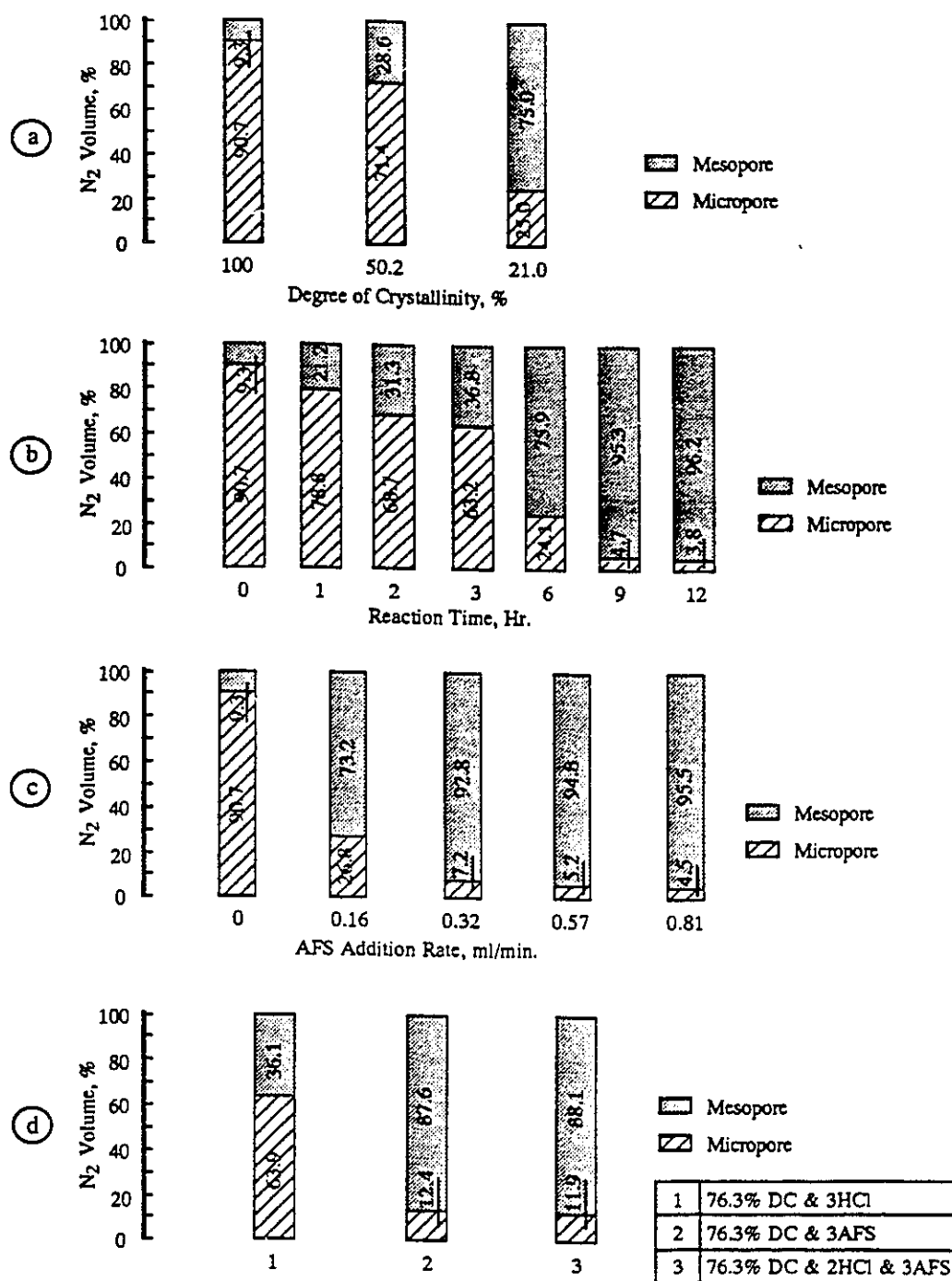
Figure 29: Percentage Volume of Nitrogen Sorbed
by Micropore and Mesopore.
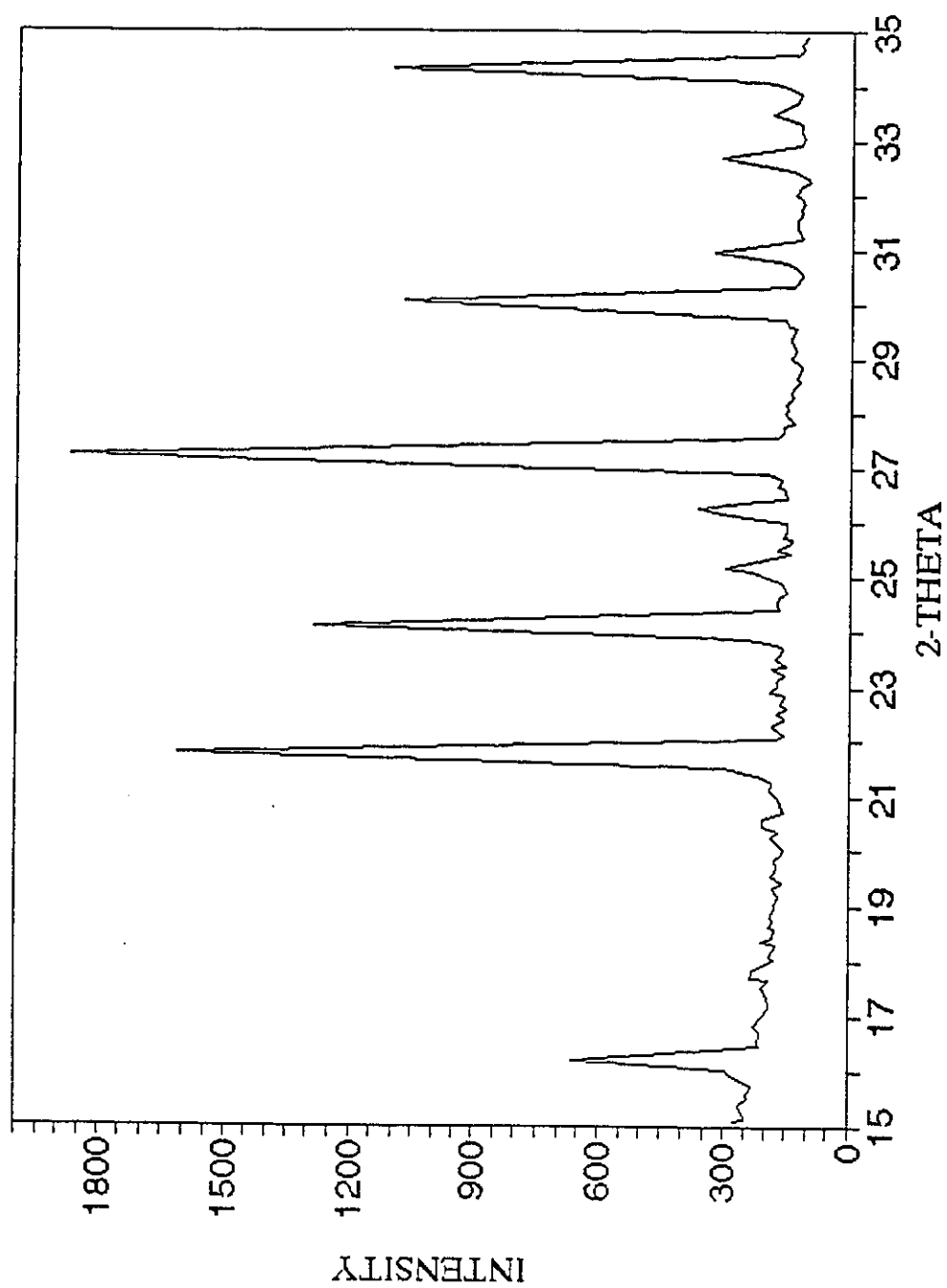
Figure 30a: X-Ray Diffraction Pattern of Untreated Ca-A
Zeolite.
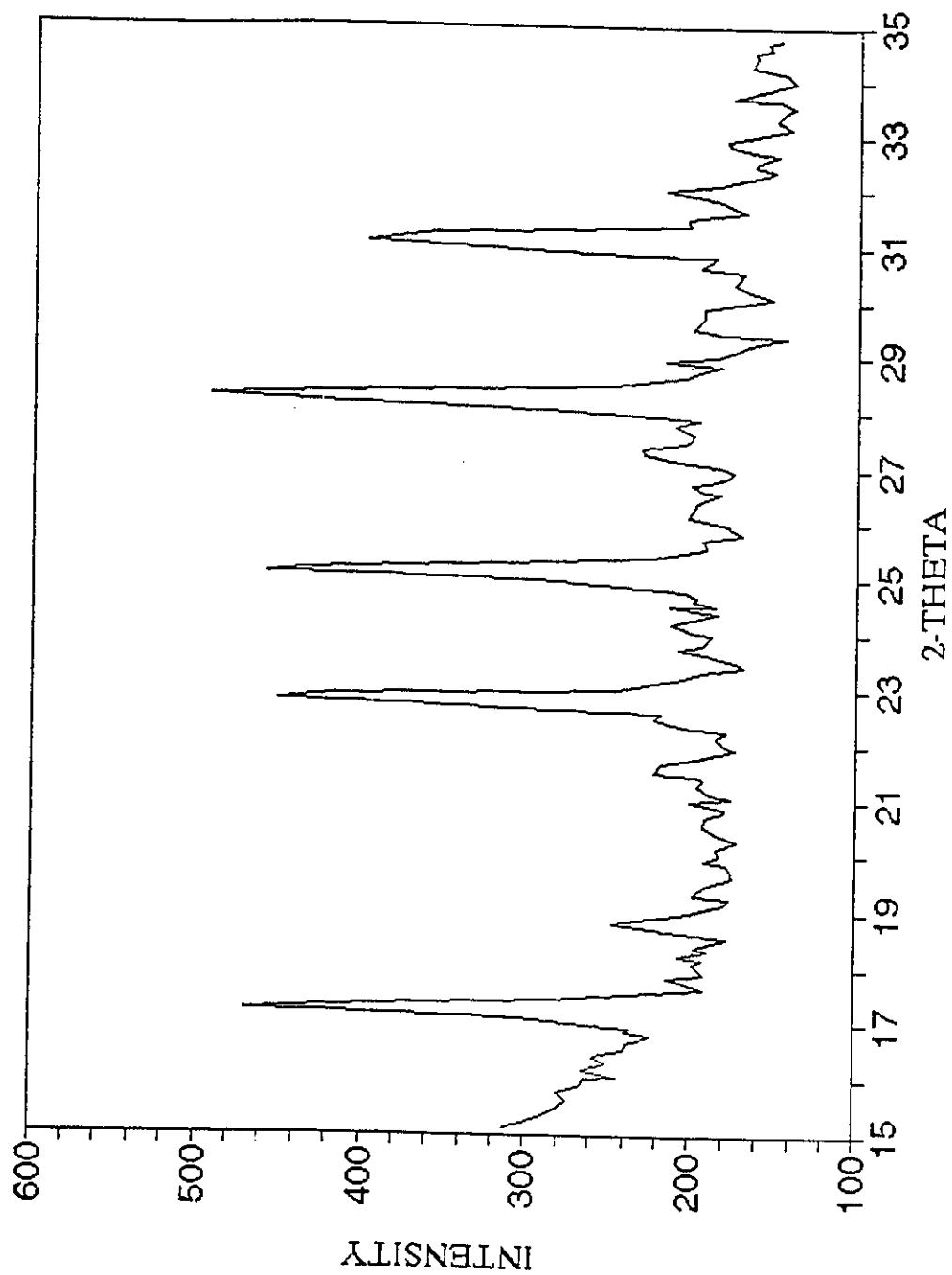
Figure 30b: X-Ray Diffraction Pattern of HT(21) Sample.
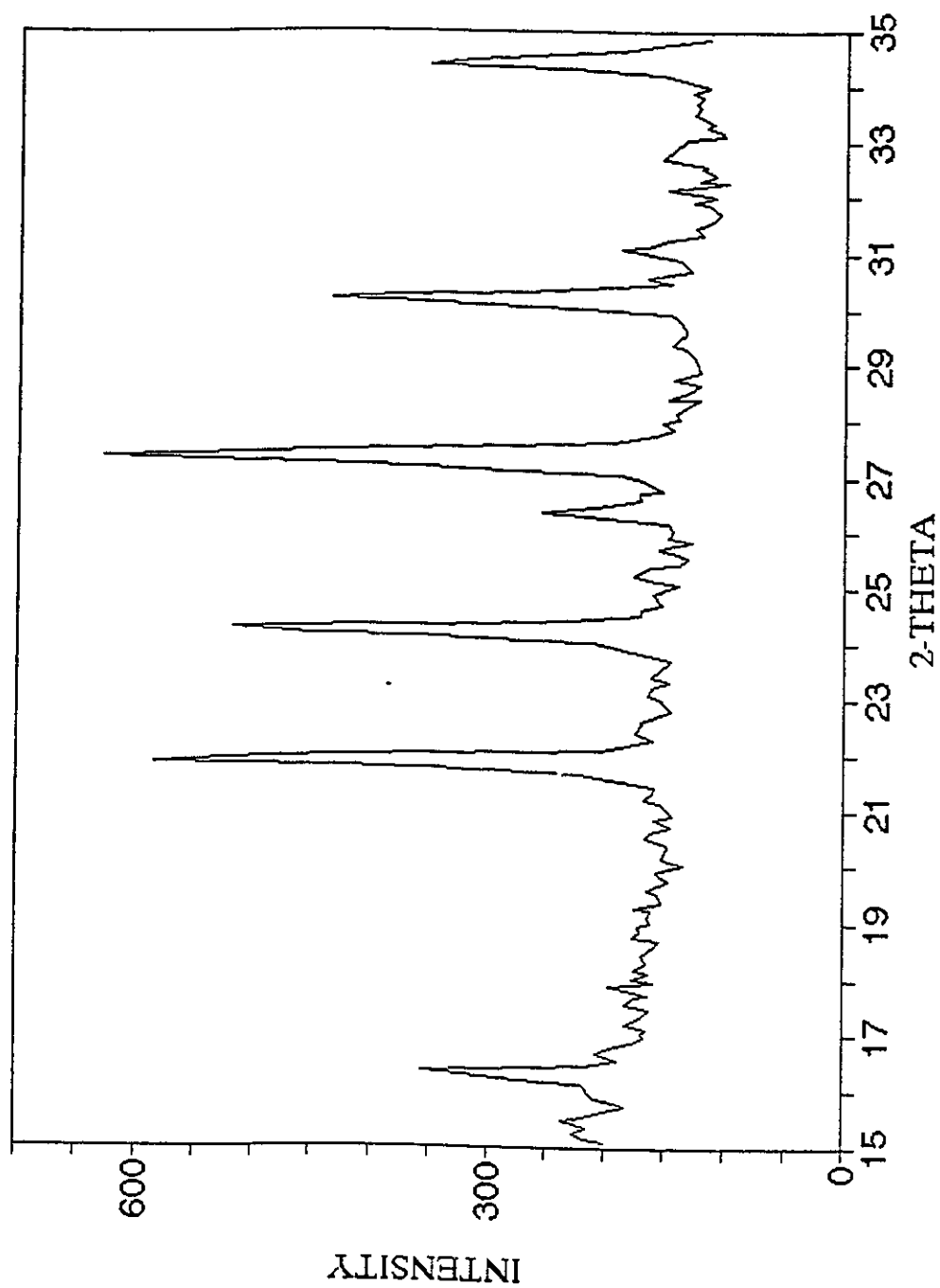
Figure 30c: X-Ray Diffraction Pattern of AT(3) Sample.
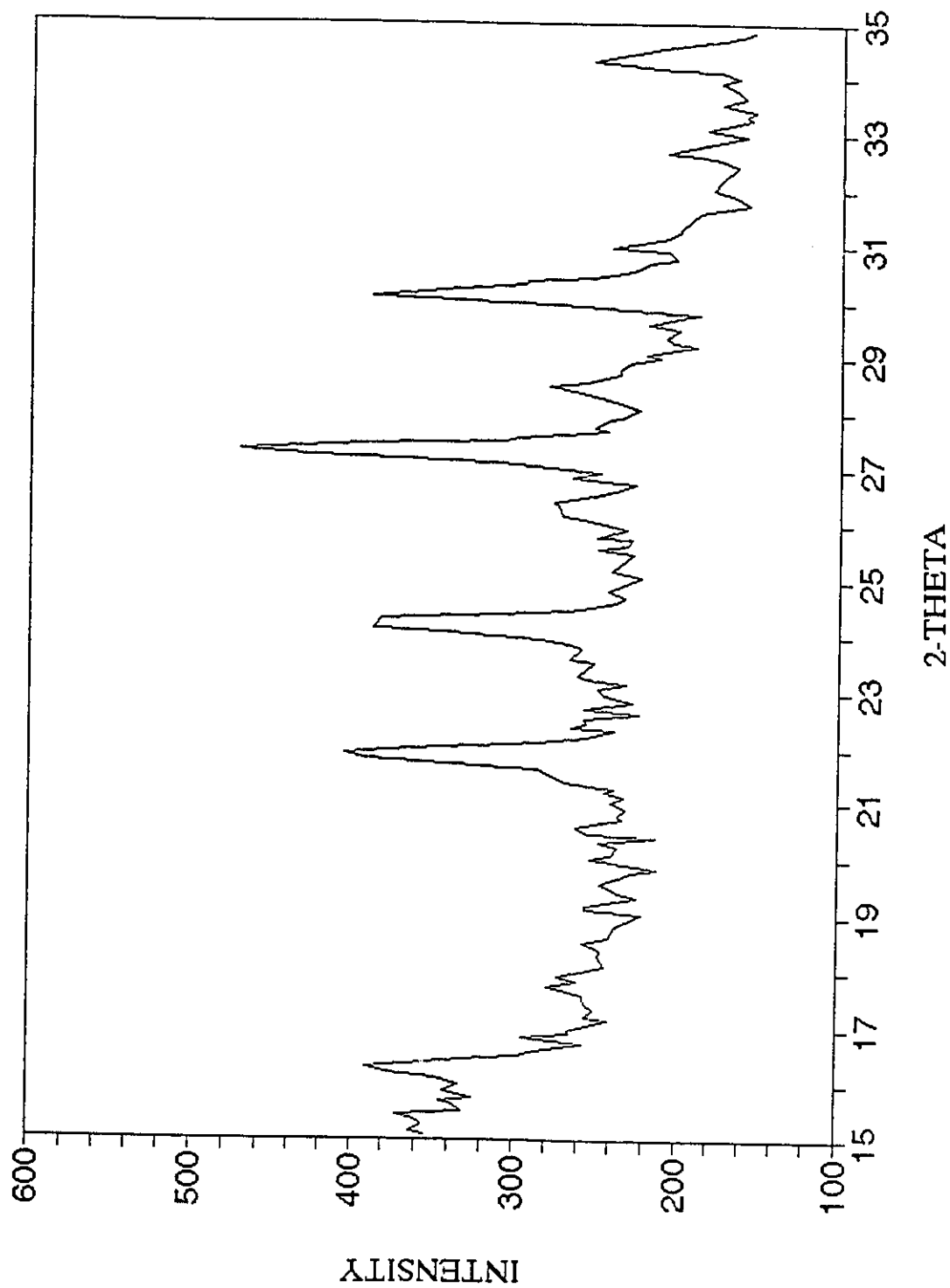
Figure 30d: X-Ray Diffraction Pattern of AFS(3)RT Sample.
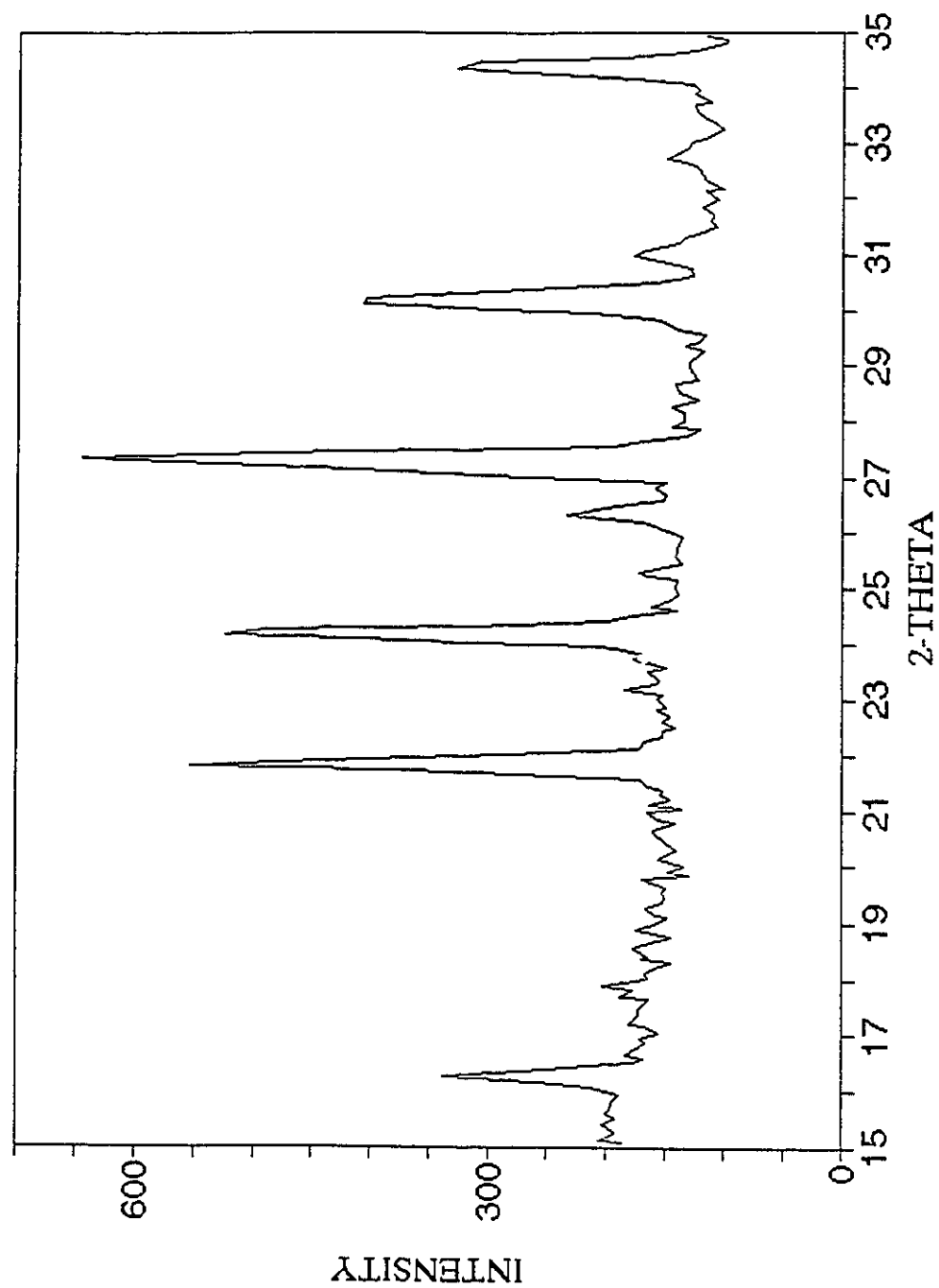
Figure 30e: X-Ray Diffraction Pattern of HTA(75,3) Sample.

v).   Activation (Thermal Stability)

Activation in air at 500 °C for 12 hours did not change significantly the shape of the pore size distribution curves of the AFS3 (Figure 19) and the AT12 samples (Figure 17).

Some positive change from the practical viewpoint is found in particular with the AFS3 sample upon heating at 500 °C: a limited increases in surface area and volume of nitrogen adsorbed, and a slight decrease in average pore diameter are observed (Table XIII). This shows that the ceramic powders obtained by AFS treatment can withstand activation temperatures of at least up to 500 °C without losing their interesting textural characteristics.

The AT samples were less resistant to heat than the AFS ones (Table XIII). The loss in surface area and volume of nitrogen sorption when these AT samples were heated at 500 °C, increased with the extent of acid treatment. This may be connected to the increasing formation of a silica-rich gel in the case of a prolonged acid treatment. Such a gel normally undergoes structural collapse when activated at high temperatures.

Table XIII: BET Results of AT and AFS Samples Activated at High Temperatures.

Sample	Tempe-rature	BET Surface Area	Volume of N_2 sorbed		Average pore diame-ter
			Total	MP	
	°C	m^2 / g	cm^3 / g	cm^3 / g	nm
AT(6)	120	182	0.133	0.032	2.1
	500	108	0.101	0.017	2.6
AT(9)	120	144	0.128	0.006	3.3
	500	64	0.072	-	5.2
AT(12)	120	145	0.131	0.005	3.5
	500	73	0.083	-	5.1
(AFS3)	120	112	0.314	0.001	11.2
	500	154	0.397	0.012	9.2

vi). **Cation-exchange capacity (C.E.C.)**

Table XIV shows the chemical composition obtained by AAS of the samples of untreated Ca-A zeolite, AFS (0.32 RT) and AT 6 and all these samples treated with 5% NaCl for two hours at room temperature. If we compare the chemical composition of the samples treated with NaCl relative to the same before the treatment, we can see clearly an enrichment in Na_2O with a decrease in the other metal oxides except Al_2O_3. As shown in Table XV, with the acid treated samples (AT series), limited restoration of the Na content is obtained whereas with the AFS treated sample, a nearly full restoration of the cation-exchange capacity of the Ca-A is observed.

In fact, in the untreated zeolite Ca-A , the total C.E.C. for Ca^{++} and Na^+ is 7.9 millieq./g or 2.3 millieq./g (with respect to Na^+) and 5.6 millieq./g (with respect to ½ Ca^{++}). The C.E.C. of the retro-exchanged AT(6) is 4.1 millieq./g or 1.4 millieq./g (Na^+) and 2.7 millieq./g (½ Ca^{++}). This represents only 52% of the C.E.C. of the parent zeolite. In the mean time, the C.E.C. of the retro-exchanged AFS(0.32, RT) is 7.8 millieq./g or 2.1 millieq./g (Na^+) and 5.7 millieq./g (Ca^{++}), which is 99% of the C.E.C. of the unreacted Ca-A zeolite.

As mentioned earlier, during the HCl acid treatment, the Na site is the first target while the Ca site can be attacked only under more severe treatment conditions. That is why the retro-exchange replaces the Na sites that were lost at first. However, since the hydronium ion H_3O^+ has more affinity towards Na than Ca in an aqueous medium, all the H_3O^+ sites which are the ex-Na sites retro exchange first, then the Ca sites will follow after. This phenomena is more visible on samples treated for longer times such as six hours instead of two hours: the Ca^{++} content of the sample AFS(0.81, RT, 6

Table XIV: Chemical Composition of Samples Before and After Treated with 5% NaCl for 2 hr at RT

Sample	Chemical composition				Si/Al ratio
	CaO	Na$_2$O	Al$_2$O$_3$	SiO$_2$	–
	Wt %				
5A	15.6	7.2	38.8	38.4	0.84
5A(2 NaCl)	14.8	12.0	38.1	35.1	0.78
AFS(0.32, RT)	16.3	0.9	31.3	51.5	1.39
AFS(0.32, RT, 2 NaCl)	16.0	6.5	34.8	42.7	1.04
AT(6)	7.6	1.2	39.4	51.8	1.11
AT(6, 2 NaCl)	7.7	4.3	35.4	52.6	1.26
AFS(0.81, RT)*	15.6	0.8	33.7	49.9	1.26
AFS(0.81, RT, 6 NaCl)*	9.5	12.9	35.6	42.0	1.00

N.B.:   (*). reference # 44

Table XV: Cation-Exchange Capacity of Samples Before and After Treated with 5% NaCl for 2hr at RT

Sample	Cation content			Total of CaO and Na_2O
	CaO	Na_2O	Al_2O_3	
	millieq./g			
5A	5.56	2.32	7.61	7.88
5A(2 NaCl)	5.28	3.87	7.47	9.15
AFS(0.32, RT)	5.81	0.29	6.14	6.10
AFS(0.32, RT, 2 NaCl)	5.71	2.10	6.83	7.81
AT(6)	2.71	0.39	7.73	3.10
AT(6, 2 NaCl)	2.71	1.39	6.94	4.10
AFS(0.81, RT)*	5.56	0.26	6.61	5.82
AFS(0.81, RT, 6 NaCl)*	3.39	4.16	6.98	7.55

N.B.: (*) reference # 44

NaCl 5%) is equal to only 60% of that of the sample before the ion-exchange treatment (3.39 out of 5.56 millieq./g) while it is 98% after ion-exchange (5.71 out of 5.81 millieq./g) for the sample of AFS(0.32, RT, 2 NaCl 5%).

CHAPTER V: CONCLUSION

This work presented here proves that it is possible to produce, from Ca-A zeolite porous solid powders which have a monomodal or a bimodal pore size distribution. Three procedures were developed to tailor the porosity. First, a very mild acid treatment with 0.2N HCl at 80 °C formed gradually mesopores. The pore size distribution of the materials obtained depended greatly on the time of exposure to the acid medium.

Second, an accurately controlled hydrothermal treatment followed by acid leaching led to mesopores having unblocked openings. It seems that the sites for acid or hydrothermal attack were located at the pore openings of the parent zeolite particles. By using the extreme operating conditions of the previously mentioned techniques, materials exhibiting monomodal pore size distributions of 3.5 - 4.5 nm and still having relatively high surface areas were also prepared.

Finally, a treatment with 0.5 M $(NH_4)_2SiF_6$ at ambient temperature provided materials which exhibited larger mesopores of about 14 nm diameter and a broad monomodal pore size distribution.

Because the AFS treatment combines two reactions: 1) extraction of Al together with Na, and 2) release of HF which attacks Al and Si indiscriminately; it results then in an enlargement of the cavity. The following ion-exchange can restore almost the same C.E.C., even though there is, of course a small loss of Al. Therefore, the product possesses the same C.E.C. properties with however, a larger pore size as compared to the parent Ca-A zeolite.

Porous solids having bimodal pore systems such as activated carbons (45) or

monomodal ones (46) are currently used for many commercial applications: adsorbents, inorganic membranes for separation and purification of bulky molecules (ultrafiltration), and catalyst support. The resulting solids studied in the present work may constitute good starting materials for such purposes.

Because of these very interesting potential applications of our products, this research should be extended to a more detailed study of the bulk density of the resulting materials and its relation to changes in composition and to the X-ray diffraction study of the crystallinity of partial framework collapse. As mentioned earlier, since the ion-exchange property gives the product a winning card, further studies with other cations should be taken. Finally, this precursor material should then be studied for the designed real ceramics, by combining it with a compatible binder and then also, for the applications proposed above.

In summary, instead of creating new zeolite types, with a larger pore size, we have enlarged the micropores of existing zeolites to the mesopore sizes. Depending on the desired result, different conditions and treatments can lead to the desired porous ceramic powders.

CHAPTER VI: REFERENCES

1)   M.E. Davis, C. Saldarriaga, C. Montes, J. Garces and C. Crowder

      Nature, Vol. 331, 698 - 699 (February 1988).

2)   S.T. Wilson, B.M. Lok, C.A. Messina, T.R. Cannan and E.M. Flanigen

      J. Am. Chem. Soc., Vol. 104, 1147 - 1149 (1982).

3)   R.M. Dessau, J.L. Schlenker and J.B. Higgins

      Zeolites, Vol. 10, 522 - 524 (July-August 1990).

4)   K.S.W. Sing et al.

      Pure and Appl. Chem., Vol. 57, No. 4, 603 - 619 (1985).

5)   D.W. Breck

      "Potential uses of natural and synthetic zeolites in industry", Union

      Carbide Molecular Sieves, Tarrytown, 1979, 35 pages

6)   D.W. Breck, W.G. Eversole, R.M. Milton, T.B. Reed and T.B. Thomas

      J. Am. Chem. Soc., Vol. 78, No. 23, 5963 - 5977 (December 1956).

7)   R. Le Van Mao

      Revue de l'institut français du pétrole, Vol. 34, No. 3, 429 - 455 (Mai-
      Juin (1979).

8)   M. Estermann, L.B. Mc Cusker, C. Baerlocher, A. Merrouche and H. Kessler

      Nature, Vol. 352, 320 - 323 (July 1991).

9)   a.   C.V. Mc Daniel and F.A. Maher

            Conf. Mol. Sieves, 1967, Soc. of Chem. Ind., London, Monogr.

186 (1968).

b.   R.M. Barrer and M.B. Makki

       Can. J. Chem., Vol. 42, 1481 (1964).

       P.E. Eberly, Jr. and C.N. Kimberlin, Jr.

       Ind. Eng. Chem. Prod. Res. Dev., Vol. 9, 335 (1970).

c.   W.E. Garwood, S.J. Lucki, N.Y. Chen, and J.C. Bailler, Jr.

       Inorg. Chem., Vol. 17, 610 (1978).

       W.E. Garwood, N.Y. Chen, and J.C. Bailler, Jr.

       Inorg. Chem., Vol. 15, 1044 (1976).

d.   B.M. Lok, F.P. Gortsema, C.A. Messian, H. Rastelli, and T.P.J. Izod

       A.C.S. Symposium Series No. 218, 1983, p.41.

e.   G.T. Kerr

       J. Phys. Chem., Vol.72, 2594 (1968).

       G.T. Kerr

       J. Phys. Chem., Vol. 73, 2780 (1969).

       G.T. Kerr, A.W. Chester and D.H. Olson

       Acta Phys. Chem., Vol. 24, 169 (1978).

f.   R. Beaumont and D. Barthomeuf

       J. Catal., Vol. 26, 218 (1972).

       R. Beaumont and D. Barthomeuf

       J. Catal., Vol. 30, 288 (1973).

g.   H.K. Beyer and I. Belenykaya

Catalysis by Zeolites, ed. B. Imelik et al. Elsevier, Amsterdam, 1980, p. 203.

h.   J. Klinowski, J.M. Thomas, M.W. Anderson, C.A. Fyfe and G.C. Gobbi

Zeolites, Vol.3, 5 (1983).

i.   W.L. Kranich, Y.H. Ma, L.B. Sand, A.H. Weiss and I. Zwiebel

Adv. Chem. Ser., Vol. 101, 502 (1970).

N.Y. Chen and F.A. Smith

Inorg. Chem., Vol. 15, 295 (1976).

j.   J. Scherzer

J. Catal., Vol. 54, 285 (1978).

V. Bosacek et al.

J. Catal., Vol. 61, 435 (1980).

10)   J. Scherzer

Catalytic Materials, Relationship between Structure and Reactivity (Eds. T.E. Whyte, R.A. Dalla Betta, E.G. Derouane and R.T.K. Baker), A.C.S. Symp. Ser. 248, Am. Chem. Soc., Washington D.C., 1984, p. 157.

11)   Q.L. Wang, G. Giannetto and M. Guisnet

Zeolites, Vol. 10, 301 - 303 (April-May 1990).

12)   G.W. Skeels and D.W. Breck

Union Carbide Corporation, Tarrytown Technique Center, Tarrytown, New York 10591.

13)   D.W. Breck

"Zeolite Molecular Sieves: Structure, Chemistry and Use", John Willey

& Sons, New York, pp. 529 - 588 (1974).

14) B.H. Davis

Chemtech, pp. 18 - 25 (January 1991).

15) A.J. Lecloux

"Catalysis: Science and Technology", Vol.2, Anderson and Boudart, Eds., Springer-Verlag, Berlin (1981), pp. 171 - 230.

16) B. Lippens and J. de Boer

J. Catal., Vol. 4, 319 (1965).

17) S.J. Gregg and K.S. Sing

"Adsorption, Surface Area and Porosity", Academic Press Inc., London (1982), pp. 111 - 190.

18) a. C. Pierce

J. Phys. Chem., Vol. 57, 149 (1953).

c. E.P. Barrett, L.G. Joyner and P.P. Halenda

"The Volume and Area Distributions in Porous Substances", 373 - 380 (January 1951).

b. D. Dollimore and G.R. Heal

J. Appl. Chem., Vol. 14, 109 - 114 (March 1964).

19) "Operator's Manual of Micromeritics - ASAP 2000 Operating Program V 1.03, Norcross, GA.

20) a. J.W. Robinson

Anal. Chem., Vol. 32, 17A (1960).

b. H. Kahn

Chem. Edu., Vol. 43, A7 (1966).

21) a. J.C. Van Loon

"Analytical Atomic Absorption Spectroscopy Selected Methods",

(Academic Press, 1980), p. 5.

b. L.R. Morris

Spectrochim. Acta, Vol. 35B, 687 (1980).

22) P. K. Kipkemboi

"Preparation and Characterization of Leached Asbestos Materials" Master

thesis, Concordia University, 1988, 177 pages.

23) M.E. Pillow

Spectrochim. Acta, Vol. 36B, 821 (1981).

24) A. Walsh

Pure and Appl. Chem., Vol. 49, 1621 (1977).

25) R.D. Dresser et al.

J. Chem. Edu., Vol. 52, A403 (1975).

26) R. Le Van Mao

React. Kinet. Catal. Lett., Vol. 12, 69 (1979).

27) R. Le Van Mao et al.

React. Kinet. Catal. Lett., Vol. 15, 293 (1980).

28) D.A. Skoog

"Principles of Instrumental Analysis", 3rd edition (Saunders   College

Publishing, 1985), p. 464.

29) G.S. Rajhans and J.L. Sullivan

"Asbestos Sampling and Analysis", Ann Arbor Science Publishers Inc., Ann Arbor, Michigan (1981), pp. 185 - 231.

30) *ASTM*, D3906, pp. 728 - 731.

31) G. Denes

Bulk Density Measurements notes, Concordia University.

32) J. Schaefer and E. Stejskal

J. Am. Chem. Soc., Vol. 98, 1031 (1976).

33) B. Shapiro, Ed.

"Heterogeneous Catalysis", A.C.S. Symp. Ser., Vol. 288, 1984, pp. 347 - 379.

34) G. Stucky and F. Dwyer, Eds.

"Intrazeolite Chemistry", A.C.S. Symp. Ser., Vol. 218, 1983, pp. 159 - 177.

35) G.C. Gerstein

Anal. Chem., Vol.55, 781A (1983).

36) D.W. Breck

"Zeolite Molecular Sieves: Structure, Chemistry, and Use", John Wiley & Sons, New York, pp. 87 - 88, 491 - 492 (1974).

37) N.S. Gnep, P. Roger, P. Cartraud, M. Guinet, B. Juguin and C. Hamon

C.R. Acad. Sci., Paris, 1743 (1989).

38) a. C.H. Elliot, Jr.

U.S. Patent no. 3 594 331 (1971).

b. D.W. Breck and G.W. Skeels

U.S. Patent no. 4 503 023 (1985).

39) J. Klinowski

Progress in NMR Spectroscopy. Vol. 16, 237 (1984).

40) G. Engelhardt, D. Michel

"High-Resolution Solid-State NMR of Silicates an Zeolites", J. Wiley & Son.

41) J. P. Gilson, G. C. Edwards, A. W. Peters and al.

J. Chem Soc., Chem. Commun., 91 (1987).

42) E. Brunner, H. Ernst, D. Freude, T. Frohlich, M. Hunger, and H. Pfeifer

Journal of catalysis, 34 (1991).

43) D.W. Breck and G.W. Skeels

Molecular Sieves II, A.C.S. Symposium Series 40, American Chemical Society, Washington, Washington D.C., 271 (1977).

44) R. Le Van Mao

Unpublished results.

45) M. Suzuki

"Adsorption Engineering", Elsevier Publ., Tokyo, 6 (1990).

46) E. Stellwagen

"Guide to Protein Purification", M.P. Deustcher, Academic Press Inc., San Diego, 327 (1990).

47) R. Le Van Mao, N.T.C. Vo, B. Sjiariel, L. Lee and G. Denes

J. Master. Chem., Vol. 2 (1992).